การเตรียมอนุพันธ์บิวทิเลเทดฟีนอลโดยใช้ตัวเร่งปฏิกิริยาวิวิธพันธุ์ชนิดกรด

นางสาววรัมพร สิงหพันธ์

วิทยานิพนธ์นี้เป็นส่วนหนึ่งของการศึกษาตามหลักสูตรปริญญาวิทยาศาสตรมหาบัณฑิต
สาขาวิชาปิโตรเคมีและวิทยาศาสตร์พอลิเมอร์
คณะวิทยาศาสตร์ จุฬาลงกรณ์มหาวิทยาลัย
ปีการศึกษา 2559
ลิขสิทธิ์ของจุฬาลงกรณ์มหาวิทยาลัย

PREPARATION OF BUTYLATED PHENOL DERIVATIVES USING ACIDIC HETEROGENEOUS
CATALYSTS

Miss Warumporn Singhapan

Thesis Title	PREPARATION OF BUTYLATED PHENOL DERIVATIVES USING ACIDIC HETEROGENEOUS CATALYSTS
By	Miss Warumporn Singhapan
Field of Study	Petrochemistry and Polymer Science
Thesis Advisor	Duangamol Tungasmita, Ph.D.

Accepted by the Faculty of Science, Chulalongkorn University in Partial Fulfillment of the Requirements for the Master's Degree

....Dean of the Faculty of Science

(Associate Professor Polkit Sangvanich, Ph.D.)

THESIS COMMITTEE

....Chairman

(Assistant Professor Warinthorn Chavasiri, Ph.D.)

....Thesis Advisor

(Duangamol Tungasmita, Ph.D.)

....Examiner

(Assistant Professor Anawat Ajavakom, Ph.D.)

....External Examiner

(Sitthipong Pengpanich, Ph.D.)

วรัมพร สิงหพันธ์ : การเตรียมอนุพันธ์บิวทิเลเทดฟีนอลโดยใช้ตัวเร่งปฏิกิริยาวิวิธพันธุ์ชนิด กรด (PREPARATION OF BUTYLATED PHENOL DERIVATIVES USING ACIDIC HETEROGENEOUS CATALYSTS) อ.ที่ปรึกษาวิทยานิพนธ์หลัก: ดร. ดวงกมล ตุงคะสมิต, 107 หน้า.

ตัวเร่งปฏิกิริยาเอสบีเอ-15 ที่มีหมู่กรดโพรพิลซัลโฟนิก และโปรตรอนเอ็มซีเอ็ม-22 สามารถ สังเคราะห์ได้ด้วยวิธีไฮโดรเทอร์มัล โครงสร้างสัณฐานวิทยาและคุณสมบัติความเป็นกรดของวัสดุที่ สังเคราะห์ได้ถูกตรวจสอบลักษณะเฉพาะด้วยเทคนิคการเลี้ยวเบนของรังสีเอกซ์ การวิเคราะห์การดูด ซับไนโตรเจน กล้องจุลทรรศน์อิเล็กตรอนแบบส่องกราดและการตรวจวัดปริมาณกรด ประสิทธิภาพ การเร่งปฏิกิริยาของเอสบีเอ-15 ที่มีหมู่กรดโพรพิลซัลโฟนิกถูกทดสอบด้วยปฏิกิริยาบิวทิเลชันของบิส ฟีนอลเอและทำการเปรียบเทียบประสิทธิภาพในการเร่งปฏิกิริยากับแอมเบอร์ลิช-15 และตัวเร่ง ปฏิกิริยาที่มีรูพรุนชนิดอื่น ภาวะที่เหมาะสมเมื่อใช้ตัวเร่งปฏิกิริยาเร่งปฏิกิริยาของเอสบีเอ-15 ที่มีหมู่ กรดโพรพิลซัลโฟนิกคืออัตราส่วนโมลของบิสฟีนอลเอต่อเมทิลเทอร์เทียรีบิวทิลอีเทอร์เท่ากับ 1: 10 ปริมาณตัวเร่งปฏิกิริยาเท่ากับ 15% โดยน้ำหนักของบิสฟีนอลเอที่อุณหภูมิ 120 องศาเซลเซียส เป็น เวลา 8 ชั่วโมง สารผสมหลังทำปฏิกิริยาให้ผลผลิตรวมของผลิตภัณฑ์สูงสุดเมื่อเทียบกับตัวเร่งปฏิกิริยา ที่มีรูพรุนเมโซพอร์รัสชนิดอื่น ยิ่งไปกว่านั้นปฏิกิริยาบิวทิเลชันของบิสฟีนอลเอถูกใช้ทดสอบ ประสิทธิภาพการเร่งปฏิกิริยาของโปรตรอนเอ็มซีเอ็ม-22 ภาวะที่เหมาะสมที่ให้ผลผลิตรวมของ ผลิตภัณฑ์สูงสุดคืออัตราส่วนโมลของบิสฟีนอลเอต่อเทอร์เทียรีบิวทานอลเท่ากับ 1: 15 ปริมาณตัวเร่ง ปฏิกิริยาเท่ากับ 10% โดยน้ำหนักของบิสฟีนอลเอที่อุณหภูมิ 120 องศาเซลเซียส เป็นเวลา 8 ชั่วโมง สารผสมหลังทำปฏิกิริยาแสดงผลผลิตรวมของอัลคิลเลทผลิตภัณฑ์สูงสุดที่ 32.8% นอกจากนี้ยังได้ ทำการศึกษากระบวนการต่อเนื่องในการเตรียม 2,6-ได-เทอร์เทียรี บิวทิล-พาราคิวมิลฟีนอล ได้ภาวะ ที่เหมาะสมคืออัตราส่วนโมลของพาราคิวมิลฟีนอลต่อเทอร์เทียรีบิวทานอลเท่ากับ 1: 5 ความเร็ว เชิงสเปซเท่ากับ 0.02 ต่อชั่วโมงที่อุณหภูมิ 120 องศาเซลเซียส เป็นเวลา 26 ชั่วโมง ผลการทดสอบได้ 2,6-ได-เทอร์เทียรี บิวทิล-พาราคิวมิลฟีนอลสูงสุดที่ 28.19% ความสามารถในการยับยั้งอนุมูลอิสระ ของผลิตภัณฑ์บริสุทธิ์และสารผสมหลังทำปฏิกิริยาถูกตรวจวัดเปรียบเทียบกับสารตั้งต้น พบว่าฤทธิ์ ต้านออกซิเดชันเพิ่มขึ้นตามลำดับดังนี้ บิสฟีนอลเอ < พาราคิวมิลฟีนอล < 2-เทอร์เทียรี บิวทิล-พารา คิวมิลฟีนอล < บิสฟีนอลเอผลิตภัณฑ์ < 2,6-ได-เทอร์เทียรี บิวทิล-พาราคิวมิลฟีนอล

สาขาวิชา ปิโตรเคมีและวิทยาศาสตร์พอลิเมอร์	ลายมือชื่อนิสิต ....
ปีการศึกษา 2559	ลายมือชื่อ อ.ที่ปรึกษาหลัก ....

5672082223 : MAJOR PETROCHEMISTRY AND POLYMER SCIENCE

KEYWORDS:

WARUMPORN SINGHAPAN: PREPARATION OF BUTYLATED PHENOL DERIVATIVES USING ACIDIC HETEROGENEOUS CATALYSTS. ADVISOR: DUANGAMOL TUNGASMITA, Ph.D., 107 pp.

Propyl sulfonic acid functionalized SBA-15 and proton MCM-22 catalysts were synthesized by using hydrothermal method. The structure morphology and acidity of synthesized materials were characterized by X-ray powder diffraction, nitrogen sorption analysis, scanning electron microscopy and acidity measurement. Propyl sulfonic acid fuctionalized SBA-15 (SBA-15-Pr-SO$_3$H) was tested catalytic activities in BisphenolA butylation and compared catalytic activity with Amberlyst-15 and other porous catalysts. The optimized condition when using SBA-15-Pr-SO$_3$H was mole ratio of BisphenolA to MTBE of 1: 10, catalytic amount 15 wt% based on BisphenolA at 120°C for 8 hrs. The reaction mixture gave the highest total yield of products compared to those of other mesoporous catalysts. Moreover, the catalytic efficiency of HMCM-22 of butylation of BisphenolA was tested. Suitable reaction condition that gave the highest total product was optimized to be mole ratio of BisphenolA to *tert*-butanol as 1: 15, catalytic amount 10 wt% based on BisphenolA at 120°C for 8 hrs. The reaction mixture exhibited the highest total yield of alkylated products as 32.8%. In addition, the condition of continuous flow process to prepare 2,6-di-*tert*-butyl *p*-cumylphenol was optimized to be mole ratio of *p*-cumylphenol to MTBE of 1: 5, LHSV = 0.02 h^{-1}, at 100°C. The results illustrated the highest 2,6-di-*tert*-butyl *p*-cumylphenol yield as 28.19%. The radical scavenging capacity of purified and reaction mixtures were measured to compare with their starting materials. It was found that antioxidant activity was increased as following order; BisphenolA < *p*-cumylphenol < 2-*tert*-butyl *p*-cumylphenol < BisphenolA products < 2,6-di-*tert*-butyl *p*-cumylphenol.

Field of Study: Petrochemistry and   Student's Signature ....

Polymer Science   Advisor's Signature ....

Academic Year: 2016

ACKNOWLEDGEMENTS

CONTENTS

LIST OF TABLES

LIST OF FIGURES

LIST OF SCHEMES

LIST OF ABBREVATIONS

Å	Angstrom
a.u.	Arbitrary unit
BET	Brunauer-Emmett-Teller
BJH	Barret, Joyner, and Halenda
°C	Degree Celsius
DPPH	α α α -Diphenyl- α -picrylhydroxyl
g	Gram (s)
HMI	Hexamethyleneimine
HPLC	High performance liquid chromatography
hrs	Hour (s)
MPTMS	(3-mercaptopropyl)trimethoxysilane
MS	Mass spectroscopy
μ m	Micrometer (s)
ml	Milliliter (s)
min	Minute (s)
M	Molarity
nm	Nanometer (s)
%	Percentage
SEM	Scanning electron microscopy
TEM	Transmission electron microscopy
TEOS	Tetraethyl orthosilicate
XRD	X-ray diffraction

CHAPTER I

INTRODUCTIONS

1.1   Statement of problems

Over the past five years, the phenol and acetone markets have seen a rapid increase in global production capacity while global demand growth for phenol, acetone and their derivatives has slowed down. The main derivative markets for phenol and acetone are bisphenol-A (BPA), polycarbonate, epoxy resins, phenolic resins and methyl methacrylate (MMA), all of which have also seen investment in new capacity in the past few years.The ongoing impact of increased capacity for these products, at a time of what seems to be lower than expected demand growth for many products, has been to increase competitive pressure on prices and change trade flows. Phenol and acetone are inextricably linked as in most instances the products are commercially produced in the cumene process, which utilises benzene and propylene as feedstocks and is therefore significantly impacted by upstream price movements. The two co-products are produced in different quantities, with around 1.5 tonnes of phenol manufactured for each tonne of acetone, but the economics of the process requires demand for both acetone and phenol [1]. Global phenol capacity is expected to have increased by more than 2.1 million tonnes between 2010 and the end of 2016. The vast majority of this additional capacity, over 2 million tonnes, has been built in Asia, with China leading the way. Most recently, in 2015, three new plants opened in China with a combined capacity of 800,000 tonnes/year [2]. Side reaction of cumene process was shown in scheme 1.1 . *p*-Cumylphenol was one of these by-products in cumene process. It can be used in the production of alkylphenol-type non ionic surfactant and as antioxidants in plastics [3]. Because *2-tert*-butyl-*p*-

cumylphenol and 2,6-di-*tert*-butyl-*p*-cumylphenol showed a terminated free radical property [4, 5] which is important for expedient life extending of oxygenated degradable item. In addition, 2,6-di-*tert*-butyl-*p*-cumylphenol was used as an antioxidant in plastic and rubber and can be applied at temperature above 120°C because of its low volatility. The butylated *p*-cumylphenols were prepared via alkylation with various butylating agents such as isobutylene, *tert*-butanol and methyl-*tert*-butyl ether (MTBE). However, butylating agent in the gas phase such as isobutylene was worried about controlling reaction parameter; instead, liquid butylating agent was selected to react with phenol derivative reactants in this study. Properly, acid was used to catalyze alkylation reaction. From the earlier patent, *p*-toluene sulfonic acid was employed as a catalyst in *p*-cumylphenol alkylation with isobutylene to prepare butylated products but this catalyst was concerned about corrosion and separation problems due to its solubility with reactants. Thus, heterogeneous catalyst was a suitable preference for green chemistry of *p*-cumylphenol derivatives synthesis and the research of *p*-cumylphenol butylation over heterogeneous catalyst in continuous flow process disappeared until now.
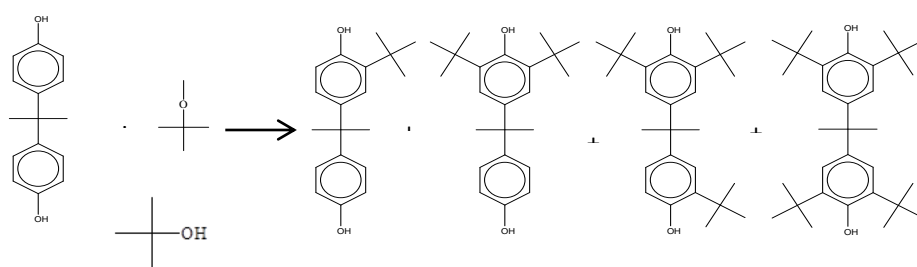
Figure 1.1   Alkylation of BisphenolA
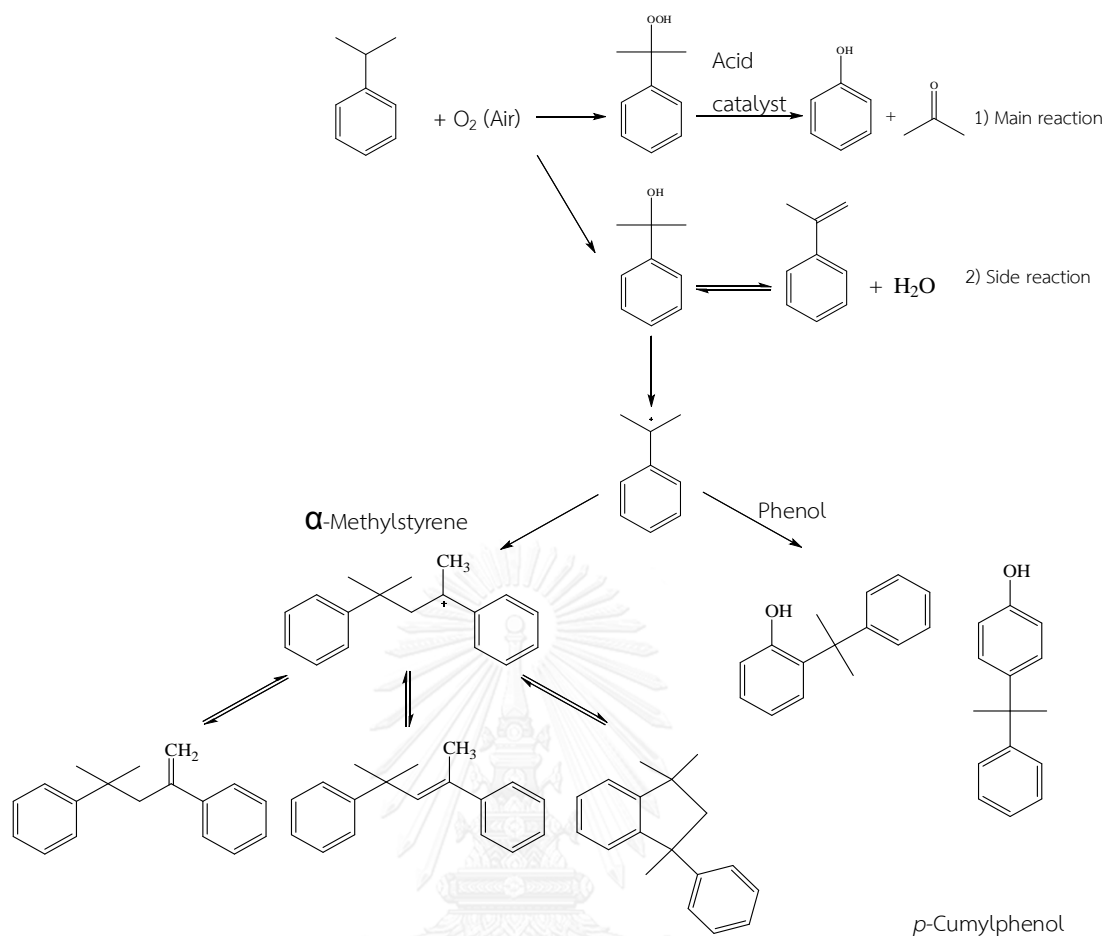
Scheme 1.1 Main reaction and side reaction of phenol production [6].

Moreover BisphenolA, commonly abbreviated as BPA, is produced commercially by the acid catalyzed condensation of phenol and acetone under mild conditions of temperature and pressure [7]. It has been in commercial use since 1957. BPA is an industrially important raw material for the preparation of epoxy resins and polycarbonates that are used to line water pipes, as coatings on the inside of many food and beverage cans and in making thermal paper that used as sales receipts and also used in the synthesis of polysulfones and polyether ketones, as an antioxidant in some plasticizers, and as a polymerization inhibitor in PVC. In 2015, an estimated 4 million tonnes of BPA chemical were produced for manufacturing polycarbonate plastic, making it one of the highest volume of chemicals produced worldwide. BPA is also used in the synthesis of polysulfones and polyether ketones, as an antioxidant in

some plasticizers, and as a polymerization inhibitor in PVC. Epoxy resins containing BPA are used as coatings on the inside of almost all food and beverage cans [8].

This work will focus on the optimization of *p*-cumylphenol in continuous flow reactor and BPA butylation condition (Figure 1.1) using acid heterogeneous catalyst for yield and selectivity of desired *C*-alkylation product in batch reactor. In addition, effects of butylating agent type (MTBE and *tert*-butanol), reaction temperature, mole ratio of BPA/butylating agent, catalytic amount, reaction time and catalytic types were examined.

1.2   Literature reviews

1.2.1 Butylated *p*-cumylphenol preparation

In 1976, Mitsui Toatsu Chemicals, Inc. [5] provided a 2 ,6 - di-*tert*-butyl-*p*-cumylphenol preparing method. *p*-Cumylphenol was reacted with isobutylene over *p*-toluene sulfonic acid at 40°C -120°C that gave 94.8% conversion and weight ratio of 2 ,6 - di-*tert*-butyl-*p*-cumylphenol to 2-*tert*-butyl-*p*-cumylphenol was more than 10. Then, kinetic mechanism of this reaction system at 80°C was studied by Masagutov, R. M. *et al.,* in 1984 [6]. The *C*-alkylation products were consecutive formation from 2-*tert*-butyl-*p*-cumylphenol and then followed by 2,6-di-*tert*-butyl-*p*-cumylphenol. The *p*-cumylphenol butylation occurred via 10 steps as shown in Scheme 1.2. The step of *p*-cumylphenol transforming to 2 -*tert*-butyl-*p*-cumylphenol was faster than the step of 2-*tert*-butyl-*p*-cumylphenol converting to 2,6-di-*tert*-butyl-*p*-cumylphenol. Besides, many of side reaction products were generated such as phenol, **α** -methylstyrene, *tert*-butylphenol, dicumylphenol and tricumylphenol.

$$X_1 + B \underset{k_{-1}}{\overset{k_1}{\rightleftharpoons}} X_2; \quad X_1 + B \underset{k_{-2}}{\overset{k_2}{\rightleftharpoons}} X_3; \quad X_3 + B \underset{k_{-3}}{\overset{k_3}{\rightleftharpoons}} X_4;$$

$$X_1 \underset{k_{-4}}{\overset{k_4}{\rightleftharpoons}} X_6 + X_7; \quad X_6 + B \xrightarrow{k_5} X_8; \quad 2\, X_7 \xrightarrow{k_6} X_9;$$

$$X_1 + X_7 \xrightarrow{k_7} X_5; \quad X_5 + B \xrightarrow{k_8} X_{10}; \quad X_5 + X_7 \xrightarrow{k_9} X_{10};$$

$$X_2 \xrightarrow{k_{10}} X_3$$
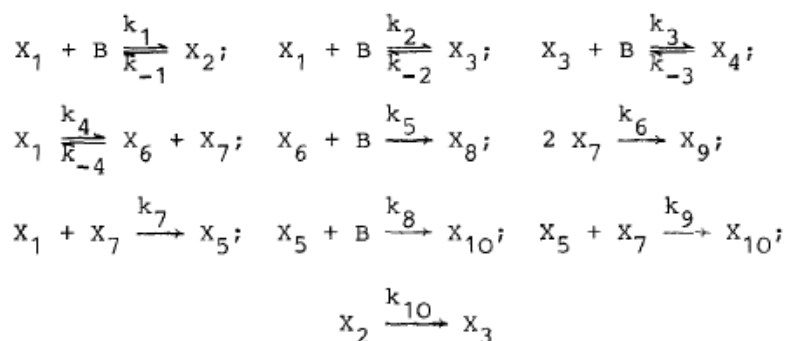
Where X_1 is *p*-cumylphenol;

X_2 is the *tert*-butyl-ether of *p*-cumylphenol;

X_3 is 2-*tert*-butyl-*p*-cumylphenol;

X_4 is 2,6-di-*tert*-butyl-*p*-cumylphenol;

X_5 are dicumylphenols;

X_6 is phenol;

X_7 is α-methylstyrene;

X_8 are *tert*-butylphenols;

X_9 are the dimers of α-methylstyrene;

X_{10} are heavy *tert*-butyl-di-cumylphenols and tricumylphenol

B is isobutylene

k_i is rate constant

Scheme 1.2 Suggested reaction scheme of p-cumylphenol alkylation with isobutylene [6].

The research of butylated *p*-cumylphenol synthesis was scarcely available. Moreover, most of the research studied about catalysis of *p*-cumylphenol butylation by homogeneous catalyst which is difficult to separate. Besides, heterogenous catalyst was examined and used in other phenol derivatives alkylation. Acidic SBA-15 was one of mesoporous catalyst and was expected to be suitable for large molecule reaction, for instance, *p*-cumylphenol butylation reaction.

1.2.2 SBA-15-Pr-SO$_3$H synthesis

In 1988, Zhao, D. *et al.* [9] reported about well-ordered hexagonal mesoporous silica (SBA-15) synthesis in acidic condition. Several poly(alkene oxide) triblock copolymers and organic molecule co-solvent were used in SBA-15 preparation. Also, SBA-15 performed 50-300 Å of pore size, 31-64 Å of wall thickness, and pore volume fractions more than 0.85.

Margolese *et al.* invented the new procedure in the preparation of sulfonic functionalized mesostructure materials. In 2000, they improved the direct synthesis method to create propyl sulfonic functionalized SBA-15 (SBA-15-Pr-SO$_3$H) [10]. This procedure involved an one-step strategy based on the co-condensation of tetraethyl orthosilicate (TEOS) and (3-mercaptopropyl)trimethoxysilane (MPTMS) in the presence of Pluronic P123 and hydrogen peroxide in HCl aqueous solution. This approach allowed in-situ oxidation of the thiol groups to sulfonic acid groups.

1.2.3 Acidic SBA-15 catalyst in butylation reaction

In 1999, Yue, Y. *et al.* The Al-SBA-15 could be synthesized by incorporating aluminium into SBA-15 *via* direct synthesis and post synthesis. Yue *et al.* studied Al-SBA-15 by direct synthesis and the resulting materials retain the hexagonal order and physical properties of purely siliceous SBA-15. The SBA-15 catalysts exhibited higher catalytic activities in the cumene cracking reaction than Al-MCM-41 [11].

In 2011, Ma, J. *et al.* researched the butylation of phenol with *tert*-butanol/ phenol as 5 by mole at 190°C and 7 hrs. for comparing catalytic activity with different structures and various synthesis methods. The percentage of conversions and reaction rate constants were decreased in the following order: AlSBA-15(20) from post synthesis method > AlSBA-15(20) from direct synthesis method > AlMCM-48(20) > AlMCM-41(20) due to larger pore size and surface area of AlSBA-15. In addition, AlSBA-15 from post

synthesis method exhibited high acid strength and could be reused 4 times without a significant catalytic activity changing [12].

Shone, J.K. *et al.* [13] reported about metal (Fe, Zn and Al) addition in mesoporous material in 2007. Metal incorporated material performed broad range of acidity from weak to strong depending on synthesis method. Also, organosilane functionalization on SBA-15 surface by direct and post synthesis was prepared to enhance acid strength. The acid strengths of organosilane were increased with following order; carboxylic group (-COOH) < alkylphosphonic group (-R-PO$_3$H$_2$) < alkylsulfonic group (-R-SO$_3$H). Under the described reaction condition; mole ratio of *tert*-butanol to phenol as 2 at 120°C, the carboxylic, alkylphosphonic and alkylsulfonic functionalized SBA-15 material were selective to *tert*-butyl phenyl ether, 2-*tert*-butyl phenol and 4-*tert*-butyl phenol, respectively. Moreover, selectivity of 2,4-di-*tert*-butyl phenol was enlarged with the reaction temperature increasing from 120°C to 150°C.

1.2.4   HMCM-22 synthesis

In 1995, MCM-22 synthesis with different SiO$_2$/Al$_2$O$_3$ ratios was observed, by Corma, A. *et al.* [14]*,* using hexamethylenimine as a template. MCM-22 at SiO$_2$/Al$_2$O$_3$ ratio about 30 showed a pure phase and obtained with good yield. Moreover, phase of sample at SiO$_2$/Al$_2$O$_3$ more than 70 was contaminated by ZSM-5 phase. MCM-22 was synthesized in rotating condition because the static condition induced the ferrierite phase appearing.

The zeolites MCM-22 with various Si/Al ratios were exchanged to proton form using 2M NH$_4$Cl aqueous solution at 80°C for 1 hr. and calcined to remove ammonia molecule at 500°C for 3 hrs. The HMCM-22 was studied in isobutene production from 1-butene isomerization, by Asensi, M.A. *et al.* [15] in 1995. About 80% selectivity of isobutene and 40% conversion were obtained with using high Si/Al ratio (Si/Al = 47) of

MCM-22.

1.2.5 HMCM-22 in butylation reaction

In 2005, Rigoreau, J. *et al*. [16] examined the toluene alkylation with propene over a HMCM-22 (Si/Al = 15) at 200°C and cymene was desired product. Toluene alkylation occurred essentially on the protonic sites of the external cups that was confirmed by collidine poisoning. HMCM-22 with large external surface exhibited high performance, stability and selective catalyst for the aromatic alkylation with propene.

In 2002, Moon, G. *et al*. [17] reported about the alkylation of phenol with methanol over H-MCM-22 was investigated and the performance of this catalyst compared with that of H-ZSM-5 and amorphous silica-alumina. The reaction was studied in the liquid phase (batch reactor) at temperatures between 200–250°C and pressures between 20–42 bar and in the gas phase (flow reactor) at temperatures between 250–400°C and feed partial pressures of 0.2 bar. The C (ring) : O (side chain)-alkylation ratio was found to be more dependent on reaction conditions (i.e. gas/liquid phase, pressure and temperature) than catalyst type. The highest C : O alkylation ratios were obtained using gas phase reactions and were similar for all three catalysts. The highest *p/o*-cresol ratios were obtained using H-MCM-22 in the liquid phase at 200°C. Reasons are proposed to explain the different ring vs side chain alkylation and cresol isomer distributions for the different catalysts and the different reaction conditions.

1.2.6 Butylated preparation

In 2000, Alkylation of phenol with *tert*-butyl alcohol catalyzed by large pore zeolites was considered by Zhang, K. *et al.* [18]. The *tert*-butylation of phenol was investigated over various zeolite catalysts using *tert*-butyl alcohol as alkylating agent

in a down-flow tubular reactor at atmospheric pressure. Zeolite HY was beneficial to the reaction. The important variables affecting the activity and selectivity of zeolite HY, such as reaction temperature, space velocity and molar ratios of *tert*-butyl alcohol to phenol, were studied. Zeolite HY hydrothermally treated at high temperatures (above 873 K) was unfavorable to the reaction. The activity and selectivity of zeolite HY were not sensitive to its crystallite diameter change. In the alkylation of phenol with *tert*-butyl alcohol over zeolite HY catalyst, the suitable reaction temperature range was from 398 to 438 K. Lower reactant molar ratios were beneficial to *p*-TBP and *o*-TBP, while higher ones were helpful to produce 2,4-DTBP. Lower space velocities (WHSV (h−1)), i.e. <1.66 (based on phenol) were beneficial to the reaction. The present study shows that zeolite HY has a potential application in the production of *tert*-butyl phenols with high activity and 2,4-DTBP selectivity.

In 2007, the different Si/Al ratios of HMCM-22 were produced using hexamethylenimine as a template. Kumar, G.S. *et al.* [19] investigated the effects of Al amount and reaction parameter in reaction of phenol with *tert*-butanol. HMCM-22 (Si/Al = 54) exhibited high selective formation of 4-*tert*-butyl phenol (76%) with 85% conversion. The experiment was carried out at 175°C, phenol: *tert*-butanol feed ratio = 1:3, WHSV = 5.13 hr.[−1] and catalyst weight = 0.5 g. From the result, 10MR ring channel in MCM-22 might be suitable for 4-*tert*-butyl phenol synthesis.

In 2004, Alkylation of *p*-cresol with *tert*-butanol catalyzed by heteropoly acid support on zirconia catalyst, which was studied by Devassy, B.M. *et al.* [20]. Butylation of *p*-cresol by *tert*-butanol was catalyzed by 12-tungstophosphoric acid supported on zirconia (TPA/ZrO$_2$) under flow conditions. Catalysts prepared with different TPA loading (5–30 wt.%) were calcined at 1023 K and acidity was estimated by temperature programmed desorption (TPD) of NH$_3$. Fifteen percent TPA/ZrO$_2$ showed the highest acidity and found to be the most active catalyst in butylation of *p*-cresol. The effects

of temperature, space velocity (LHSV) and molar ratio of the reactants on the conversion of p-cresol and products selectivities were optimized and the optimum reaction conditions evaluated were 403 K, tert-butanol/p-cresol (Bu/Cr) molar ratio 3 and LHSV = $4h^{-1}$. Under the optimized conditions, conversion of p-cresol was found to be 61 mol% with product selectivity for 2-tert-butyl-p-cresol (TBC) 81.4%, 2,6-di-tert-butyl-p-cresol (DTBC) 18.1% andtert-butyl-p-tolyl ether (ether) 0.5%. Study of time on stream (TOS) performed as a function of time for 100 h showed that the loss in activity in terms of conversion of p-cresol was 6%.

In 2006, Synthesis, Characterization, and Catalytic Performance of Mesoporous were considered by Shujie, W. *et al*. [21]. Mesoporous Al-SBA-15 was synthesized by the post-synthesis grafting of Al atoms on a parent siliceous SBA-15. Both SBA-15 and Al-SBA-15 with different Si/Al ratios were characterized by powder X-ray diffraction, transmission electron microscopy, and N_2adsorption–desorption. The alkylation of phenol with *tert*-butanol was carried out at atmospheric pressure in a continuous flow, fixed-bed quartz reactor (id=6 mm) using 0.3 g catalysts. Prior to use, the catalysts were activated in N_2 at 500°C for 1 hr, and the reactor was then cooled down to the required reaction temperature. The reaction mixture was injected from the top using a syringe pump. After reaction for 2 h, the products were collected and quantified by a gas chromatograph. During the alkylation of phenol with *tert*-butanol, the Al-SBA-15 catalyst showed a higher conversion of phenol and selectivity for 2,4-di-*tert*-butyl phenol (2,4- DTBP) than the traditional Al-MCM-41 catalyst. At a reaction temperature of 145°C, a higher phenol conversion of 75.2% and a 2,4-DTBP selectivity of 31.3% over Al-SBA-15 were observed as compared to those over Al-MCM-41, which were 61.3% and 13.4%, respectively. Due to the large pore size (about 9 nm), which allows a faster diffusion of reactants and products, catalyst deactivation of Al-SBA-15 was not observed even after reaction for 5 hr.

1.3   Objectives

1.3.1   Continuous flow process

To study the effect of parameters on butylated product yield for optimum reaction conditions in continuous flow reactor with Amberlyst-15 catalyst which give high selective to di-*tert*-butylated phenol product.

1.3.2   Batch process

To synthesize the acidic porous heterogeneous catalysts for prepare di-*tert*-butylated phenol derivatives.

To study the effect of reaction parameters on butylated product yield and product distribution in butylation reaction of phenol derivatives.

1.4   Scopes of work

1.4.1   Continuous flow process

Determine the optimum condition of butylation reaction by studying the effect of *p*-cumylphenol to butylating agent mole ratio and reaction temperature.

- Type of butylating agent   Methyl *tert*-butyl ether (MTBE)
                                                         and *tert*-butanol

- Reaction temperature   90°C - 110°C

- Molar ratio of phenol derivative
  to butylating agent mole ratio   1: 3 - 1: 10

1.4.2   Batch process

1.4.2.1 Synthesis SBA-15 and MCM-22 via hydrothermal method

1.4.2.2 Functionalize SBA-15, Al-SBA-15 and MCM-22 with propyl sulfonic group

1.4.2.3 Increase acidity of MCM-22 with proton exchange

1.4.2.4 Characterize resulting porous materials

1.4.2.5 Determine the reaction parameters of butylation reaction affect on yield and selectivity of butylated products

- Type of butylating agent   Methyl *tert*-butyl ether (MTBE) and *tert*-butanol

- Type of catalyst

  Microporous catalysts   HZSM-5, HMCM-22 and HBeta

  Mesoporous catalysts   MCA-Pr-SO$_3$H and SBA-15-Pr-SO$_3$H

  Clay   Treated acidic bentonite

  Commercial catalysts   Amberlyst-15

- Reaction temperature   100°C - 120°C

- Molar ratio of phenol derivative

  to butylating agent mole ratio   1: 5-1:20

- Catalytic amount based on

  phenol derivative weight   0 - 20 wt%

- Reaction time   2 hrs. - 10 hrs.

1.4.3 Evaluation antioxidant

CHAPTER II

THEORY

2.1   Catalysts

A catalyst is a substance that increased the rate of a chemical reaction by reducing the activation energy (E_a) as shown in Figure 2.1. The highest peak position performing the highest energy refers to the transition state. In typically reaction, the energy required to enter the transition state is high, whereas the energy to transition state decreases in catalytic reaction. In addition, the catalyst may participate in multiple chemical transformations and is not consumed by the reaction.
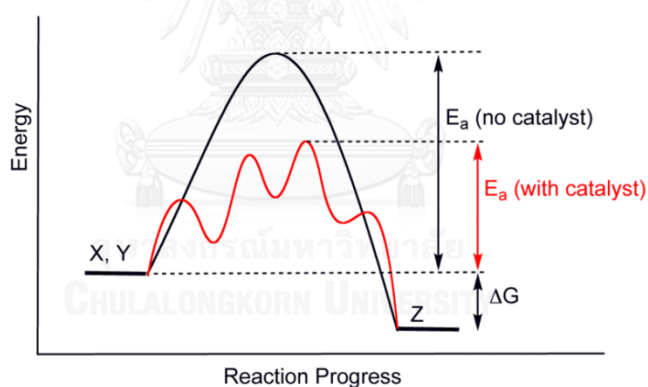
Figure 2.1   The relationship between activation energy (E_a) and enthalpy (ΔH) of the reaction with and without a catalyst [22].

2.1.1   Type of catalyst

Catalysts can be classified into two main types by the boundary of the catalyst and the reactant. Heterogeneous reaction is the different phase reaction between catalyst and reactants, whereas the catalyst in the same phase of reactant is called homogeneous reaction. Thus, the solid catalysts are identified as heterogeneous catalysts, and the liquid catalysts are specified as homogeneous catalysts when assume

reactant is liquid. Homogeneous catalyst has a higher degree of dispersion than heterogeneous catalyst only the surface atoms are active [23]. Summary of the advantage and disadvantage of two-type catalyst is presented in Table 2.1.

Table 2.1   Comparison of homogeneous and heterogeneous catalysts [23]

Consideration	Homogeneous catalyst	Heterogeneous catalyst
1. Active centers	All metal atoms	Only surface atoms
2. Concentration	Low	High
3. Selectivity	High	Low
4. Diffusion problems	Practically absent	Present (mass-transfer-controlled reaction)
5. Reaction conditions	Mild (50-200°C)	Severe (often >250°C)
6. Applicability	Limited	Wide
7. Activity loss	Irreversible reaction with product (cluster formation), poisoning	Sintering of the metal crystallites, poisoning
8. Modification possibility	High	Low
9. Thermal stability	Low	High
10. Catalyst separation	Sometimes laborious (chemical decomposition, distillation, extraction)	Fixed-bed: unnecessary Suspension: filtration
11. Catalyst recycling	Possible	Unnecessary (fixed-bed) or easy (suspension)
12. Cost of catalyst	High	Low

The major disadvantage of homogeneous catalyst is the difficulty of separating the catalyst from the product. Heterogeneous catalysts are either automatically

removed in the process (*e.g.* vapor-phase reaction in fixed bed reactor) or separated by simple methods such as filtration or centrifugation. However, in more complicated processes, distillation, liquid-liquid extraction and ion exchange are necessarily used homogeneous catalysts.

2.1.2 Porous molecular sieves

Molecular sieves are porous materials that perform selective adsorption properties. They can be classified into three main types depending on their pore size: and the IUPAC definitions: microporous materials, mesoporous materials, and macroporous materials. Properties and examples of these materials are summarized in Table 2.2.

Table 2.2 IUPAC classification of porous materials

Type of porous molecular sieve	Pore size (Å)	Examples
Microporous materials	< 20	Zeolites, Activated carbon
Mesoporous materials	20 – 500	M41s, SBA-15, Pillared clays
Macroporous materials	> 500	Glasses

2.1.3 Microporous materials

Zeolite is one of microporous crystalline alumino silicates. Each zeolite framework topology is identified by a three capital letter code, establish by the Structure Commission of the International Zeolite Association (IZA). Zeolites comprise naturally about 40 Å but zeolite or zeolite-like materials have been synthesized more than 170 Å. Although several structures exist, only 17 Å are of commercial interest: MER, MFI, MOR, MTT, RHO, TON and MWW. The different applications of these materials

are related to their properties of ion exchange, acidity, high activity, thermal stability and shape selectivity [24].

2.1.3.1 Structure of zeolites

Zeolites, a type of molecular sieves, are crystalline aluminosilicates that contain uniform pores and cavities with molecular dimensions. A zeolite has a three dimensional network structure of tetrahedral primary building unit (PBU) which consists of four oxygen anions with either silicon or aluminum cation in the center as shown in Figure 2.2.

Oxygen

Silicon or Aluminum
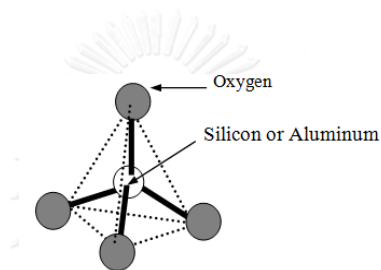
Figure 2.2   A primary building unit of porous materials [24].

A secondary building unit (SBU) consists of selected geometric groupings of those tetrahedral. These units will be assemble to originate large lattices by repeating identical building blocks (unit cells) as shown in Figure 2.3 for the FAU zeolite.

Sodalite cage   FAU zeolite

24 tetrahedral

Figure 2.3   Tetrahedral arrangement forming the sodalite cage and finally the structure of the zeolite FAU [24].

The tetrahedrons are mutually connected by sharing oxygen atom as shown in Figure 2.4 which produces the framework of zeolite. The negative charge of the lattice is neutralized by the positive charge of the metal cations. In the basic zeolites these are usually cation of univalent and bivalent metals or their combination. The general formula for the composition of zeolite is

$$M_{x/n} [(AlO_2)_x (SiO_2)_y]. \ w \ H_2O$$

Where M is the cation of valence n, generally from the group I or II ions, although other metals, nonmetals, and organic cations are also possible, w is the number of water molecules. Water molecules are located in the channels and cavities, as the cations that neutralize the negative charge created by the presence of the AlO_2^- tetrahedral unit in the structure.

Figure 2.4   The structure of zeolites [24].

The different ring sizes found in zeolites, based on the different number of tetrahedral atoms defining the opening, are shown in Figure 2.5. The ring sizes are often mentioned as the number of oxygen atoms which are equal to the number of tetrahedral atoms.

(a)   (b)   (c)
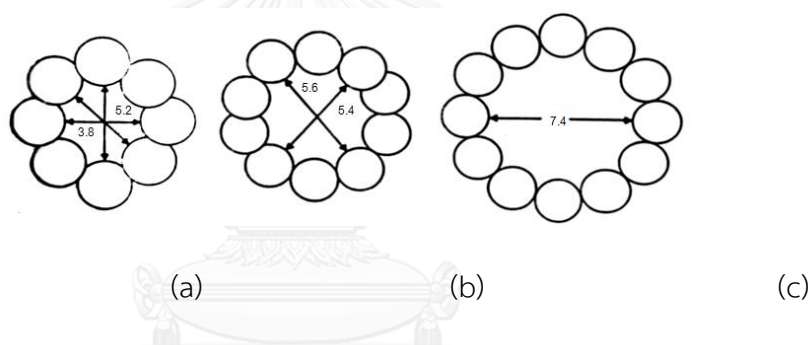
Figure 2.5   Examples of the three types of pore openings in the porous material molecular sieves (a) an 8 ring pore opening (small pore), (b) a 10 ring pore opening (medium pore) and (c) a 12 ring pore opening (large pore) [24].

2.1.3.2 Acid site of zeolites

In addition to the shape and size selective catalysis, the generation of acidic sites in the zeolite pores leads to a highly efficiency in solid-acidic catalysis. The isomorphous replacement of silicon atom with aluminum atom in a tetrahedral site gives rise to a charge imbalance because aluminum atom has lower coordination ability than silicon atom and must be neutralized. This is achieved in two ways in natural zeolites:

- The length of Al-O bond becomes slightly longer.

- A coordination site is made avail for cation to counter the excess negative charge.

In natural zeolites, the excess negative charge is balanced by various cations are present in the neighboring environment *e.g.* K^+, Na^+, Mg^{2+} and Ca^{2+} as exhibited in Figure 2.6 and Figure 2.7. The type of counter ion used to balance the charge plays an important part in the use of the zeolite. For uncomplicated understanding, the cation is replaced with a proton by hydrothermal treatment to form a hydroxyl group at the sharing oxygen atom. The acid site formed behaves as a classic Brønsted, proton donating acidic site as shown in Figure 2.8.
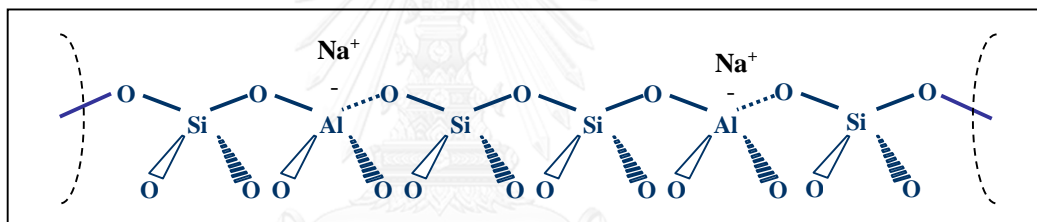
Figure 2.6   Sodium balanced zeolite framework [25].
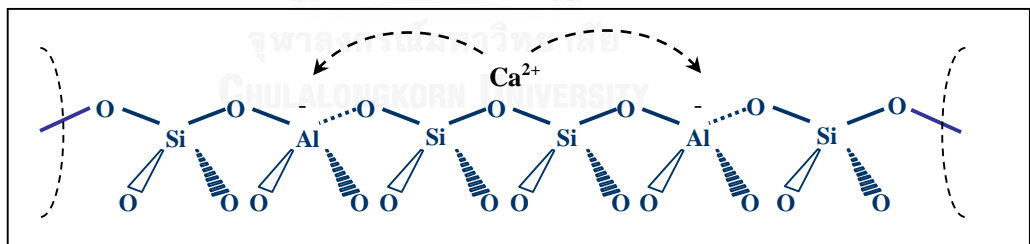
Figure 2.7   Calcium balanced zeolite framework [25].
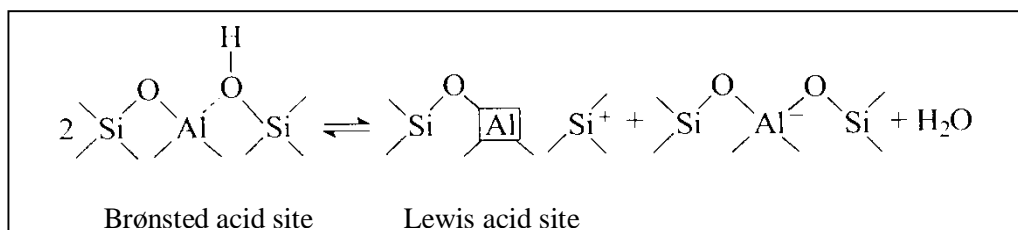
Figure 2.8   Brønsted and Lewis acid sites in zeolites [22].

2.1.4   MCM-22 zeolite

2.1.4.1 Structure and properties

MCM-22 zeolite (MWW structure type) was firstly synthesized by Mobil in 1990. This zeolite has a very original structure (Figure 2.9) and is considered as an intermediate pore size zeolite. It contains two independent bi-dimensional pore systems each accessible through 10 MR openings located on the ab-plane: sinusoidal channels delimitated by 10 MR (4.1 Å × 5.1 Å), with intersections of (6.4 Å × 6.9 Å) (Figure 2.10 (a), Figure 2.11 (a)), and large supercages with 12 MR (inner diameter 7.1 Å and 18.2 Å height) each connected to six others through 10MR windows (4.0 Å × 5.5 Å) (Figure 2.10 (b-c); Figure 2.11 (b)). The supercages stack one above the other by double 6-membered ring openings (hexagonal prisms), through which molecules cannot practically diffuse. Then, there is no access to the internal pores along the c-direction through the top or bottom surface of the crystal plates. Moreover, the outer surface of crystals presents large 12 MR pockets (hemicages, cups) which correspond to half supercages (diameter of 7.1 Å, depth of 7.0 Å) (Figure 2.12).

External cups
Ø 7.1 Å; Depth 7.0 Å

Hexagonal prism

10MR opening of
supercage (4.0 x 5.5 Å)

Sinusoidal channels
(4.0 x 5.1 Å)

MWW
supercage
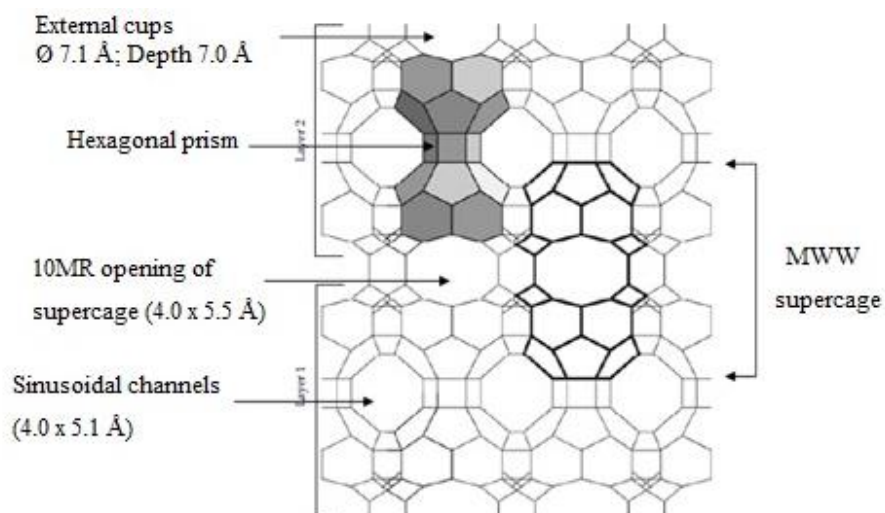
Figure 2.9 MWW framework structure (the supercage is highlighted and the shaded region shows two 12 MR cups back to back connect by a double six ring (hexagonal prism)) [24].

a) Sinusoidal channel system b) Supercage channel system   c) Supercage

Channel
(4.0 x 5.5 Å)

Supercage

18.2 Å
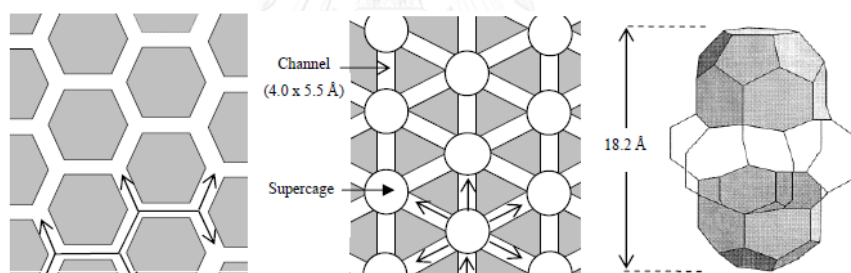
Figure 2.10 (a) Projection along the [001] direction of the sinusoidal channels and (b) supercages channel system of MCM-22 with various diffusion pathways are demonstrated by arrows. (c) Supercage with its six 10-ring apertures, having an inner diameter of 7.1 Å (defined by 12-MR) and a height of 18.2 Å. [24].

(a)   (b)

5.1   5.5

4.1   4.0
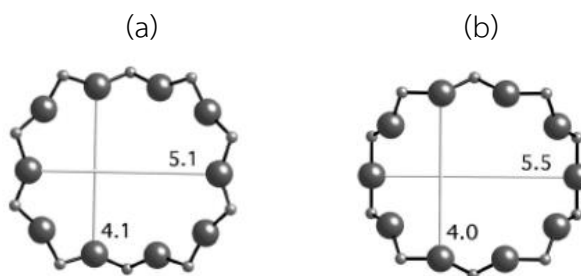
Figure 2.11   Pore size apertures of (a) sinusoidal channels and (b) supercages viewed normal to [001] [24].
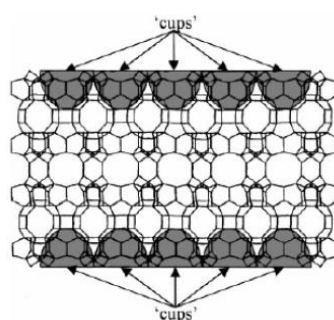
Figure 2.12   MCM-22 structure with the large cavities (''cups'') [24].

MCM-22 crystallizes as a layered precursor, generally denominated as MCM-22(P) (Figure 2.13). Each sheet contains the sinusoidal channels and 12 MR ''external cups'' (diameter of 7.1 Å, depth of 7.0 Å).
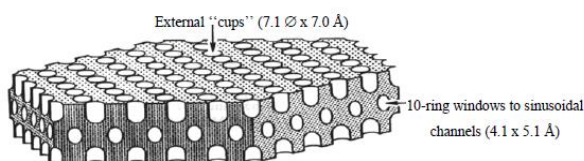
Figure 2.13   Single sheet of MCM-22 precursor [24].

During the first calcination of the MCM-22 precursor (MCM-22 (P)), in order to remove the template, it occurs dehydration and condensation between facing silanols of the sheets, forming Si-O-Si interlayer bridges, which origins the supercages and the final structure of MCM-22 zeolite (Figure 2.14). The sinusoidal channels, which already exist in the sheets of the layered precursor, are also designated ''interlayer micropores'' whereas supercages are denominated as ''intralayer micropores''.
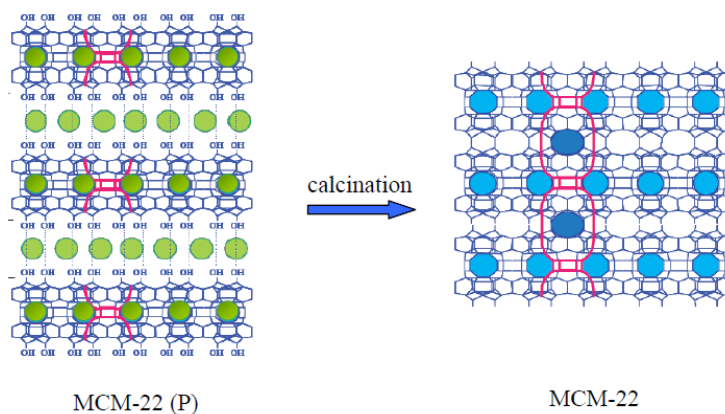
MCM-22 (P)　　　　　　　　　MCM-22

Figure 2.14 MCM-22 structure formation from calcination of the MCM-22 (P) precursor. Vertices represent the framework T atoms (Si or Al). --- Groups SiOH condensation, ● organic template, ● 10 MR sinusoidal channels pore apertures, -- 12 MR semicavities (MCM-22P) and 12 MR supercages and cups in MCM-22, ● 10 MR pore apertures to supercages in MCM-22 [24].

2.1.5 Mesoporous materials

Mesoporous silica has uniform pore sizes from 20 to 500 Å and has found great utility as catalysts and sorption media because of the regular arrays of uniform channels. Larger surface area is desired for enhancing of the efficient in the reactions [26].

The silica surface contains reactive silanol (Si-OH) groups which easily react with organic functionalities (Figure 2.15) for allowing to organic/inorganic hybrid material creation. The silica surface comprises a combination of isolated silanols (Figure 2.15 (a)), germinal silanols (Figure 2.15 (b)), vicinal silanols (Figure 2.15 (c)) and siloxane bridge (Figure 2.15 (d)). All of silanol species can be alter to prepare organic/inorganic hybrid material [27].

(a) (b) (c) (d)
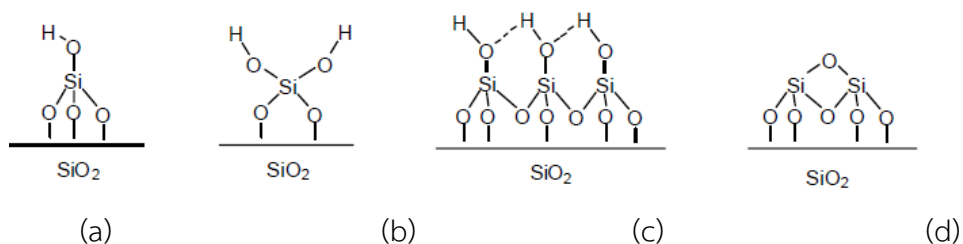
Figure 2.15   Types of silica surface Si-O species [27].

2.1.6   SBA-15

2.1.6.1 Structure and properties

Generally, silica materials was synthesized by the polymerization of $Si(OR)_4$ (tetraalkyl orthosilicate, where R is the alkyl chain) to form a of SiO_2 network (Scheme 2.1). The structure and properties of the silica was depending on reaction conditions. SBA-15, which is one of mesoporous material, was prepared by using non-ionic triblock copolymer (Pluronic 123) as a non-ionic triblock copolymer (Pluronic 123), which serves as a structure directing agent [27].
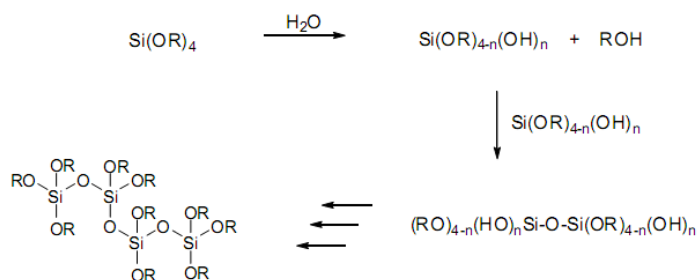
Scheme 2.1   Amorphous SiO_2 framework [27].

Specially, the micelles were formed by triblock copolymer in acidic aqueous ethanol solution (Scheme 2.2A). After the micelles dispersion, tetraethyl orthosilicate was adjusted as the silica source and polymerized surrounding the micelles to appearance the inorganic framework (Scheme 2.2B and 2.2C). TEOS was used as the silica source because it could be prevent the contamination of silica

material with residual halogen compounds that can be incorporated when used the other silica sources, such as $SiCl_4$ (Scheme 2.2D).
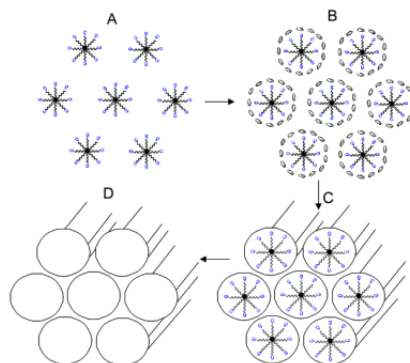
Scheme 2.2   Synthesis of SBA-15 [27].

In addition, the properties listed in Table 2.3, SBA-15 shows a better performance than MCM-41 in almost of properties.

Table 2.3   Comparison of two well-known mesoporous materials, MCM-41 and SBA-15 in their characteristic properties [9, 28]

Properties	MCM-41	SBA-15
Pore size (Å)	20-100	46-300
Pore volume (mL/g)	>0.7	0.8-1.23
Surface area (m²/g)	>1000	690-1040
Wall thickness (Å)	10-15	31-64

2.1.6.2   Synthesis of SBA-15 and formation mechanism

For SBA-15 materials, aging time and temperature are particularly important. Some research found that mesoporous SBA-15 prepared from calcination of an 'as-prepared' hybrid precursor contained a significant fraction of microporosity; further aging of the precursor in the mother liquors leads to an improvement on the pore size distribution as shown in Figure 2.16.
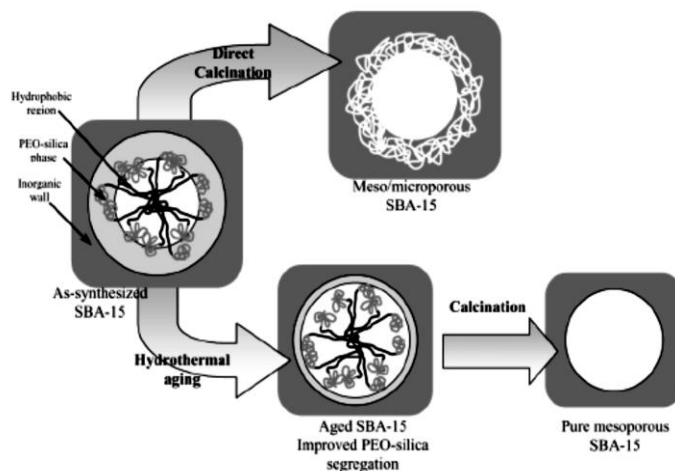
Figure 2.16 Pore evolution upon thermal treatment, depending on pre-treatment and aging [29].

2.1.7 Modification of SBA-15 by organic functionalization

Nowadays, the attachment of organic functionalities such as sulfonic acid groups to the surface of siliceous SBA-15 mesoporous material is an interesting research area in heterogeneous catalysis and green chemistry. Basically, two strategies have been generally used to anchor organic groups onto a mesostructured silica surface.

2.1.7.1 Direct synthesis

The preparation of sulfonic-acid modified mesostructured materials is illustrated in Figure 2.17. This method is simplicity, because the incorporation of the organic precursor and the formation of the mesoporous material occur in a single synthetic step. To have a useful catalyst after synthesis, one must be able to extract the template from within the pores to create porosity. Calcination the synthetic material will destroy the incorporated organic functional groups. Extraction technique can be most effectively accomplished by ethanol solution [30-32].
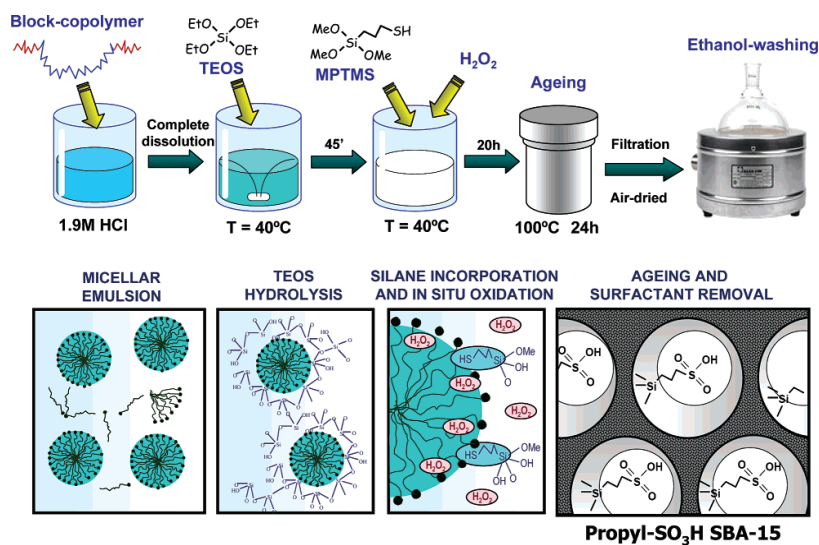
Figure 2.17 In-situ oxidation synthesis strategy for the preparation of sulfonic-acid-modified mesostructured materials [31].

2.1.7.2 Post synthesis

Grafting procedure based on modification of the silica surface with organic groups through silylation reaction occurring on isolated ($\equiv$ Si-OH) and germinal (=Si(OH)$_2$) silanol groups using trichloro- or trialkoxyorganosilane and silylamines as organic precursors [31].

Synthesis of sulfonic functionalized SBA-15 by post synthesis is shown in Scheme 2.3. In typical procedure, calcined SBA-15 is treated with a silating agent like 3-mercaptopropyltrimethoxysilane (MPTMS) in nonpolar solvent (commonly toluene) to immobilize thiol groups on the surface. These thiol functionalities are then oxidized, normally using hydrogen peroxide. The most apparent advantage of this procedure is good preservation of the mesostructure after post-modification.
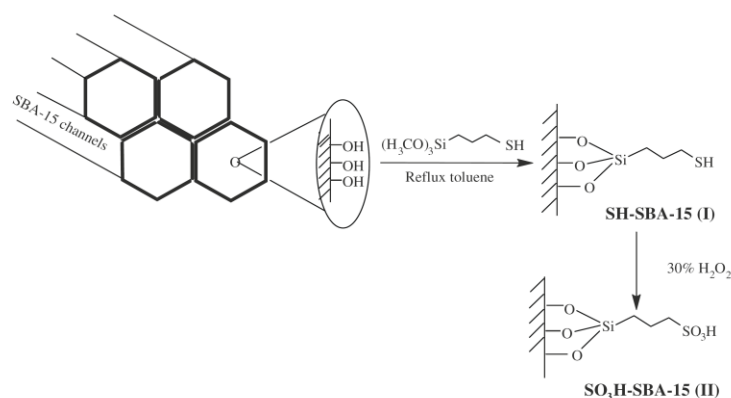
Scheme 2.3   Post synthesis procedure for the preparation of sulfonic-acid-modified mesostructured materials [33].

The difference between the two methods mainly involves the location of the organic functional group on the resulting silica material. The co-condensed material contained the groups on the surface and within the walls of the silica framework whereas the functional groups of grafted material only exhibited on the surface (Figure 2.18).

co-condensation   grafting
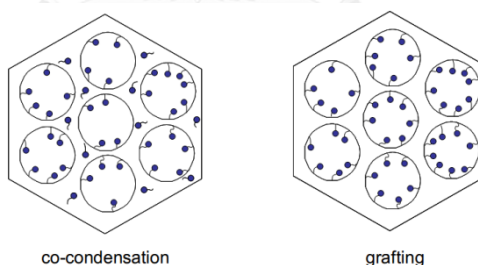
Figure 2.18   Comparison of functionalization via co-condensation or grafting [27].

2.1.8   Al-SBA-15

Presently, several post synthesis method where aluminum was grafted onto the mesoporous wall with various aluminum sources such as $Al(CH_3)_3$, $AlCl_3$ have been developed without the mesoporous structure seriously destroyed. Figure 2.19 shows that synthesis of Al-SBA-15 use basic probe (L) (e.g. pivalonitrile, the terminal silanol groups) including to form the bridging hydroxyl groups.
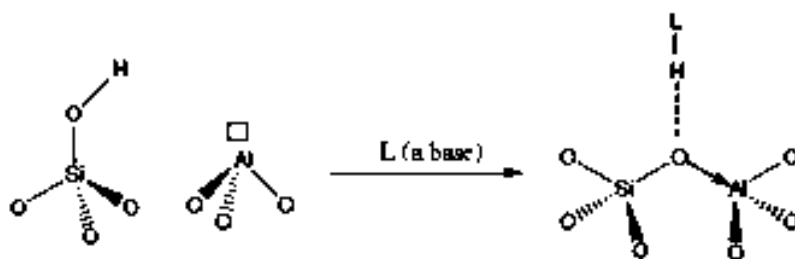
Figure 2.19 Aluminosilicates material using basic probe (L) inducing to form the
bridging hydroxyl group.

2.1.9 Amberlyst-15

Amberlyst-15 is a registered trademark of Rohm and Hass Company. It is an ion-exchange resin which is composed of styrene divinylbenzene copolymer crosslinked with sulfonic acid group. It has been used in a wide range of acid-catalyzed reaction due to having strong acidity. Especially, Amberlyst-15 with dry form that contains moisture amount ≤ 1.5 % was used in many reactions such as alkylation, esterification, etherification or condensation hydrolysis [34, 35]. However, surface area of Amberlyst-15 is negligible and thermal stability is very limited. The structure of Amberlyst-15 unit is illustrated in Figure 2.20
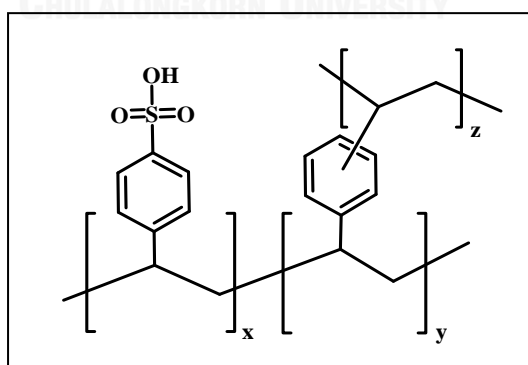
Figure 2.20   The structure of Amberlyst-15 unit [35].

2.1.10 Characterization of materials

2.1.10.1 X-ray powder diffraction (XRD)

X-ray powder diffraction (XRD) is an instrumental technique used to identify minerals, as well as other crystalline materials. This technique can provide information including the degree of crystallinity and specifying hexagonal mesoporus struture. In addition, it can allowed information that is the degree of hydration of sample. X-ray powder diffraction is based on constructive inference of monochromatic X-rays and crystalline samples.
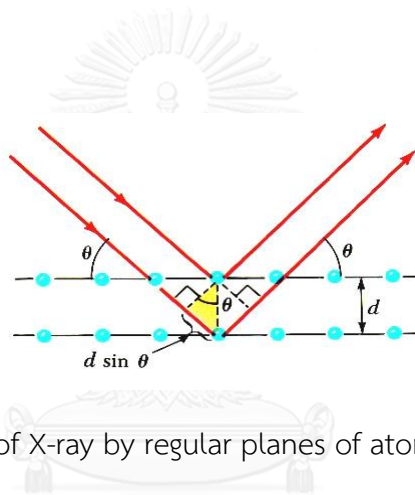
Figure 2.21   Diffraction of X-ray by regular planes of atoms [36].

Figure 2.21 shows a monochromatic beam of X-ray incident on the surface of crystal at an angle θ. The scattered intensity can be measured as a function of scattering angle 2θ. The resulting XRD pattern efficiently determines the different phases present in the sample. Using this method, Braggs' law is able to determine the interplanar spacing of the samples, from diffraction peak according to Bragg's angle.

$$n\lambda \ = \ 2\,d\,\sin\theta$$

Where the integer n is the order of the diffracted beam, λ is the wavelength of XRD source; d is the distance between adjacent planes of the crystal (the d-spacings) and θ is the angle between the incident beam and these planes.

2.1.10.2 Nitrogen adsorption-desorption technique

The N_2 adsorption-desorption technique is used to classify the porous materials and its physical properties such as surface area, pore volume, pore diameter and pore-size distribution of solid catalysts. Adsorption of gas by a porous material is described by an adsorption isotherm, the amount of adsorbed gas by the material at a fixed temperature as a function of pressure. Porous materials are frequently characterized in terms of pore sizes derived from gas sorption data [37, 38]. The IUPAC classification of adsorption isotherms is illustrated in Figure 2.22.
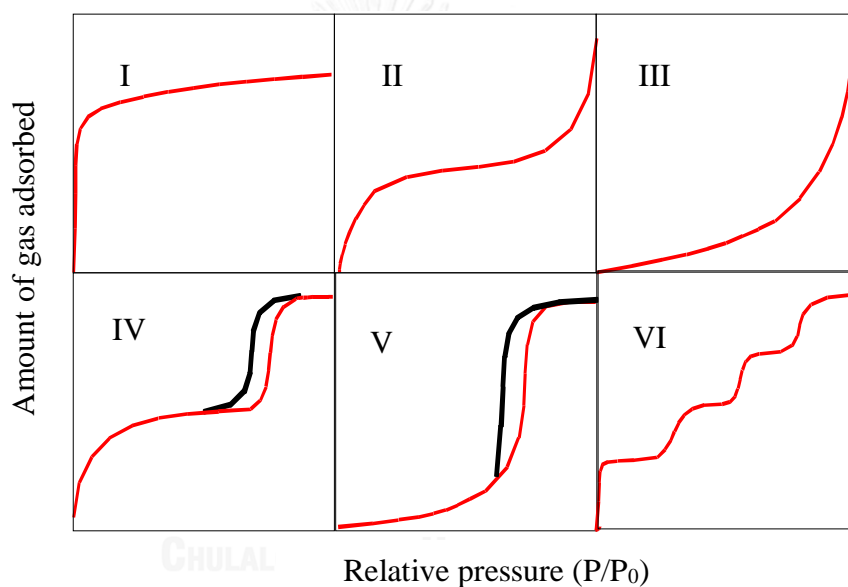
Figure 2.22 The IUPAC classification of adsorption isotherm [38].

Adsorption isotherms are described as shown in Table 2.4 base on the strength of the interaction between the sample surface and gas adsorbate, and the existence or absence of pore.

Table 2.4   Features of adsorption isotherms

Type	Characters	
	Interaction between sample surface and gas adsorbate	Porosity
I	relatively strong	Micropores
II	relatively strong	Nonporous
III	weak	Nonporous
IV	relatively strong	Mesopore
V	weak	Micropores
		Mesopore
VI	relatively strong sample surface has an even distribution of energy	Nonporous

2.1.10.3 Scanning electron microscope (SEM)

The scanning electron microscope (SEM) has unique capabilities for analyzing surfaces and morphology of materials. The electron microscope produces images of a sample by scaning it with a focus beam of electrons. The electrons interact with atoms in the sample, producing various signals that contain information about the sample's surface topography and composition. The electron beam is scanned in a raster scan pattern, and the beam's position is combined with the detected signal to produce an image. SEM can achieve resolution better than 1 nanometer. The process of SEM are showed in Figure 2.23.
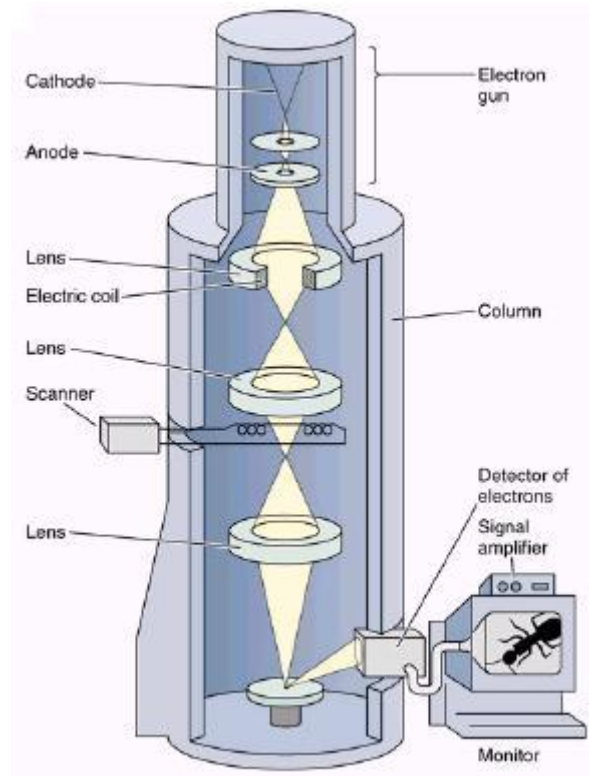
Figure 2.23   The process in SEM [39].

2.1.10.4 Inductively Coupled Plasma Mass Spectroscopy (ICP-MS)

Inductively Coupled Plasma Mass Spectrometer (ICP-MS) combines mass spectrometric detector with an inductively coupled plasma source. It can analyze metal elements from lithium to uranium with the concentration from 0.1 ppm to 1 wt.% In principle, solutions are vaporized using a nebulizer while solid samples can be examined using laser ablation. In order to split material into individual atoms, the samples are introduced into high-energy argon plasma that consists of electrons and positively charged argon ion. Then, this material atom show positive charge. In the hot plasma, most of elements ionize very efficiently (>90%). To allow their identification, the elemental ions must be transferred from 7000K to room temperature and from atmospheric pressure to high vacuum. After that, the ions are extracted through a number of apertures. The process of ICP-MS are demonstrated in Figure 2.24.
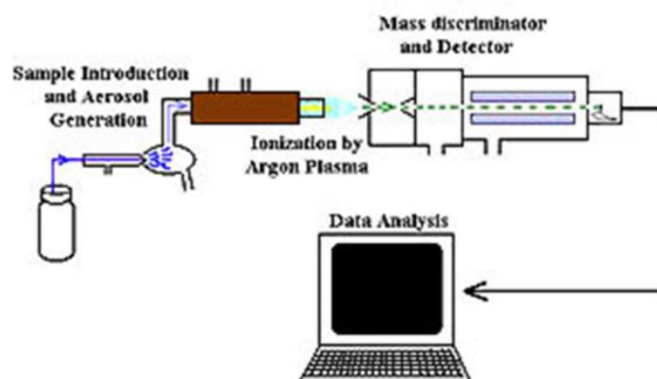
Figure 2.24   The process in ICP-MS [40].

2.2   Evaluation of antioxidant activity

Antioxidant activity of compound is assessed as resistance to oxidation of substance in the presence of that particular compound. The radical scavenging method uses the induction period, percentage inhibition or rates of hydroperoxide formation or decomposition, or IC_{50} value (concentration required to achieve 50% inhibition) based quantification.

DPPH is a well-known radical and a trap ("scavenger") for other radicals. Therefore, rate reduction of a chemical reaction upon addition of DPPH is used as an indicator of the radical nature of that reaction. Because of a strong absorption band centered at about 520 nm, the DPPH radical has a deep violet color in solution, and it becomes colorless or pale yellow when neutralized [41]. This property allows visual monitoring of the reaction, and the number of initial radicals can be counted from the change in the optical absorption at 517 nm and in this way the antioxidative potential of a substance can be determined as shown in Figure 2.25.
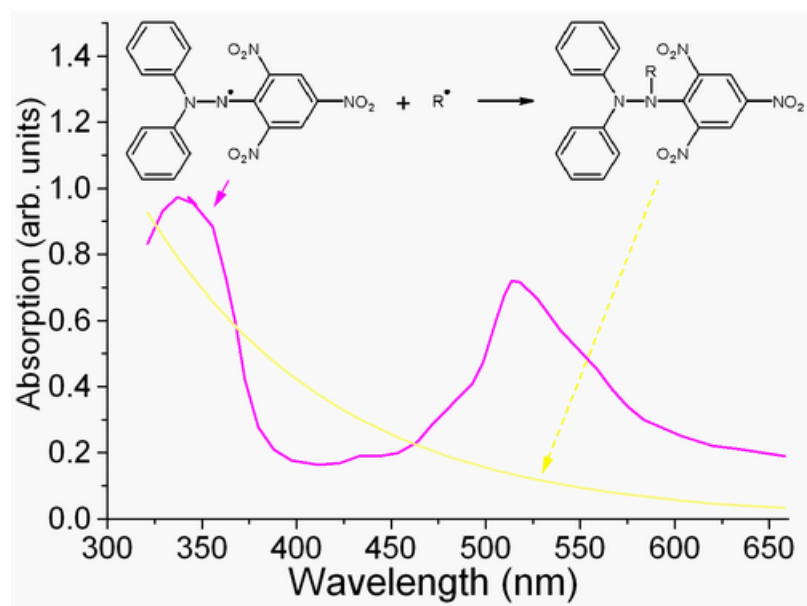
Figure 2.25   Redox reaction with the 2,2-diphenyl-1-picrylhydrazyl radical [41].

CHAPTER III

EXPERIMENTS

3.1 Starting materials

3.1.1 Starting materials for propyl sulfonic acid functionalized SBA-15 (SBA-15-Pr-SO₃H) preparation

1) Triblock copolymer pluronic P123, PEO_{20}-PPO_{70}-PEO_{20}, average molecular weight = 5800 (Aldrich)

2) Tetraethyl orthosilicate, TEOS (Fluka, 98 %)

3) Hydrochloric acid, HCl (Fluka, 37 %)

4) (3-Mercaptopropyl)trimethoxysilane, MPTMS (Aldrich, 95 %)

5) Hydrogen peroxide, H_2O_2 (Merck, 30 %)

6) Toluene, C_7H_8 (CARLO ERBA, 99.5%)

7) Sulfuric acid, H_2SO_4 (Merck, 95-97%)

8) Deionized water

3.1.2 Starting materials for HMCM-22 preparation

1) Fumed silica (Riedel-de Haën, Cab-osil®M-5)

2) Sodium aluminate, $NaAlO_2$ (Riedel-de Haën, reagent grade)

3) Hexamethyleneimine, HMI (Fluka, ≥97.0%)

4) Sodium hydroxide, NaOH (Lab-Scan, ≥99.0%)

5) Ammonium chloride, NH_4Cl (Fluka, reagent grade)

3.1.3 Chemicals for butylation reaction

1) *p*-Cumylphenol, $C_{15}H_{16}O$ (Aldrich, 99%)

2) Bisphenol-A (PTT company)

3) Methyl *tert*-butyl ether, $C_5H_{12}O$ (Merck, ≥99.5%)

4)   *tert*-Butanol, $C_4H_{10}O$ (Fluka, ≥99%)

3.1.4 Chemicals for quantitative analysis

1)   Methanol, CH_4O (Merck, HPLC grade, 99.9%)

3.1.5 Chemicals for antioxidant test

1)   Butylated hydroxytoluene, $C_{15}H_{24}O$ (Merck, 99%)

2)   2,2-diphenyl-1-picrylhydrazyl, $C_{18}H_{12}N_5O_6$ (Aldrich)

3.2 Instruments, apparatus and analytical measurements

3.2.1 Oven and furnace

Crystallization of SBA-15 during the synthesis was carried out at $100^{\circ}C$ for 48 hrs. in static condition using a Memmert UM-500 oven as heater. Moreover, as-synthesized SBA-15 and MCM-22 were dried in this oven at $100^{\circ}C$ for 24 hrs. Organic template was removed from SBA-15 and MCM-22 channels by calcination using a Carbolite RHF 1600 muffle furnace in air. The calcination temperature programs of SBA-15 and MCM-22 were shown in Figure 3.1.
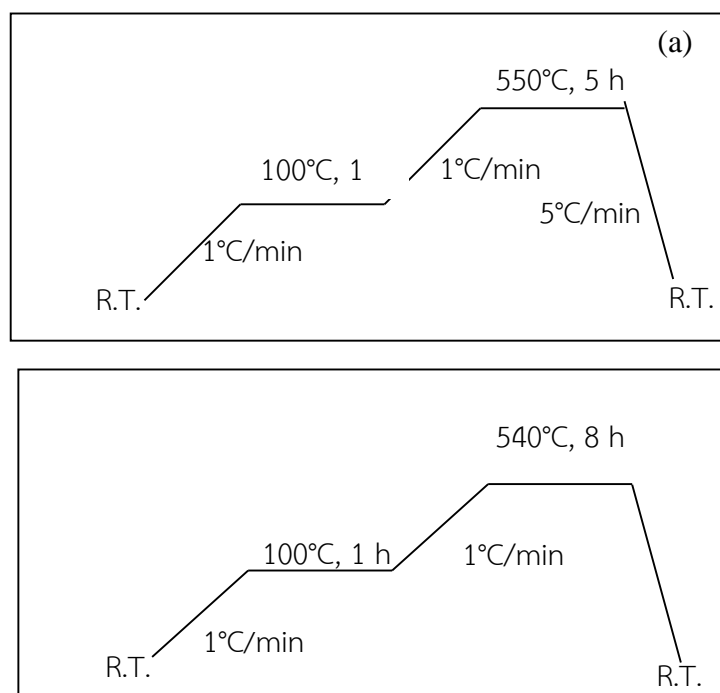
Figure 3.1   The temperature program for the calcination of (a) SBA-15
                   and (b) MCM-22.

3.2.2   X-ray powder diffractometer (XRD)

The XRD patterns of resulting materials were characterized using a Rigaku D/MAX-2200 Ultima$^+$ X-ray diffractometer equipped with Cu target X-ray tube (40 kV, 30mA). The 2-theta angle was ranged from 0.5 to 3.00 degree for SBA-15 and from 2 to 40 degree for MCM-22. The scan speed was used at 1.00 degree/min and sampling width of 0.02 degree. The scattering slit, divergent slit and receiving slit were fixed at 0.5 degree, 0.5 degree, and 0.15 mm, respectively. The measured diffractograms were analyzed using MDI software (Jade 6.5).

3.2.3 Surface area analyzer

Characterization of catalyst porosity in term of N_2 adsorption-desorption isotherms, BET specific surface area, and pore size distribution of the catalysts were measured using a BEL Japan, BELSORP-mini instrument. Before analysis, the calcined sample was weighed about 40 mg that was pretreated 400°C for 2-3 h under vaccum. Adsorption isotherms were measured at 77 K (liquid nitrogen) using highly pure nitrogen as an adsorbate.

3.2.4 Scanning electron microscope (SEM)

The morphology of catalysts was observed with a JEOL JSM-6480 LV scanning electron microscope with 15 kV of acceleration voltage. All materials were coated with spluttering gold under vacuum for conductivity.

3.2.5 ICP-MS spectrometer

Aluminium content in Al-SBA-15, Al-SBA-15-Pr-SO$_3$H and MCM-22 were analyzed by using the Themo Scientific ICAP^{TM} RQ inductively coupled plasma-quadruples mass spectrometer (ICP-QMS).

3.2.6 <u>High-performance</u> liquid chromatography (HPLC) analysis

The reaction mixtures from butylation were analyzed using a 600Waters analytical high-performance liquid chromatography equipped with a 250 mm length ✕ 4.6 mm inner diameter, 5 μm film thickness of ultra C18 capillary column which is a reverse phase column. The detector was a 2996 photodiode array (PDA) at 254 nm. Mobile phase in chromatographic condition was 85% of methanol: 15% of water and flow rate was 0.8 ml/min at 30°C. The sample concentration was prepared in 1 mg of alkylation mixture product in 1 ml of methanol solvent. The analysis sample volume *was* 10 μl. In the later, 1525Waters analytical high-performance liquid chromatography

with 2489 photodiode array (PDA) detector was used to analyze in the same method as a previous description.

3.2.7 Acid-base titration

The acid amount of catalyst was measured using 2M NaCl solution as the ion-exchange agent (Scheme 3.1). Approximately 0.05xx g of the catalysts was added into 15 ml of NaCl solution to equilibrate for 30 min under stirred at room temperature. After that, it was titrated with 0.01 M NaOH as titrant and phenolphthalein as indicator [42].


```
┌─────────────────────────────────────────────────┐
│  ┌───────────────────────────────────────────┐  │
│  │  0.05 g of catalyst + 15 mL of 2M NaCl (aq) │  │
│  └───────────────────────────────────────────┘  │
│                      │                           │
│                 Equilibrate for 30 min           │
│                      ▼                           │
│            ┌────────────────────┐                │
│            │   -SO₃Na + HCl     │                │
│            └────────────────────┘                │
│                      │                           │
│                 Titrate with 0.01M NaOH          │
│                      ▼                           │
│                  (use phenolphthalein as indicator) │
│            ┌────────────────────┐                │
│            │    NaCl + H₂O      │                │
│            └────────────────────┘                │
└─────────────────────────────────────────────────┘
```
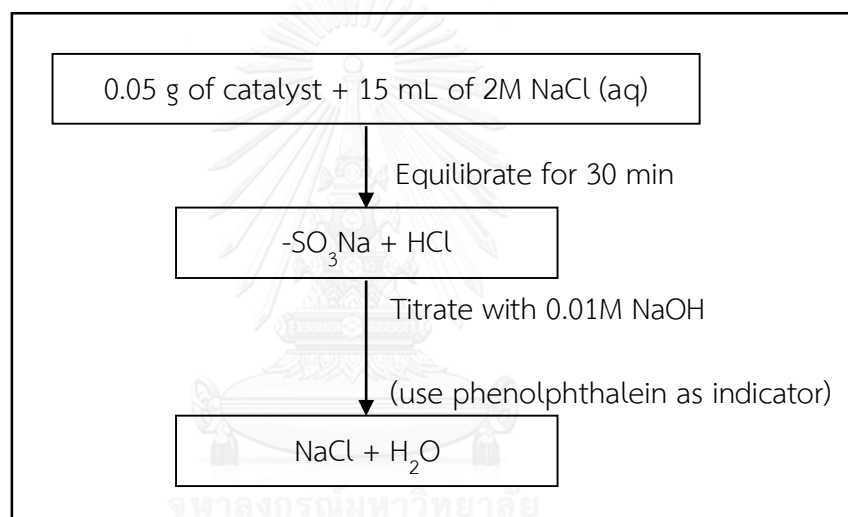
Scheme 3.1   Diagram for acid-base titration.

3.2.8 Parr reactor

The butylation reaction of phenol derivatives (BisphenolA) were performed in 100 ml PARR reactor. The temperature for the reaction are 100 - 120°C

3.3   Catalyst preparation

3.3.1   Synthesis of Al-SBA-15

In this work, mesoporous Si-SBA-15 was incorporated with aluminium *via* post synthesis. Post-synthesized of Al-SBA-15 following Luan *et al.* method [42, 43] was conducted by stirring 0.5 g of calcined SBA-15 in 50 ml of water containing 0.1288 g of $NaAlO_2$ at room temperature for 12 h. The Al-containing mesoporous material was filtered and thoroughly washed with deionized water and then dried at room temperature. After post-treatment, the remained Na^+ ion was removed by ion-exchange with of 0.01M NH_4Cl solution for 24 h. Then material was calcined at 550 °C for 5 h. The solid was designated as Al-SBA-15 at Si/Al mole ratio = 14. The procedure for preparing Al-SBA-15 was shown in Scheme 3.2.
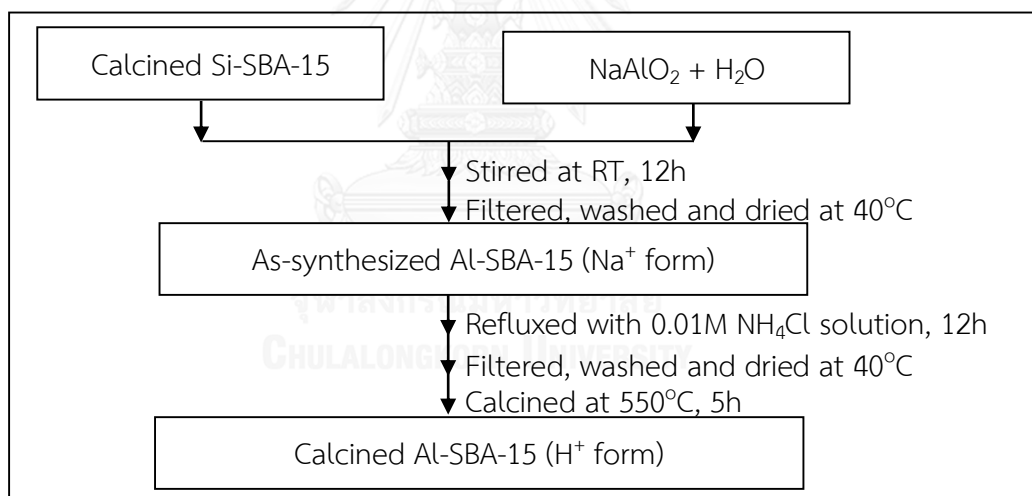
Scheme 3.2   Alumination of Al-SBA-15.

3.3.2 Propyl sulfonic acid functionalized SBA-15 (SBA-15-Pr-SO$_3$H) preparation

3.3.2.1 SBA-15 synthesis by hydrothermal method

SBA-15 synthesis was preformed by hydrothermal method reported by Zhao, D. *et al.* [9]. The gel mole composition of 1.0TEOS: 0.0165 P123: 5.88 HCl: 192 H$_2$O was prepared by dissolving 4.0 g Pluronic P123 as template was dissolved with stirring in 30 g of deonized water and 120 g of 2.0 M HCl solution at room temperature. Subsequently, TEOS was added dropwise and stirred for 60 min. After that, the mixture was aged at 40°C for 8 hrs. with stirring. The resulting gel was transferred to a Teflon-lined autoclave for hydrothermal crystallization at 100°C for 48 hrs. As-synthesized SBA-15 was separated by filtration, washed with deionized water for several times, and overnight drying. The template was removed by calcination at 550°C for 5 hrs. The procedure for synthesizing the SBA-15 was illustrated in Scheme 3.3.

```
┌─────────────────────────────────────────────────────────────┐
│                                                               │
│   ┌───────────────────────────────────────────┐              │
│   │  Template Pluronic P123 + 2.0 M HCl       │              │
│   └───────────────────────────────────────────┘              │
│                        │                                      │
│                        │    -  Stirred until homogeneous solution │
│                        ▼                                      │
│   ┌───────────────────────────────────────────┐              │
│   │  Template solution                        │              │
│   └───────────────────────────────────────────┘              │
│                        │                                      │
│                        │    -  Added TEOS with addition funnel │
│                        │    -  Stirred at room temperature for 60 min │
│                        ▼                                      │
│   ┌───────────────────────────────────────────┐              │
│   │  Gel mixture                              │              │
│   └───────────────────────────────────────────┘              │
│                        │                                      │
│                        │    -  Aged with stirring at 40°C for 24 hrs. │
│                        │    -  Crystallized at 100°C for 48 hrs. │
│                        │    -  Filtered, washed and dried     │
│                        ▼                                      │
│   ┌───────────────────────────────────────────┐              │
│   │  As-synthesized SBA-15                    │              │
│   └───────────────────────────────────────────┘              │
│                        │    -  Calcined at 550°C for 5 hrs.   │
│                        ▼                                      │
│   ┌───────────────────────────────────────────┐              │
│   │  SBA-15                                   │              │
│   └───────────────────────────────────────────┘              │
│                                                               │
└─────────────────────────────────────────────────────────────┘
```
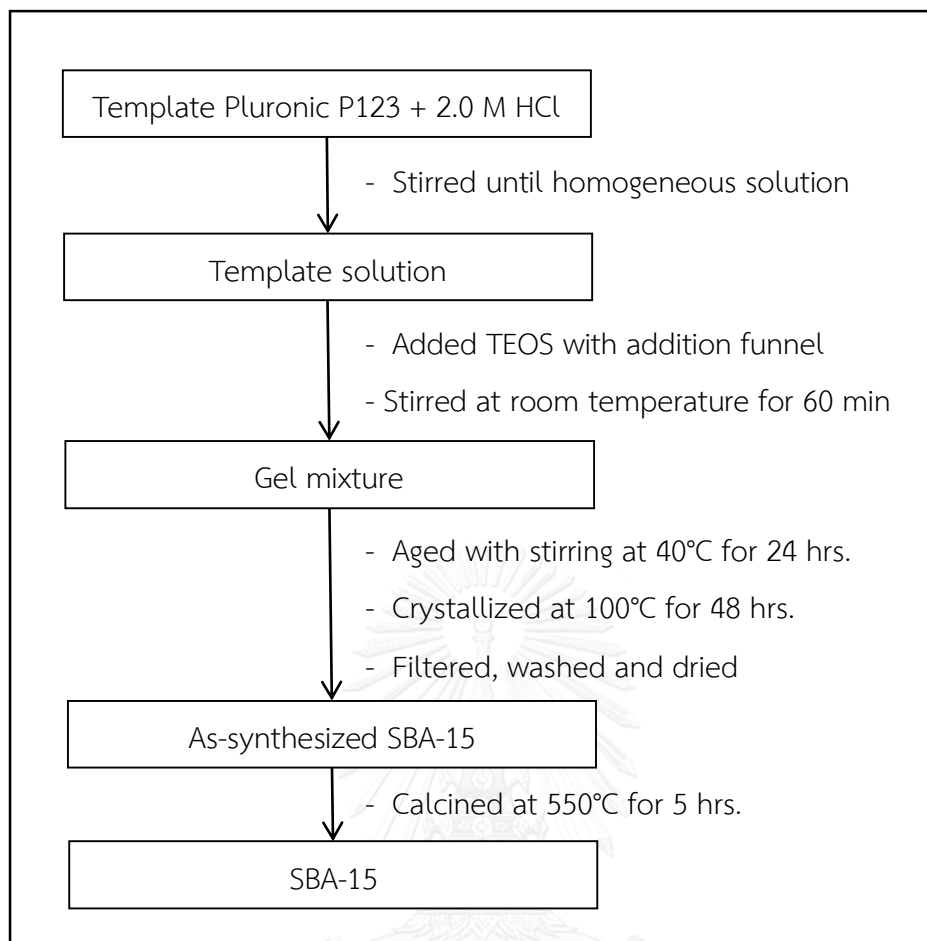
Scheme 3.3   Diagram of SBA-15 synthesis.

3.3.2.2 Addition of propyl sulfonic acid functional group

Three grams of SBA-15 and Al-SBA-15 were suspended with (3-mercaptopropyl)tri-methoxysilane in dry toluene and refluxed at 60°C for 6 hrs. After that, the thiol groups were oxidized to sulfonic acid groups by 30%H_2O_2. The wet material was suspended in 0.2 M H_2SO_4 for 2 hrs [44]. Finally, the functionalized material was filtered and dried in oven for overnight at 60°C.

3.3.3 HMCM-22 preparation

3.3.3.1 Synthesis of MCM-22

The layer MCM-22 (P) precursor was synthesized using hexamethyleneimine (HMI) as the directing agent, fume silica (SiO_2; Cab-osil M-5), sodium aluminate ($NaAlO_2$: 40-45 wt% Na_2O, 50-56 wt% Al_2O_3, 0.05 wt% Fe_2O_3), sodium hydroxide (NaOH) and deionized water. The MCM-22 which contained SiO_2/Al_2O_3 = 30 was prepared in the following way: 37.19 g of HMI was added dropwise to a mixture that comprised 25.04 g of fume silica, 3.53 g of NaOH and 150 g of H_2O under vigorous stirring. A solution of 2.65 g of $NaAlO_2$ in 150 g of water was added dropwise and the mixture was stirred constantly for 1 hr to receive a homogenous gel with a composition of SiO_2 : 0.15 NaO_2 : 0.033 Al_2O_3 : 0.9 HMI : 40 H_2O by mole. The resulting gel was filled into a Teflon line stainless-steel autoclave, rotated at 70 rpm and heated at 140°C for 7 days. The solid outcome was filtered, washed with deionized water until the pH was below 9, and accordingly dried at 80°C overnight to obtain lamellar precursor of MCM-22. The preparation procedure for MCM-22 (P) was shown in scheme 3.4. Then MCM-22 (P) was calcined in air at 540°C for 8 hrs. to remove directing agent and the yield was MCM-22 [14].
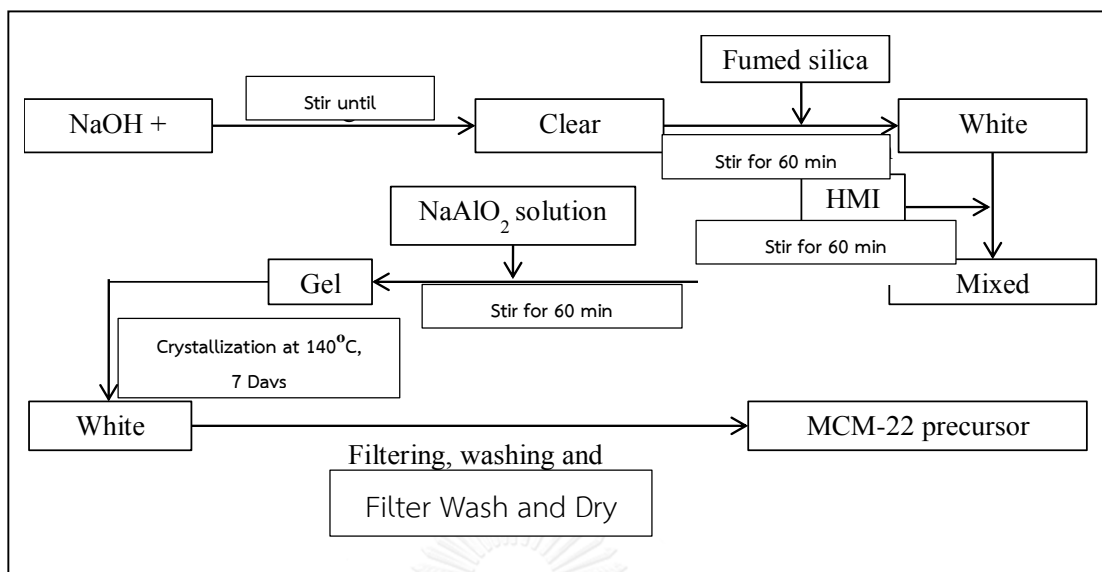
Scheme 3.4   Preparation diagram for MCM-22 precursor.

3.3.3.2 Ion exchange of MCM-22 material

MCM-22 zeolite was changed to H-form by according process: MCM-22 (P) and 1 M NH_4Cl solution (20 ml/g) were loaded in a round bottom flask that connected with air condenser. The suspension was stirred at 80°C for 18 hrs. Next, the mixture was filtered and washed with DI water. The result solid was dried at 80°C overnight. The dried material was once again treated with 1 M NH_4Cl as the same procedure. This cycle was repeated four times to reach the maximum proton exchange capacity. Finally, the exchange material was calcined in air at 540°C for 8 hrs. [15].

3.3.3.3 Addition of propyl sulfonic acid functional group

3 grams of MCM-22 was suspended with (3-mercaptopropyl)tri-methoxysilane in dry toluene and refluxed at 60°C for 6 hrs. After that, the thiol groups were oxidized to sulfonic acid groups by 30%H_2O_2. The wet material was suspended in 0.2 M H_2SO_4 for 2 hrs [44]. Finally, the functionalized material was filtered and dried in oven for overnight at 60°C.

3.4   Procedure in butylated phenol derivatives preparation with continuous flow reactor

The synthesis of mono- and di-butylated *p*-cumylphenol were carried out in a fixed bed continuous stainless steel reactor. The *p*-cumylphenol and butylating agent (MTBE or *t*-butanol) was used with 1:3, 1:5, 1:10 mole ratio and flowed in of pack bed reactor with flow rate of 0.03 ml/min. About 12 grams of Amberlyst-15 catalyst was packed in the reactor that was covered by heating jacket. At termination of reaction time, the reaction mixture was cooled down, collected and analyzed by high-performance liquid chromatography equipped with ultra C_{18} capillary column as show in scheme 3.5.

```
┌─────────────────────────────────────────────────────────────────┐
│                                                                   │
│   ┌──────────────────┐        ┌──────────────────┐               │
│   │  p-Cumyl phenol  │   +    │ Butylating agent │               │
│   │    derivative    │        │                  │               │
│   └──────────────────┘        └──────────────────┘               │
│              │                                                    │
│              │         -   Heated and feed containing a           │
│              │             mixture of p-cumylphenol and           │
│              │             tert-butanol passed into the           │
│              ▼                                                    │
│   ┌──────────────────────┐                                       │
│   │  Reaction mixture    │                                       │
│   │ (Collected every 2 hrs.)│                                    │
│   └──────────────────────┘                                       │
│              │          -   Sampling   1   mg   of               │
│              │              reaction mixture                      │
│              ▼          -   Added 1 ml of                         │
│   ┌──────────────────┐       methanol as a solvent               │
│   │  HPLC analysis   │       and vigorously shook                 │
│   └──────────────────┘                                           │
│                                                                   │
└─────────────────────────────────────────────────────────────────┘
```
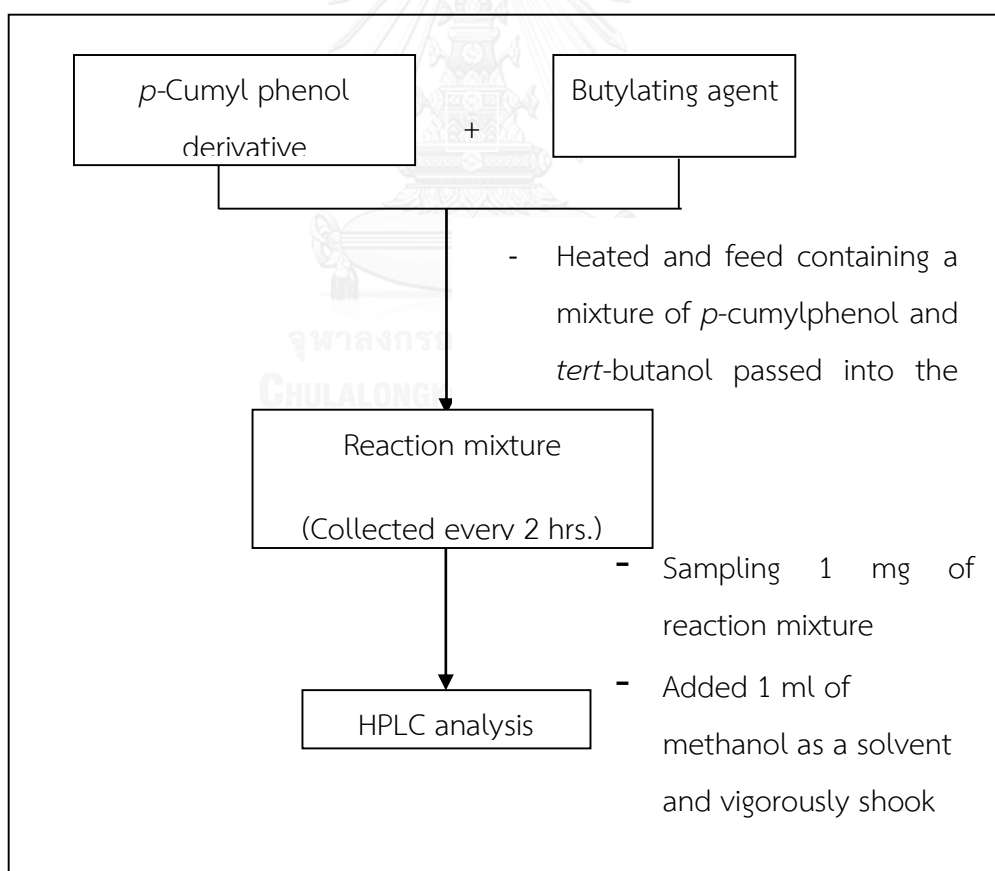
Scheme 3.5   Diagram for butylated phenol derivative preparation and analysis in continuous flow reactor.

3.5 Parameters affecting butylated phenol derivatives preparation with continuous flow reactor

3.5.1 Effect of butylating agent type

Butylation of *p*-cumylphenol over Amberlyst-15 catalyst was carried out using MTBE and *tert*-butanol as butylating agent.

3.5.2 Effect of reaction temperature

The reaction temperature was varied in the range of 90°C - 110°C.

3.5.3 Effect of phenol derivative to butylating agent mole ratio

The mole ratio of phenol derivative to butylating agent was changed from 1: 3- 1: 10.

3.6 Procedure in butylated phenol derivatives preparation with batch reactor

The catalytic efficiency was investigated in BisphenolA alkylation with butylating agent. Before the reaction, the catalysts were heated overnight at 70°C. BisphenolA alkylation was carried out in autoclave reactor which received from Parr instrument company. The total weight of phenol derivative (Bisphenol-A) and butylating agent (MTBE or *tert*-butanol) was used constantly at ten grams and added to the *batch reactor* with the agitation speed of 200 rpm. Percentage of catalyst was calculated base on weight of phenol derivative. At termination of reaction time, the reaction mixture was cooled down and separated from spent catalyst by centrifugation. The reaction mixture was collected and analyzed by high-performance liquid chromatography equipped with ultra C_{18} capillary column as shown in scheme 3.6.
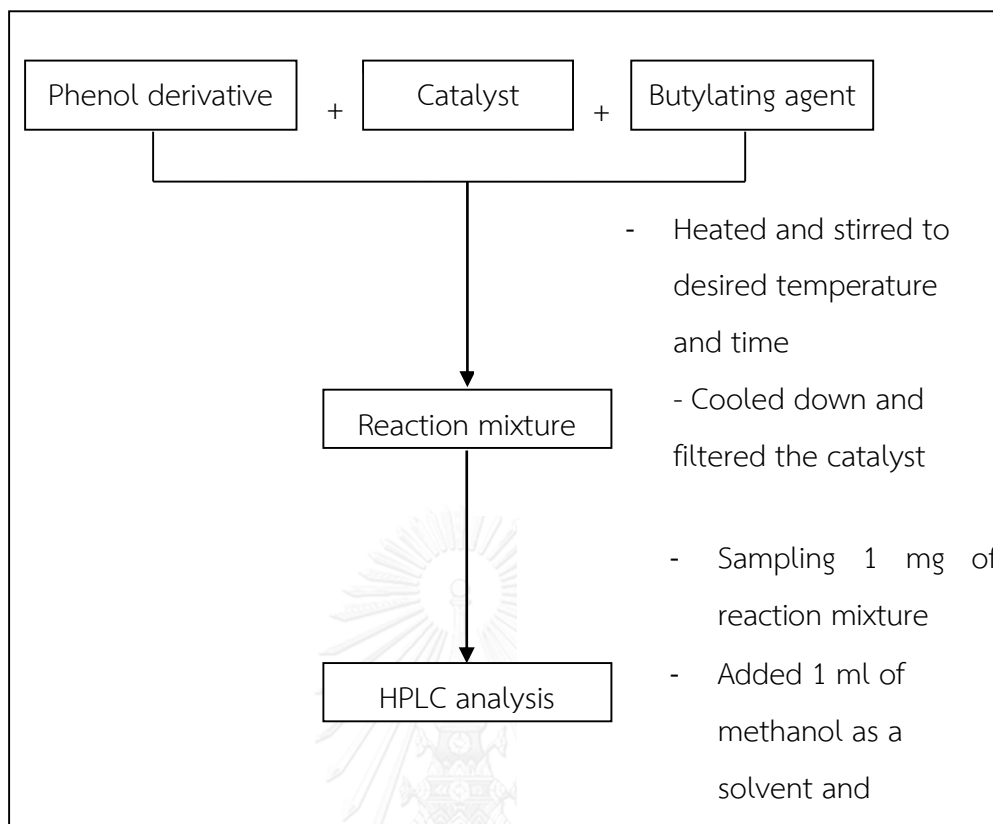
Scheme 3.6   Diagram for butylated phenol derivative preparation and analysis.

3.7   Parameters affecting butylated phenol derivatives preparation with batch reactor

3.7.1   Effect of butylating agent type

Butylation of Bisphenol-A over Amberlyst-15 catalyst was carried out using MTBE and *tert*-butanol as butylating agent.

3.7.2   Effect of catalytic type

Catalytic activities of SBA-15-Pr-SO$_3$H and HMCM-22 were compared with HZSM-5, HBeta, treated bentonite, MCA-Pr-SO$_3$H, MCM-22-Pr-SO$_3$H, Al-SBA-15, Al-SBA-15 Pr-SO$_3$H and commercial catalysts such as Amberlyst-15.

3.7.3 Effect of reaction temperature

The reaction temperature was varied in the range of 100°C - 120°C.

3.7.4 Effect of phenol derivative to butylating agent mole ratio

The mole ratio of phenol derivative to butylating agent was changed from 1: 5-1: 20.

3.7.5 Effect of catalytic amount

The catalytic loading was varied from 0 to 20 wt% based on weight of phenol derivative reactant.

3.7.6 Effect of reaction time

The reaction time was differed in the range 2 hrs. - 10 hrs.

3.8 Antioxidant activity

p-Cumylphenol, Bisphenol-A, purified butylated products and reaction mixture from butylation reaction were examined for antioxidant activity by using UV-visible method. This method was used to estimate half maximal inhibitory concentration (IC_{50}) value of them.

3.8.1 Antioxidant test by UV-visible method

The radical scavenging activity of the butylated phenol derivatives against 2,2-diphenyl-1-picrylhydrazyl radical was determined by measuring UV absorbance at 517 nm by Sunrise™ microplate reader. Butylated hydroxytoluene (BHT) was used as standard for comparison. All evaporated samples and standard were prepared with methanol in the following concentrations, 1 ppm, 0.5 ppm, 0.25 ppm, 0.125 ppm and 0.0625 ppm. The 50 μl of each prepared concentrations and blank were placed into microplate. Then 250 μl of DPPH solution (11.8 mg in 100 ml of methanol) was added to all of them and incubated for 30 min and the absorbance was read [45].

The radical scavenging percentage was calculated using the following formula:

$$\% \text{ radical scavenging} = \left(\frac{A_{\text{blank}} - A_{\text{sample}}}{A_{\text{blank}}} \right) \times 100$$

Where A_{blank} = absorbance of DPPH radical without the sample

A_{sample} = absorbbance of DPPH radical and added of sample

The calculated % radical scavenging relative with concentration was plotted to compute concentration at 50% radical scavenging or half maximal inhibitory concentration (IC_{50} value) as seen in Figure 3.2.
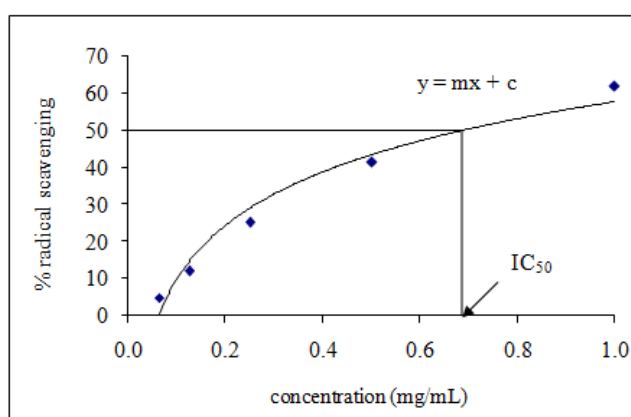
Figure 3.2   Curve of concentration versus % radical scavenging of inhibitor.

CHAPTER IV
RESULTS AND DISCUSSION

4.1 Catalytic activities of Amberlyst-15 in butylated *p*-cumylphenol preparation in continuous flow reactor

In this study, *p*-cumylphenol butylation reaction employed a variety of liquid butylating agent, such as methyl *tert*-butyl ether (MTBE) and *tert*-butanol, to compare efficiency for 2,6-di-*tert*-butyl *p*-cumylphenol (2,6-DTCP) preparation. The optimum reaction condition over Amberlyst-15 for 2,6-DTCP synthesis was investigated with various reaction parameters (reaction temperature and *p*-cumylphenol to butylating agent mole ratio).

4.1.1 Butylated *p*-cumylphenol preparation from *p*-cumylphenol with MTBE

| *p*-cumylphenol | MTBE | 2-*tert*-butyl *p*-cumylphenol (2-TCP) | 2,6-di-*tert*-butyl *p*-cumylphenol (2,6-DTCP) |
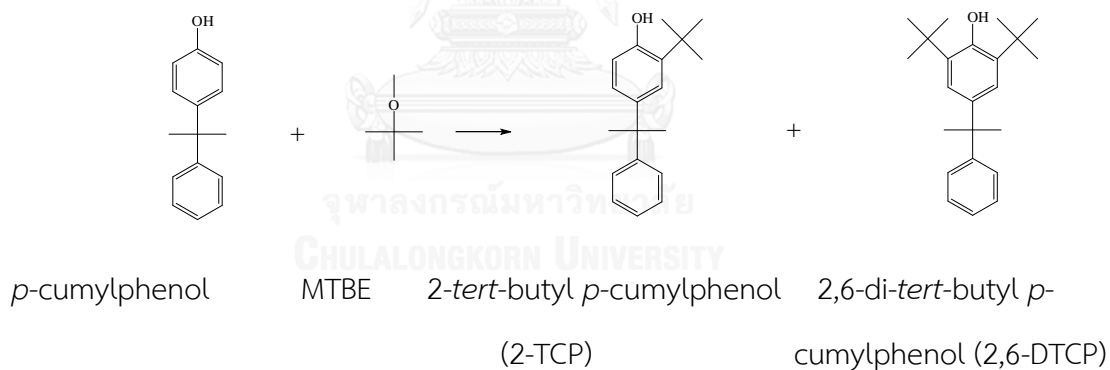
4.1.1.1 Effect of reaction temperature

Catalytic performance of Amberlyst-15 was studied with the reaction temperature range between 90°C - 110°C in *p*-cumylphenol butylation. The *p*-cumylphenol conversion, butylated product yields and 2,6-DTCP selectivity were shown in Table 4.1. When increasing reaction temperature from 90°C to 100°C, the butylated product yields were rapidly increased. On the other hand, a further reaction temperature rising from 100°C to 110°C caused the by-products to increase with conversion enhancing. The *p*-cumylphenol could be decomposed in the presence of acid at high temperature [46] that was the reason for large *p*-cumylphenol conversion but low desired product yield was obtained.

Table 4.1   Effect of reaction temperature in continuous flow reactor with MTBE

Temperature ($^{\circ}$C)	Time (hrs)	%conversion	Butylated product yield (%)	
			2-TCP	2,6-DTCP
90	26	98.60	59.00	20.08
100	26	98.39	70.20	28.19
110	26	98.39	71.35	28.65

N Reaction condition CP:MTBE= 1:5, using Amberlyst-15 as a catalyst, flow rate: 0.03ml/min, HPLC pump, total feed 100 ml, LHSV = 0.02 h^{-1}.
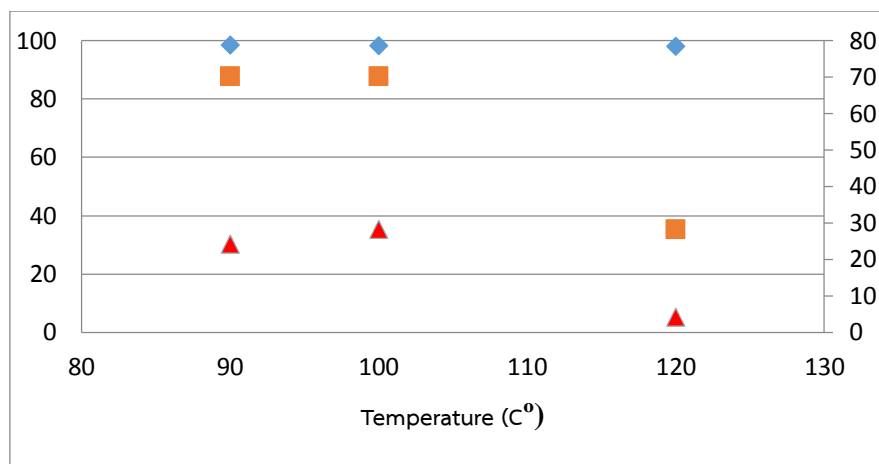
Figure 4.1   Influence of temperature on the butylated products yield over

Amberlyst-15(Butylation condition: reaction temperature 100°C; flow

rate = 0.03 ml/m and reaction time 26 hrs. (Symbols: (◆) *p*-

cumylphenol conversion, (■) 2-TCP yield and (▲) 2,6-DTCP.

4.1.1.2 Effect of *p*-cumylphenol to MTBE mole ratio

The result of *p*-cumylphenol to MTBE as 1:5 by mole showed the highest *p*-cumylphenol conversion (98.39%) and 2,6-DTCP yield (28.19%), as seen in Table 4.2. Additionally, the butylation using very low MTBE amount, 1: 3 by mole, gave high *p*-cumylphenol conversion (98.20%) close to the result at 1:5 mole ratio but it demonstrated deficiency of 2,6-DTCP selectivity and large number of other products were formed. Moreover, the conversions at other mole ratios (1:3 to 1:10) were decreased with mole ratio increasing because the excess amount of MTBE was consumed in other reactions. Scheme 4.1 showed the oligomerization of isobutylene could be formed as side reaction of MTBE that was depended on reaction condition; mole ratio, temperature and catalytic amount [47].

Table 4.2   Effect of mole ratio in continuous flow reactor with MTBE

CP : MTBE mole ratio	Time (hrs)	%conversion	Butylated product yield (%)	
			2-TCP	2,6-DTCP
1 : 3	26	98.20	78.35	19.85
1 : 5	26	98.39	70.20	28.19
1 : 10	26	98.52	33.59	22.01

Reaction condition Amberlyst-15 as a catalyst, 100ºC, flow rate: 0.03ml/min, HPLC pump, total feed 100 ml, LHSV = 0.02 h^{-1}.
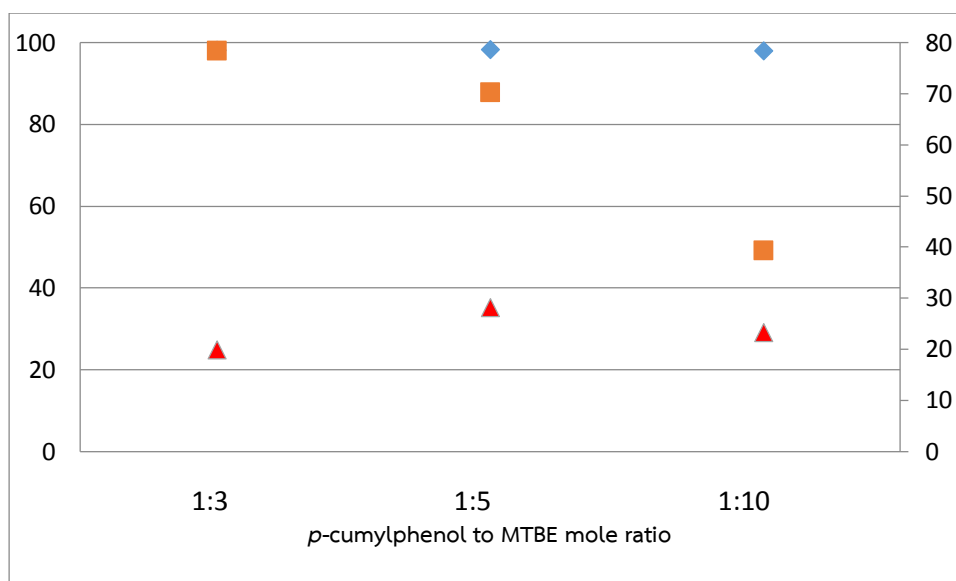
Figure 4.1   Influence of mole ratio on the butylated products yield over

Amberlyst-15

(Butylation condition: reaction temperature 100°C; flow rate = 0.03

ml/m and reaction time 26 hrs. (Symbols: (◆) *p*-cumylphenol

conversion, (■) 2-TCP yield and (▲) 2,6-DTCP.
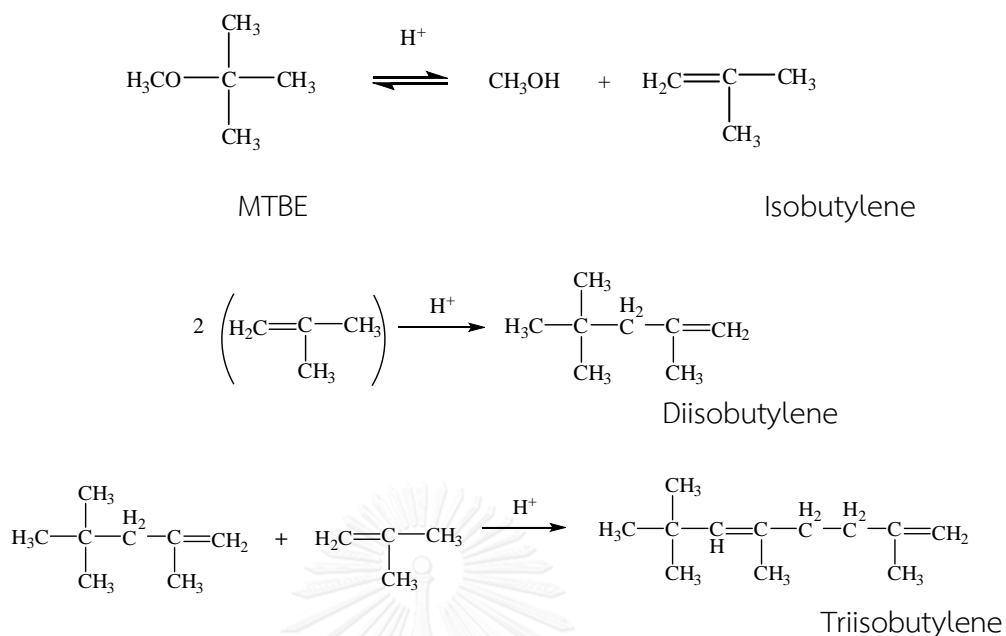
Scheme 4.1   Parallel reactions of MTBE.

4.1.2   Butylated *p*-cumylphenol preparation from *p*-cumylphenol with *tert*-butanol

p-cumylphenol   *tert*-butanol   2-*tert*-butyl *p*-cumylphenol   2,6-di-*tert*-butyl *p*-

(2-TCP)   cumylphenol (2,6-DTCP)
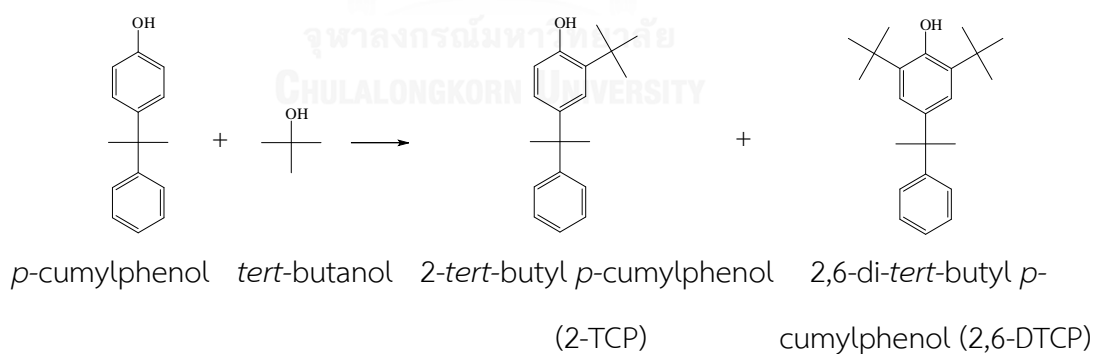
4.1.2.1 Effect of reaction temperature

To determine the effect of reaction temperature, the experiments were conducted at temperature ranging from 90℃ to 110℃. The results were shown in Table 4.3. The *p*-cumylphenol conversion and other products were increased with reaction temperature rising. The effect of temperature was studied by

carrying out the reaction at different temperatures, keeping the feed composition and space velocity constant. When increasing reaction temperature from 90 to 110°C the *p*-cumylphenol conversion and the product composition were changed with variation in reaction temperature % yield of 2,6-DTCP were increased. The suitable temperature should be 100°C because this condition gave di-butylated product higher than other conditions.

Table 4.3   Effect of reaction temperature in continuous flow with t-butanol

Temperature (°C)	Time (hrs)	%conversion	Butylated product yield (%)	
			2-TCP	2,6-DTCP
90	44	68.20	60.69	0.00
100	44	94.05	75.37	18.67
110	44	97.77	81.58	3.89

Reaction condition CP:*t*-BuOH= 1:5, using Amberlyst-15 as a catalyst, flow rate: 0.03ml/min, HPLC pump, total feed 100 ml, LHSV = 0.02 h^{-1}.
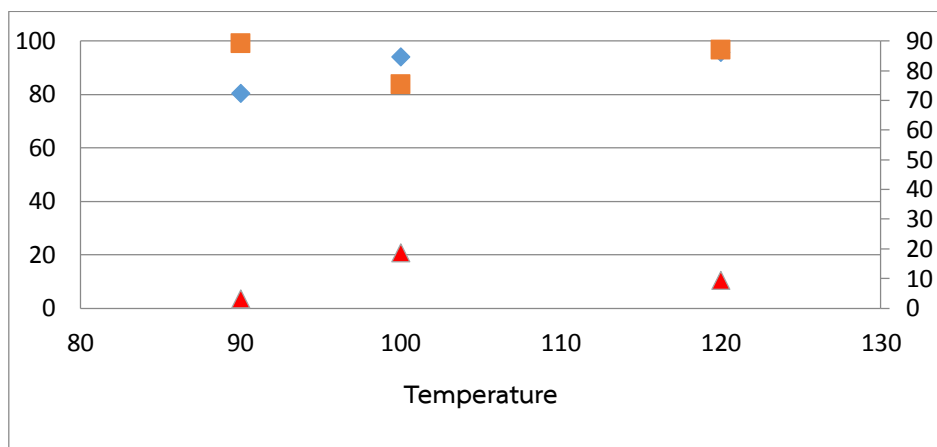
Figure 4.1   Influence of temperature on the butylated products yield over

Amberlyst-15(Butylation condition: reaction temperature 100°C; flow

rate = 0.03 ml/m and reaction time 44 hrs. (Symbols: (◆) *p*-

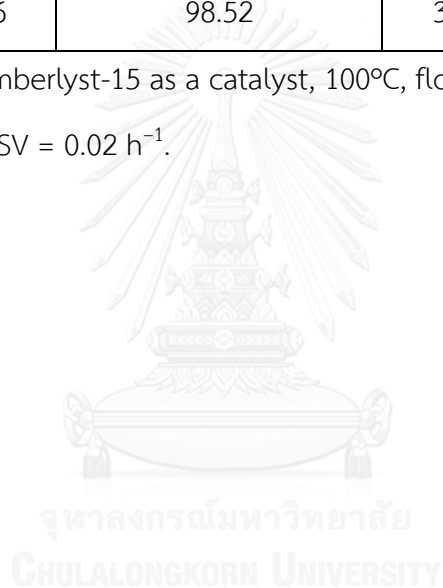cumylphenol conversion, (■) 2-TCP yield and (▲) 2,6-DTCP.

4.1.2.2 Effect of *p*-cumylphenol to tert-butanol mole ratio

The effect of *p*-cumylphenol to *tert*-butanol mole ratio on conversion

and butylated product yield over Amberlyst-15 was differed in the range of 1:3 to 1:

10 and the results were shown in Table 4.4. From the Table 4.4, the other products

were decreased with amount of *tert*-butanol increasing from 1:3 to 1:5. The conversion

and butylated product yield of 2,6-DTCP were increased when *p*-cumyl phenol to *tert*-

butanol mole ratio was raised from 1:3 to 1:5 at reaction temperature 100°C. A further

increased in mole ratio from 1:5 to 1:10 showed decreasing of conversion and

butylated product yields which may be caused by the parallel reaction of *tert*-butanol

and led to the formation of its side product as showed in Scheme 4.2.

Table 4.4   Effect of mole ratio in continuous flow with t-butanol

CP:*t*-BuOH mole ratio	Time (hrs)	%conversion	Butylated product yield (%)	
			2-TCP	2,6-DTCP
1 : 3	44	63.19	6.45	0.0
1 : 5	44	94.05	75.37	18.67
1 : 10	44	97.53	85.10	12.42

Reaction condition Amberlyst-15 as a catalyst, 100ºC, flow rate: 0.03ml/min, HPLC

pump, total feed 100 ml, LHSV = 0.02 h^{-1}.
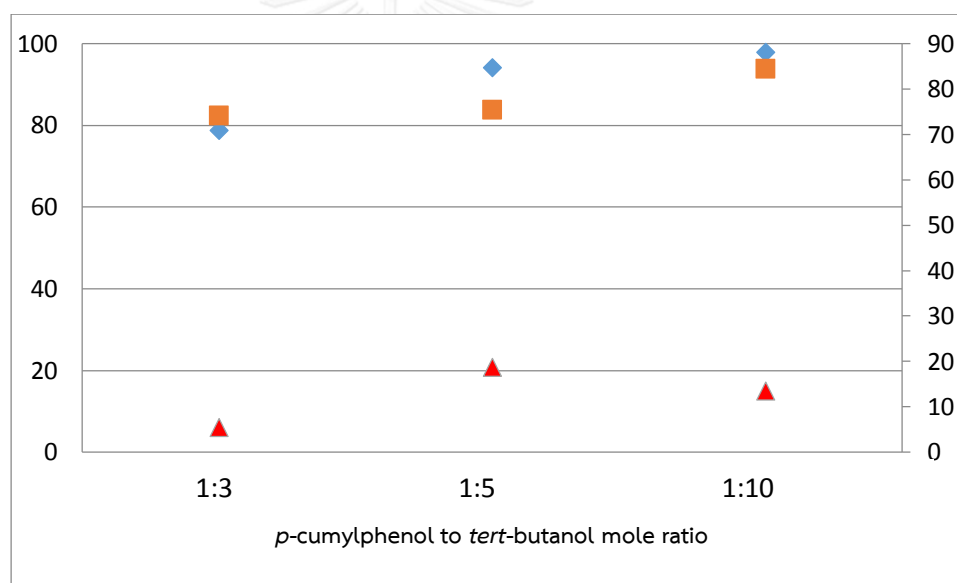
Figure 4.1   Influence of mole ratio on the butylated products yield over

Amberlyst-15

(Butylation condition: reaction temperature 100°C; flow rate = 0.03

ml/m and reaction time 44 hrs. (Symbols: (♦) *p*-cumylphenol

conversion, (■) 2-TCP yield and (▲) 2,6-DTCP.
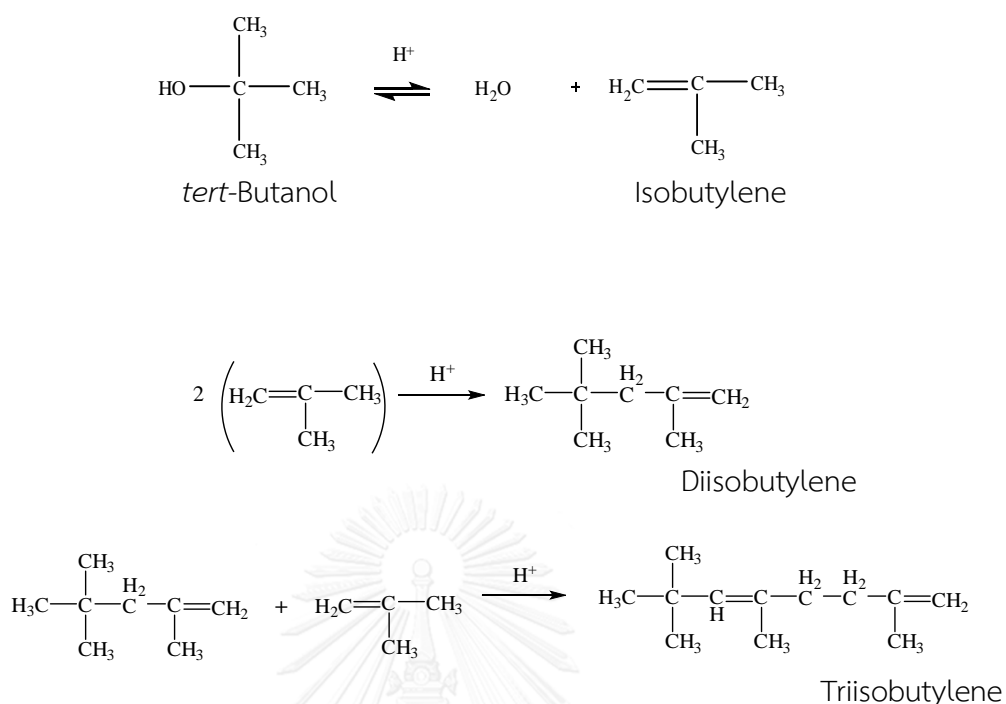
**Scheme 4.2**   Parallel reactions of tert-butanol.

4.2   Catalytic activities of Amberlyst-15 in butylated Bisphenol A preparation in batch reactor

In this study, BisphenolA butylation reaction employed a variety of liquid butylating agent, such as methyl *tert*-butyl ether (MTBE) and *tert*-butanol, to compare efficiency for butylated phenol preparation. The optimum reaction condition over Amberlyst-15 for butylated phenol derivatives synthesis was investigated with various reaction parameters (catalyst type, reaction temperature, BisphenolA to butylating agent mole ratio, catalytic amount and reaction time).

4.2.1   Butylated BisphenolA preparation from BisphenolA with MTBE
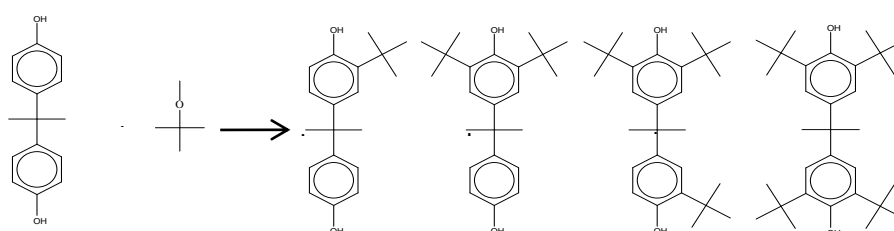
BisphenolA   MTBE   1   2   3   4

1.) 2-tert-butyl-4-(2-(4-hydroxyphenyl)propan-2-yl)phenol : 2-TBP

2.) 2,6-di-tert-butyl-4-(2-(4-hydroxyphenyl)propan-2-yl)phenol : 2,6-DTBP

3.) 2,6-di-tert-butyl-4-(2-(3-tert-butyl-4-hydroxyphenyl)propan-2-yl)phenol :
    2,6-DTBPP

4.) 4,4'-(propane-2,2-diyl)bis(2,6-di-tert-butylphenol) : 4,4-B-2,6-DTBP

4.2.1.1 Effect of reaction temperature

Catalytic performance of Amberlyst-15 was studied with the reaction temperature range between 100°C - 120°C in BisphenolA butylation. The BisphenolA conversion, butylated product yields were shown in Table 4.5. The temperature at 120°C gave the highest yield of product (42.6%) and the selectivity of 2-TCP and 2.6-DTCP as 24.8, 7.5, respectively.

Table 4.5   Effect of reaction temperature on conversion and product distribution over Amberlyst-15 in batch reactor with MTBE

Temperature ($^{\circ}$C)	Conversion (%)	Selectivity (%)				Total yield of product %
		2-TCP	2,6-DTCP	2,6-DTBPP	4,4-B-2,6-DTBP	
100	89.5	15.9	5.3	0.0	0.0	23.1
110	96.2	19.2	6.5	3.7	6.4	37.2
120	96.1	24.8	7.5	3.3	5.1	42.6

Butylation condition: BisphenolA/MTBE mole ratio as 1:10; catalytic amount 15 wt% base on BisphenolA; reaction time 8 hrs. and stirring speed 200 rpm. (SD ± 1)

4.2.1.2 Effect of BisphenolA to MTBE mole ratio

The result of BisphenolA to MTBE as 1:10 by mole showed the highest BisphenolA conversion (96.2%), as seen in Table 4.6. Additionally, the butylation using very high MTBE amount, 1: 15 by mole, gave high total yield of product than the other but it demonstrated deficiency of 2,6-DTBPP and 4,4-B-2,6-DTBP selectivity. This result showed that mole ratio at 1:10 was an optimum condition.

Table 4.6   Effect of mole ratio on conversion and product distribution over Amberlyst-15 in batch reactor with MTBE

Mole ratio (BisphenolA : MTBE)	Conversion (%)	Selectivity (%)				Total yield of product %
		2-TCP	2,6-DTCP	2,6-DTBPP	4,4-B-2,6-DTBP	
1:5	95.3	15.1	6.1	2.7	4.4	29.7
1:10	96.2	24.9	7.5	3.3	5.3	42.6
1:15	88.5	37.8	2.0	0.0	0.0	44.9

Butylation condition: reaction temperature 120°C; catalytic amount 15 wt% base on BisphenolA; reaction time 8 hrs. and stirring speed 200 rpm. (SD ± 1)

4.2.1.3 Effect of catalytic amount

In order to investigate the effect of catalytic amount, 0 - 20 wt% of Amberlyst-15 was used in butylation of BisphenolA with MTBE. From the Table 4.7, non-catalyst (0 wt%) reaction showed negligible conversion and BisphenolA conversion

was enhanced with increasing amount of catalyst. It can be observed that the yield of product was increased by raising the catalyst amount from 5 to 15 wt%. This result was expected because catalyst loading increment was proportional to availability of active site. Whereas, the lower yield was surprisingly obtained when the catalyst amount was increased from15 to 20 wt%. The reason might be the slurry was formed and caused mixing problem. This result showed that catalytic amount at 15 wt% was an optimal catalytic loading that gave the highest yied of product (42.6%) and conversion (96.2).

Table 4.7 Effect of catalytic amount on conversion and product distribution over *Amberlyst-15 in batch rector with MTBE*

| Catalytic amount (wt%) | Conversion (%) | Selectivity (%) | | | | Total yield of product % |
		2-TCP	2,6-DTCP	2,6-DTBP	4,4-B-2,6-DTBP	
0	3.4	0.0	0.0	0.0	0.0	0.0
5	95.0	17.8	2.3	0.0	0.0	21.2
10	94.9	13.7	3.4	1.4	4.2	24.0
15	96.2	24.8	7.4	3.3	5.3	42.6
20	95.3	19.3	5.9	4.00	2.3	32.9

Butylation condition: reaction temperature 120°C; BisphenolA/MTBE mole ratio as 1:10; reaction time 8 hrs. and stirring speed 200 rpm. (SD ± 1)

4.2.1.4 Effect of reaction time

The influence of reaction time on butylation of BisphenolA was investigated in the range of 2 hrs. - 10 hrs. and the results were shown in Table 4.8.

The reaction time was 8 hrs gave highest conversion as 96.2%. In addition, this time also exhibited the highest 24.9% of selectivity when compare with the other reaction time.

Table 4.8   Effect of reaction time on conversion and product distribution over Amberlyst-15 in batch reactor with MTBE

Time (hrs.)	Conversion (%)	Selectivity (%)				Total yield of product %
		2-TCP	2-TCP	2,6-DTBPP	4,4-B-2,6-DTBP	
2	92.3	11.2	2.7	0.0	0.0	15.1
4	93.7	19.1	5.2	0.0	0.0	25.9
6	94.8	17.2	3.5	0.0	0.0	21.8
8	96.2	24.9	7.5	3.3	5.3	42.6
10	94.6	16.2	4.1	2.9	5.3	30.1

Butylation condition: reaction temperature 120°C; BisphenolA/MTBE mole ratio as 1:10; catalytic amount 15 wt% base on BisphenolA and stirring speed 200 rpm.   (SD ± 1)

For MBTE reaction, the optimum condition gave 96.2% conversion, 24.9% yield of 2-TCP and 42.6% toatal yield of product that was carried out with

BisphenolA to MTBE mole ratio as 1:10, 15 wt% of Amberlyst-15 based on BisphenolA at 120°C for 8 hrs.

4.2.2 Butylated *p*-cumylphenol preparation from *p*-cumylphenol with *tert*-butanol
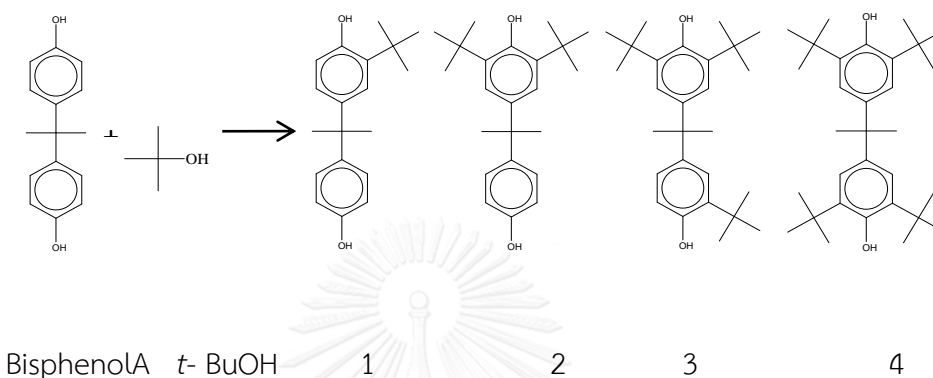
BisphenolA   *t*- BuOH   1   2   3   4

1.) 2-tert-butyl-4-(2-(4-hydroxyphenyl)propan-2-yl)phenol : 2-TBP

2.) 2,6-di-tert-butyl-4-(2-(4-hydroxyphenyl)propan-2-yl)phenol : 2,6-DTBP

3.) 2,6-di-tert-butyl-4-(2-(3-tert-butyl-4-hydroxyphenyl)propan-2-yl)phenol : 2,6-DTBPP

4.) 4,4'-(propane-2,2-diyl)bis(2,6-di-tert-butylphenol) : 4,4-B-2,6-DTBP

4.2.2.1 Effect of reaction temperature

The impact of the reaction temperature on yield and selectivity of the butylated product was investigated at various temperature from 100-120°C. From Table 4.9, when the temperature was increased from 100 up to 120°C the conversion and total yield of product increased and reached the maximum to 97.7% and 45.1% respectively. At the same, selectivity of 2-TCP gave the highest of butylated products.

Table 4.9   Effect of reaction temperature on conversion and product distribution over Amberlyst-15 in batch reactor with tert-butanol

Temperature (°C)	Conversion (%)	Selectivity (%)				Total yield of product %
		2-TCP	2,6-DTCP	2,6-DTBPP	4,4-B-2,6-DTBP	
100	69.5	2.9	0.0	0.0	0.0	4.2
110	88.8	9.1	1.6	0.0	0.0	12.1
120	97.7	17.8	10.0	6.0	10.2	45.1

Butylation condition: BisphenolA /*tert*-butanol mole ratio as 1:15; catalytic amount 10 wt% base on BisphenolA; reaction time 8 hrs. and stirring speed 200 rpm. (SD ± 1)

4.2.2.2 Effect of p-cumylphenol to tert-butanol mole ratio

The effect of BisphenolA to *tert*-butanol mole ratio was investigated in the range of 1:5 to 1: 20 and shown in Table 4.10. When the amount of *tert*-butanol increased from 1:5 to 1:15, the conversion was enhanced and attained 97.7% as like the total yield of products attained to a maximum value 45.1%. On the other hand, when the mole ratio was further increase to 1:20, there was a significant change in the rate of reaction, the total yield of product was lower (43.1%) than that of 1:15 mole ratio. This effect may be caused by the consumption of butylating agent by side reaction of excess *tert*-butanol. That include high volume of isobutylene and subsequency to produce di-isobutylene and tri-isobutylene [48], respectively.

Table 4.10   Effect of mole ratio on conversion and product distribution over Amberlyst-15 in batch reactor with tert-butanol

Mole ratio (BisphenolA : *tert*-butanol)	Conversion (%)	Selectivity (%)				Total yield of product %
		2-TCP	2,6-DTCP	2,6-DTBPP	4,4-B-2,6-DTBP	
1:5	86.4	10.8	5.1	1.4	2.0	22.4
1:10	96.9	17.8	7.3	3.9	8.4	38.6
1:15	97.7	17.8	10.0	6.0	10.2	45.1
1:20	84.5	14.7	7.9	5.0	9.0	43.4

Butylation condition: reaction temperature 120°C; catalytic amount 15 wt% base on BisphenolA; reaction time 8 hrs. and stirring speed 200 rpm. (SD ± 1)

4.2.2.3 Effect of catalytic amount

The effect of catalytic amount on the reaction was studied by varying from 0 to 20 wt% of the reactant as shown in Table 4.11. With increase in catalytic amount up to 10 wt%, the conversion and yield of products increased. The greatest yield of product (45.1%) was obtained at the catalytic loading of 10 wt%. At 10 to20 wt%, the conversion and yield of products decreased. The acid catalyst was important to induce the *tert*-butyl cabocation intermediate of butylation. However, the catalyst overloading might be impeded the phase mixing of BisphenolA and *tert*- butanol.

Table 4.11 Effect of catalytic amount on conversion and product distribution over Amberlyst-15 in batch reactor with tert-butanol

Catalytic amount (wt%)	Conversion (%)	Selectivity (%)				Total yield of product %
		2-TCP	2,6-DTCP	2,6-DTBPP	4,4-B-2,6-DTBP	
0	14.4	0.0	0.0	0.0	0.0	0.0
5	80.6	0.0	0.0	0.0	0.0	0.0
10	97.7	17.8	10.0	6.0	10.2	45.1
15	88.4	10.7	6.2	5.8	3.1	29.2
20	77.7	10.9	9.9	1.9	3.4	33.6

Butylation condition: reaction temperature 120°C; *p*-cumylphenol/*tert*-butanol mole ratio as 1:15; reaction time 8 hrs. and stirring speed 200 rpm. (SD ± 1)

4.2.2.4 Effect of reaction time

The influence of reaction time on butylation was shown in Table 4.12. The conversion and butylated products yield were enchanced with increasing reaction time from 2 hrs to 10hrs. On the other hand, when the reaction was continued to 10 hrs., the conversion and yield of product were gradually decreased. It could be explained by de-alkylation or elimination of butyl group. Therefore, the suitable reaction time was concluded at 8 hrs.

Table 4.12 Effect of reaction time on conversion and product distribution over Amberlyst-15 in batch reactor with tert-butanol

Time (hrs.)	Conversion (%)	Selectivity (%)				Total yield of product %
		2-TCP	2,6-DTCP	2,6-DTBPP	4,4-B-2,6-DTBP	
2	76.2	2.3	0.0	0.0	0.0	3.0
4	72.8	6.4	1.1	0.0	0.0	8.8
6	77.6	17.4	2.7	0.0	0.0	20.9
8	97.7	13.5	10.0	6.0	10.2	45.1
10	92.2	9.3	7.7	2.3	7.8	29.4

Butylation condition: reaction temperature 120°C; BisphenolA/*tert*-butanol mole ratio as 1:15; catalytic amount 10 wt% base on BisphenolA and stirring speed 200 rpm. (SD ± 1)

For *tert*-butanol reaction, the optimum condition gave 97.7% conversion and 45.1% total yield of product that was carried out with BisphenolA to *tert*-butanol mole ratio as 1:15, 10 wt% of Amberlyst-15 based on BisphenolA at 120°C for 8 hrs.

4.3 Screening of catalysts in *p*-cumylphenol butylation

The optimum condition of BisphenolA butylation with MTBE gave 96.2% conversion and 41.0% total of yield product that was proceeded with BisphenolA to MTBE mole ratio as 1:10, 15 wt% of Amberlyst-15 based BisphenolA at 120°C for 8 hrs. Whereas, 97.9% conversion and 44.1 % total of yield product were received in the optimum condition of *tert*-butanol that performed with BisphenolA to *tert*-butanol mole ratio as 1:15, 10 wt% of Amberlyst-15 based on BisphenolA at 120°C for 8 hrs. As

the results, *tert*-butanol exhibited higher performance as a butylating agent. The both of optimum conditions were tested with several types of catalyst to discover the catalyst that was suitable for gave the highest total yield of product. Table 4.13 demonstrated BisphenolA conversion, total yield of product and selectivity over various heterogeneous catalyst types.

Table 4.13 Effect of catalytic type on conversion and product distribution with different butylating agent types

Catalytic type (acidity, mmol/g)	Butylating agent	Conv. (%)	2-TCP Yield (%)	2,6-DTCP Yield (%)	2,6-DTBPP Yield (%)	4,4-B-2,6-DTBP Yield (%)	%Total Yield Prouct.	Butylating agent	Conv. (%)	2-TCP Yield (%)	2,6-DTCP Yield (%)	2,6-DTBPP Yield (%)	4,4-B-2,6-DTBP Yield (%)	%Total Yield Prouct.
Microporous catalyst														
HZSM-5 (0.66)		13.2	0.0	0.0	0.0	0.0	0.0		0.0	0.0	0.0	0.0	0.0	0.0
HBeta (0.72)		23.8	0.0	0.0	0.0	0.0	0.0		0.0	0.0	0.0	0.0	0.0	0.0
MCM-22 (0.62)		80.5	5.5	1.2	1.3	0.0	8.0		90.4	16.9	5.7	13.1	0.0	35.7
HMCM-22 (1.12)		27.4	4.4	0.0	0.0	0.0	4.4		93.8	16.8	7.1	14.3	0.0	38.2
MCM-22-Pr-SO₃H (0.72)		14.7	10.4	2.1	0.0	0.0	12.5		89.5	22.8	2.9	0.0	0.0	25.7
Mesoporous catalyst														
MCA-Pr-SO₃H (0.88)		0.0	0.0	0.0	0.0	0.0	0.0		13.6	0.0	0.0	0.0	0.0	0.0
Al-SBA-15 (0.71)		15.9	1.2	0.0	0.0	0.0	1.2		0.0	0.0	0.0	0.0	0.0	0.0
Al-SBA-15-Pr-SO₃H (0.94)	MTBE	14.9	10.8	4.3	0.0	0.0	15.1	tert-butanol	0.0	0.0	0.0	0.0	0.0	0.0
SBA-15-Pr-SO₃H (1.02)		86.5	11.0	5.2	0.0	0.0	16.2		29.8	1.7	0.0	0.0	0.0	1.7
SBA-15 pure (0.47)		0.0	0.0	0.0	0.0	0.0	0.0		0.0	0.0	0.0	0.0	0.0	0.0
Clay														
Treated bentonite (4,4)		82.1	11.5	10.0	0.0	0.0	21.5		90.6	19.2	7.3	0.0	0.0	26.5
Commercial catalyst														
Amberlyst-15 (4.76)		96.2	24.9	7.5	3.3	5.3	41.0		97.9	17.9	10.0	6.0	10.2	44.1

Reaction cond. for MTBE: 120°C; BisphenolA/MTBE =1:10 by mole; catalytic amount 15 wt% base on BisphenolA and stirring speed 200 rpm. (SD ± 1)

Reaction cond. for *tert*-butanol: 120°C; BisphenolA /*tert*-butanol =1:15 by mole; catalytic amount 10 wt% base on BisphenolA and stirring speed 200 rpm. (SD ± 1

From the Table 4.13, Amberlyst-15 performed the higher BisphenolA conversion and total yield of product than HMCM-22 and SBA-15-Pr-SO$_3$H, respectively. This result was related to acid amount from titration as following order; Amberlyst-15 > HMCM-22 > SBA-15-Pr-SO$_3$H.

The difference of zeolites, including prepared HMCM-22, commercial HZSM-5 and commercial HBeta with SiO$_2$/Al$_2$O$_3$ ratios about 30 and Commercial sulfonic acid functionalized catalyst as Amberlyst-15, were utilized for BisphenolA butylation catalysis. The physical properties of zeolites were shown in Table 4.14. HZSM-5 and HBeta showed lower of acidity including total specific surface area and pore volume than HMCM-22. Also, HMCM-22 exhibited the highest activity among zeolite catalysts.

Table 4.14 Physicochemical and textural properties of Amberlyst-15 and zeolites

| Catalyst (SiO$_2$/Al$_2$O$_3$)	Pore volume[a] (cm$^3 \cdot$g^{-1})	Total specific surface area[b] (m$^2 \cdot$g^{-1})	Micropore distribution, d$_p$[c] (Å)	Acid capacity[d] (mmol/g)
HZSM-5 (28.2)	0.28	435	6.0	0.66
HBeta (30.3)	0.18	210	6.0	0.72
HMCM-22 (30)	0.15	384	7.0	1.12
Amberlyst-15	0.05	47	-	4.76

[a]Calculated using the *t*-plot method.

[b]Calculated using the BET plot method.

[c]Calculated using the MP plot method,

[d]Calculated using the acid titration

Furthermore, HMCM-22 with the large 12 ring cups which corresponding to half supercage (diameter of 7.1 Å, depth of 7.0 Å) [24] was shown in Figure 4.1. That revealed more activity due to easier diffusion of the BisphenolA and butylated products because pore size of HMCM-22 was too fit with comparison to molecular size of BisphenolA and butylated products, as showed in Table 4.15. Additionally, the oxygen membered ring dimension of HZSM-5 and HBeta were relatively too small to compare with the width and length of BisphenolA and butylated products, therefore

all of the butylated products were negligible in HZSM-5 and HBeta catalysis pore syetems. For the both of MTBE and *tert*-butanol reaction results were similarly.
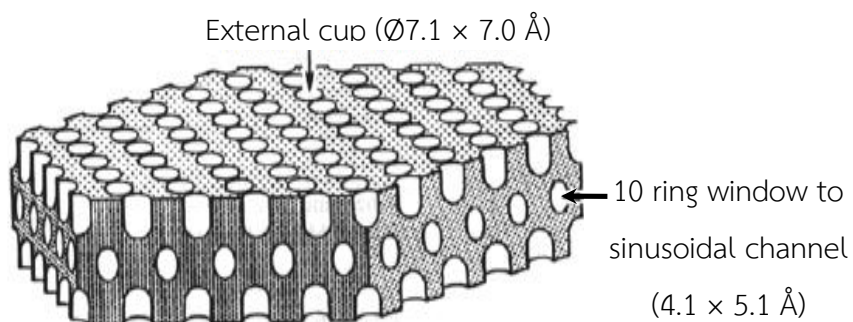
Figure 4.1 Single sheet of MCM-22 precursor with showing a half of supercage or hemicage [24].

Table 4.15 Molecular width and length calculation by HyperChem program

Molecule	Width (Å)	Length (Å)
BisphenolA	5.980	8.263
2-tert-butyl-4-(2-(4-hydroxyphenyl)propan-2-yl)phenol	8.018	10.392
2,6-di-tert-butyl-4-(2-(4-hydroxyphenyl)propan-2-yl)phenol	12.187	6.388
2,6-di-tert-butyl-4-(2-(3-tert-butyl-4-hydroxyphenyl)propan-2-yl)phenol	13.280	7.997
4,4'-(propane-2,2-diyl)bis(2,6-di-tert-butylphenol)	12.522	7.8972

The hexagonal mesoporous catalysts (SBA-15-Pr-SO$_3$H) showed greater activity than microporous catalysts (HZSM-5 and HBeta) whereas Al-SBA-15-Pr-SO$_3$H, which was a mesoporous structure, presented low catalytic activity in the MTBE reaction, as shown in Table 4.13. Moreover, using MTBE as butylating agent SBA-15-Pr-SO$_3$H displayed the highest selectivity than the other catalyst in mesoporous catalyst that gave total yield of product and conversion were 16.16% and 86.47%, respectively. This result was related to acid amount from titration. In contrast Al-SBA-15-Pr-SO$_3$H contained higher surface area and acid amount than SBA-15-Pr-SO$_3$H catalyst but gave lower activity than SBA-15-Pr-SO$_3$H that might be unsuitable for BisphenolA butylation. On the other hand, SBA-15 revealed the barely reaction conversion due to the low acidity of free hydroxy group in silica framework. Furthermore, treated bentonite was tested in this reaction and gave low butylated products yields. Although, it was a rather high acid amount catalyst (4.4 mmol/g) but low specific surface area (42 m^2/g) that might be unsuitable for BisphenolA butylation. This result was shown in Table 4.16

Table 4.16 Textural properties of sulfonic acid functionalized of MCA-Pr-SO3H, SBA-15, SBA-15-Pr-SO3H, Al- SBA-15- Pr-SO3H and Treated bentonite

Catalyst	Total specific surface area[a] ($m^2 \cdot g^{-1}$)	Pore size distribution[b] (Å)	Pore volume[b] ($cm^3 \cdot g^{-1}$)	Acidity[c] (mmol/g)
MCA-Pr-SO$_3$H	430	61.8	0.62	0.88
SBA-15	684	80.6	1.02	0.47
SBA-15-Pr-SO$_3$H	570	24.3	0.57	1.12
Al-SBA-15-Pr-SO$_3$H	630	80.6	0.90	0.94
Treated bentonite	42	-	-	4.4

[a]Calculated using the BET plot method,

[b]Calculated using the BJH method,

[c]Calculated using the acid titration

4.4   Characterization of catalysts

4.4.1   The physico-chemical properties of SBA-15 materials

4.4.1.1 XRD results

The XRD patterns of as-synthesized SBA-15, SBA-15, Al-SBA-15, Al-SBA-15-Pr-SO$_3$H and SBA-15-Pr-SO$_3$H were shown in Figure 4.10. For all materials, a very intense peak and two weak peaks indexed to (100), (110) and (200) diffractions that specified the prepared materials contained well-ordered hexagonal structure [47]. After calcined,

the XRD pattern showed that the hexagonal structure was remained and peak intensity at (100) reflection increase which resulting from removal of organic template form the pores of the materials. Al-SBA-15 compared to calcined SBA-15 showed the intensity of the (100) reflection increases when Al was added in SBA-15 structure. In addition (100) reflection was shifted slightly to higher angle comparing to SBA-15 resulting from the shrinkage during the recalcination process or change in lattice parameters and d-spacing due to Al inclusion in crystal structure of SBA-15 [9]. The diffraction peaks of SBA-15-Pr-SO_3H and Al-SBA-15-Pr-SO_3H were slightly shifted to higher 2 theta values when compared with SBA-15, indicating pore size was decreased by bulky sulfonic group grafting on the surface of SBA-15.
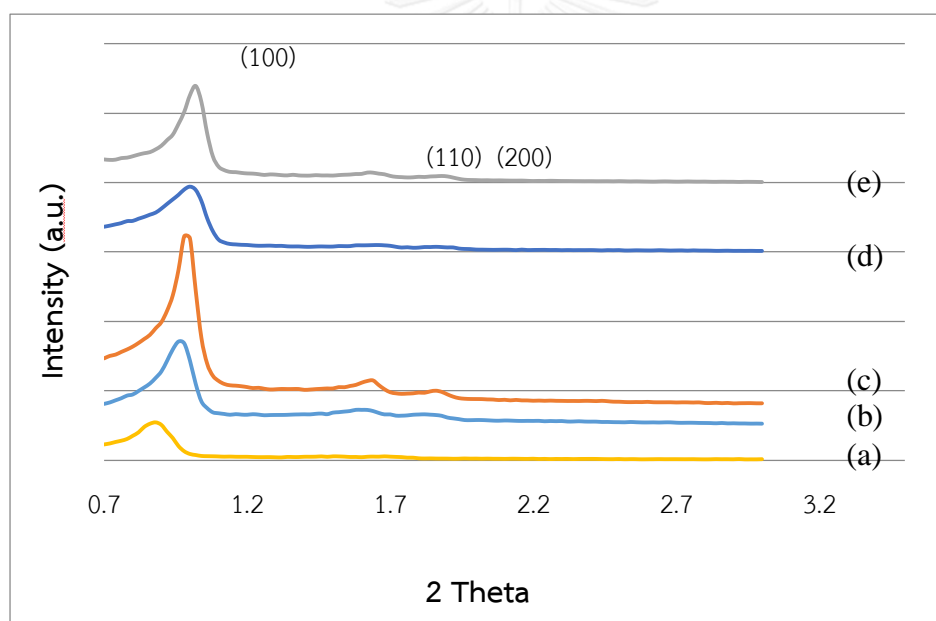
Figure 4.2   X-ray powder diffraction patterns of (a) as-synthesized SBA-15, (b) SBA-15, (c) Al-SBA-15, (d) SBA-15-Pr-SO_3H and (e) Al-SBA-15-Pr-SO_3H.

4.4.1.2 Nitrogen sorption properties of SBA-15 materials

The N_2 adsorption-desorption isotherm of SBA-15 and functionalized SBA-15 were defined as a type IV of IUPAC classification and hysteresis loop was performed a H1-type, as shown in Figure 4.3, that was a nature pattern of mesoporous

materials [53]. In addition, textural properties of SBA-15 Al-SBA-15 and Al-SBA-15-Pr-SO$_3$H, with Si/Al ratio as14 was indicate in Table 4.17. Aluminium was load in SBA-15 framework that decreased the amount of nitrogen up take in SBA-15 owing to the decreaseing of pore volume as 0.90 cm^3·g^{-1}. In addition, the loading Al into SBA-15 framework afffected to decreased the BET surface area (647 m^2·g^{-1}). When the organo sulfonic acid group was functionalized into pore structure of Al-SBA-15, the pore volume was decreased from 647 m^2·g^{-1} to 521 m^2·g^{-1}. Moreover, SBA-15-Pr-SO$_3$H performed the lower pore volume and total specific surface area with comparison to SBA-15 material. The decrease in the BET surface area after Pr-SO3H functionalization indicated the organo-sulfonic acid group to be incorporated both into and on the mesoporous structure and surface.

Table 4.17   Textural properties of SBA-15 and sulfonic acid functionalized SBA-15

Catalyst	Total specific surface area^a (m^2·g^{-1})	External surface area, S$_{ext}$^{c} (m^2·g^{-1})	Pore size distribution^b (Å)	Mesopore volume^b (cm^3·g^{-1})	Acidity^d (mmol/g)
SBA-15	719	657	80.6	0.93	0.50
Al-SBA-15	647	465	80.6	0.90	0.71
SBA-15-Pr-	635	603	80.6	0.90	1.02
Al-SBA-15- Pr-SO$_3$H	521	497	80.6	0.77	0.94

^{a}Calculated using the BET plot method,

^{b}Calculated using the BJH method,

^{c}Calculated using t-plot method,

[d]Calculated using the acid titration
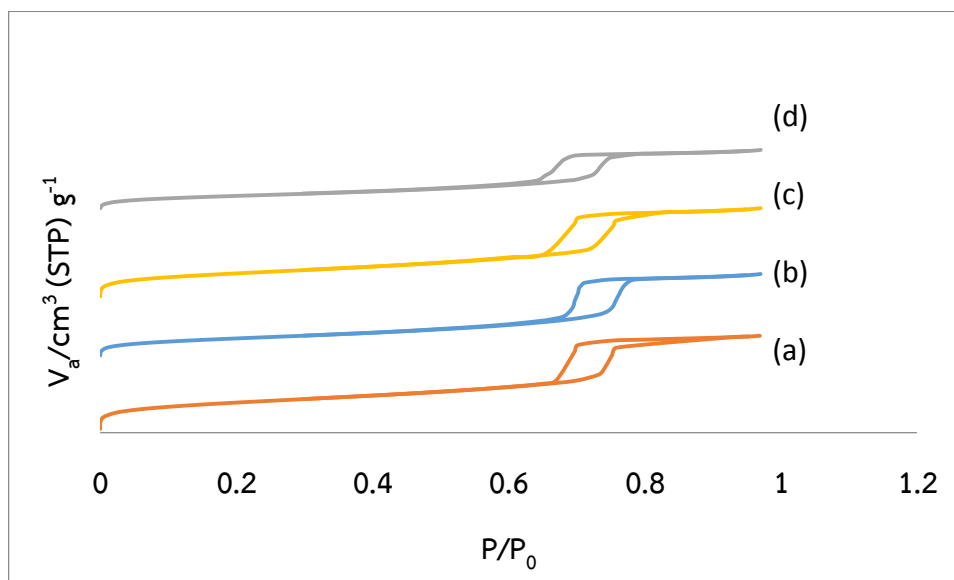
Figure 4.3 N$_2$ adsorption-desorption isotherm of (a) SBA-15and b) Al-SBA-15, (c) SBA-15-Pr-SO$_3$H and (d) Al-SBA-15-Pr-SO$_3$H.

4.4.1.3 SEM images

The SEM images showed the morphology of SBA-15, Al-SBA-15, SBA-15-Pr-SO$_3$H and Al-SBA-15-Pr-SO$_3$H in Figure 4.4 (a-d). Calcined SBA-15 were aggregated particles with rope-liked structure. After aluminum addition, some small rod particles were separated from the rope-liked agglomeration of SBA-15. Al-SBA-15 performed many rod particles that were broken from SBA-15. However the rod shape of individual particle remained the same as pure silica matter. After propyl sulfonic acid group addition, some particles were separated from the rope-liked agglomeration and the round particles change to ellipse.
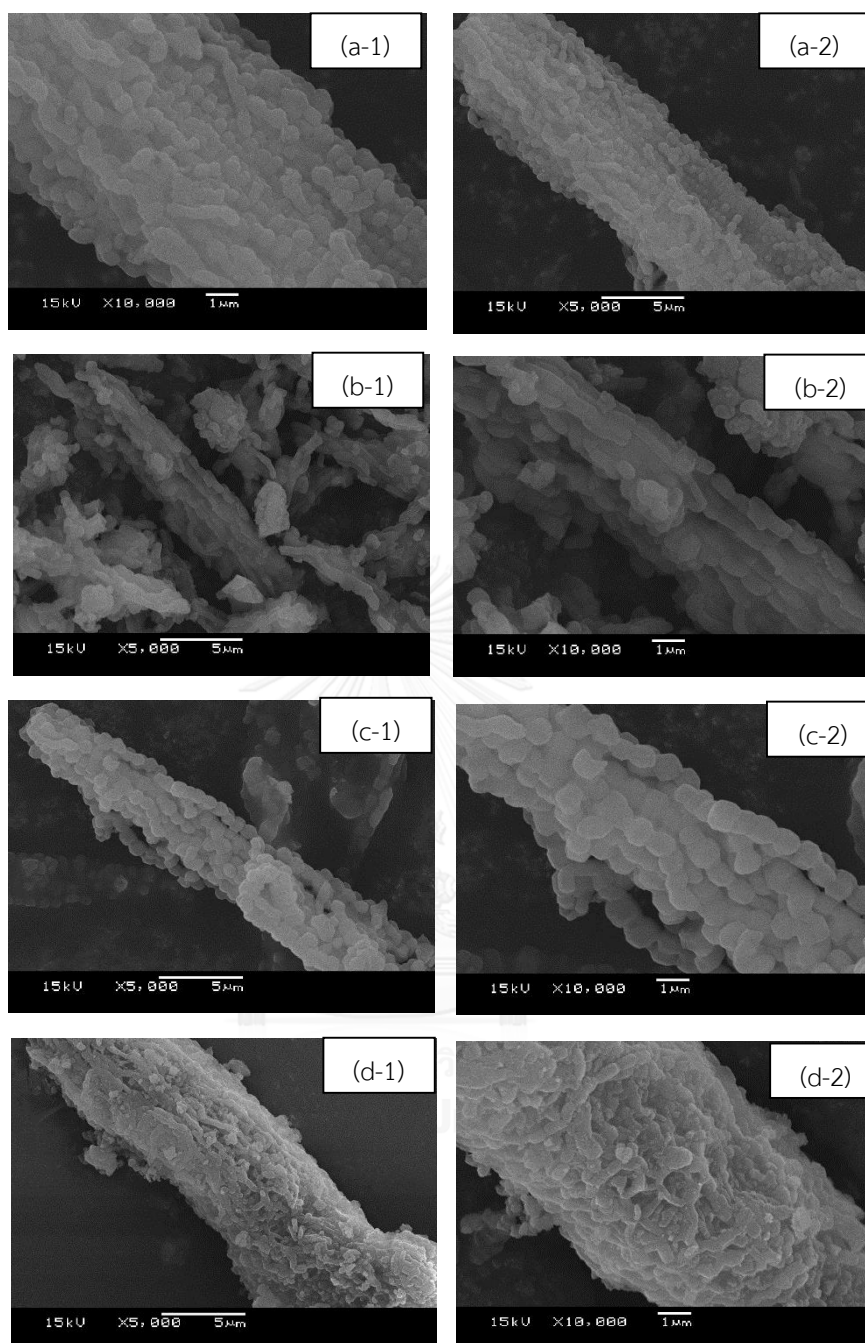
Figure 4.4   SEM images of SBA-15((a-1)×5,000 and (a-2)×10,000), Al-SBA-15 ((b-1)×5,000 and (b-2)×10,000) and SBA-15-Pr-SO₃H ((c-1)×5,000 and (c-2)×10,000) and Al-SBA-15-Pr-SO₃H ((d-1)×5,000 and (d-2)×10,000) .

4.4.2 The physico-chemical properties of MCM-22 materials

4.4.2.1 XRD results

Figure 4.25 (a) showed some of as-synthesized MCM-22 diffraction peaks were broad and overlapping peaks at low 2 theta angle. On the other hand, XRD peaks of NaMCM-22 sample were sharpened after calcination. Moreover, XRD patterns of calcined (Figure 4.25 (b)), exchanged MCM-22 (Figure 4.25 (c) and MCM-22- Pr-SO$_3$H (Figure 4.25 (d)) showed clearly parent peak and position of diffraction peaks that referred to crystalline phases of MCM-22 as the previous research [19, 48] with no significant difference between before and after improve acidity.
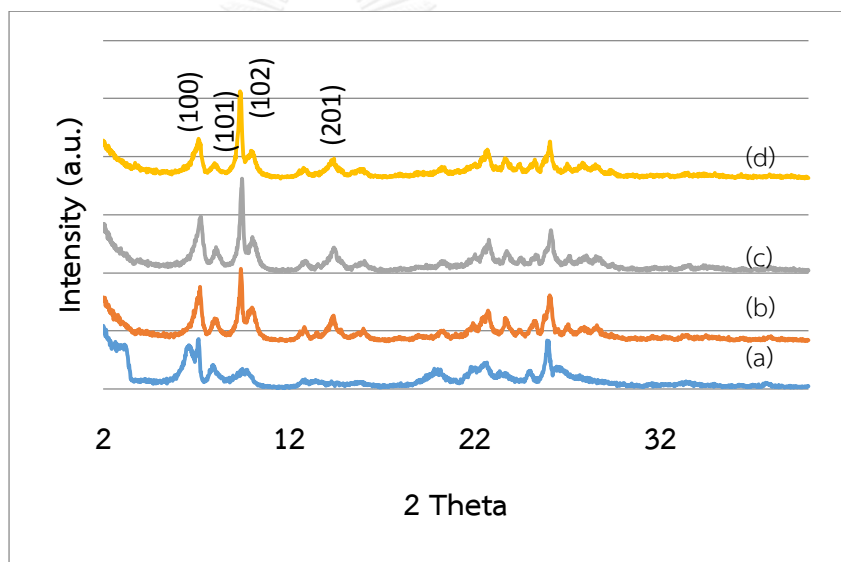
Figure 4.5   X-ray powder diffraction patterns of (a) as-synthesized NaMCM-22, (b) NaMCM-22, (c) HMCM-22 and MCM-22- Pr-SO$_3$H.

4.4.2.2 Nitrogen sorption properties of MCM-22 materials

Figure 4.26 showed the N_2 adsorption-desorption isotherm of NaMCM-22, HMCM-22 and MCM-22- Pr-SO$_3$H was a type I isotherm that indicated the existence of microporosity in the material. The pore size distribution of HMCM-22 was a narrow distribution and pore diameter was about 7.0 Å that was measured by MP-plot method. The total specific surface area of HMCM-22 was 384 m^2/g. The *t*-plot method was used to determine the external surface area and pore volume that was 61.5 m^2/g and 0.15 cm^3/g, respectively. Moreover, when the organic functional group were increased in the pore, the total specific area and pore volume decreased as 246 m$^2 \cdot$g^{-1}, 0.13 cm$^3 \cdot$g^{-1}, respectively. This result as shown in Table 4.18

**Table 4.18**   Textural properties of NaMCM-22, HMCM-22 and MCM-22-Pr-SO$_3$H

Catalyst	Total specific surface area^a (m$^2 \cdot$g^{-1})	Micropore distribution, d$_p$^{b} (Å)	External surface area, S$_{ext}$^{c} (m$^2 \cdot$g^{-1})	Micropore volume, V$_p$^{c} (cm$^3 \cdot$g^{-1})	Acidity^d (mmol/g)
MCM-22	387	7.0	41.8	0.09	0.62
HMCM-22	384	7.0	61.5	0.15	1.12
MCM-22-Pr-SO$_3$H	246	7.0	79.7	0.13	0.72

^{a}Calculated using the BET plot method,

^{b}Calculated using the MP plot method,

^{c}Calculated using the *t*-plot method,

^{d}Calculated using the acid titration
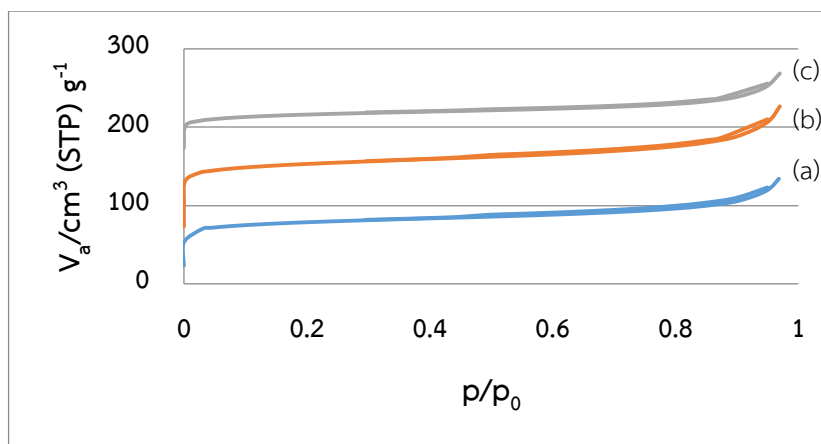
Figure 4.6   N$_2$ adsorption-desorption isotherms of (a) NaMCM-22, (b) HMCM-22 and (c) MCM-22- Pr-SO$_3$H.

4.4.2.3 SEM images

Figure 4.27 presented NaMCM-22 HMCM-22 and MCM-22- Pr-SO$_3$H morphology. Comparative between MCM-22 and HMCM-22, MCM-22 exhibits aggregation of plates-like morphology. After exchange to proton-form, H-MCM-22 shows the distribution of plates. Although the small plates are spreading, but also have a disc-like platelet structure. The last one, MCM-22-Pr-SO$_3$H that was grafted with propyl sulfonic acid group displayed a similar shape and particle size as other MCM-22 materials. The crystal shape of NaMCM-22 and HMCM-22 in this study well agreed with previously reported [19, 49].
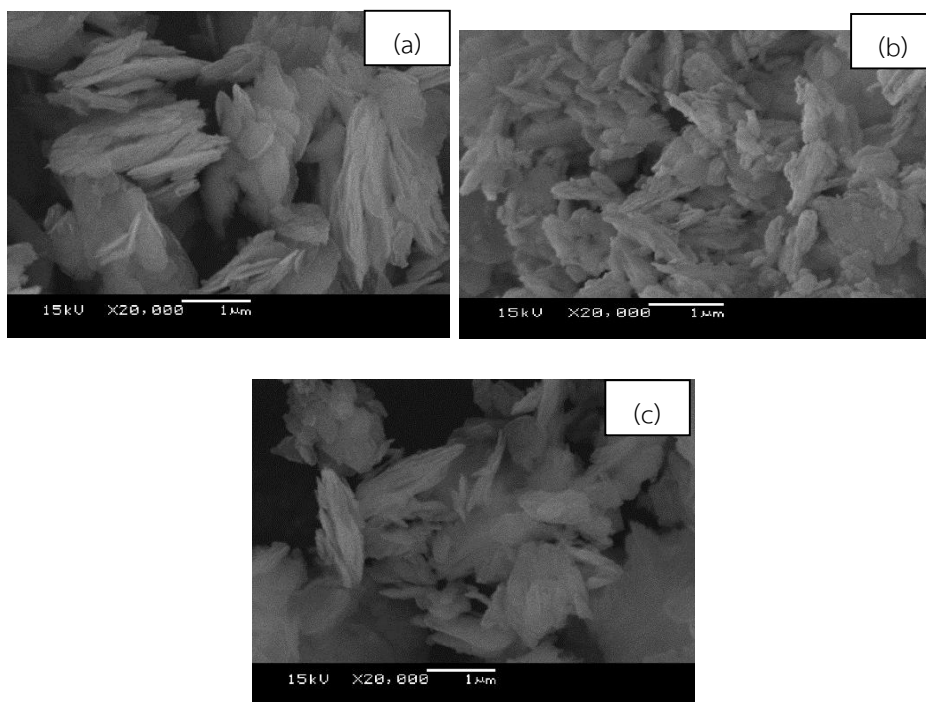
Figure 4.7 SEM images of (a) NaMCM-22, (b) HMCM-22 and (c) MCM-22- Pr-SO₃H.

4.5 Elemental analysis of Al-SBA-15, Al- SBA-15-Pr-SO₃H and HMCM-22

The number of aluminium atoms in catalysts was determined in ICP-MS. The Si was caculated by deduction of Al- form the total number of tetrahedral atoms. It was found that the Al contents in the catalyst as shown in Table 4.19. It was found that Al contents in the catalyst of MCM-22-Pr-SO₃H that was not significant difference Si/Al ratio of theory which about 14.0-15.0. In addition, the Si/Al ratio in gel calculated from gel composition and in Al-SBA-15 product calculated by ICP-MS technique were 14.00 and 23.1, respectively. The elemental analysis result proved that little of aluminum elements were in the solid structure of SBA-15. The Si/Al molar ratio in the gel of Al-SBA-15 in preparation step was lower than found in synthetic matter. That may be caused by the structural framework of pure silica SBA-15 was not suitable for increase aluminium. Also, this trend was similar Al- SBA-15-Pr-SO₃H.

Table 4.19   Si/Al mole ratio os Al-SBA-15, Al- SBA-15-Pr-SO$_3$H and MCM-22-Pr-SO$_3$H

Catalyst	Si/Al mole ratio in catalyst
Al-SBA-15	23.1
Al- SBA-15-Pr-SO$_3$H	55.6
MCM-22-Pr-SO$_3$H	17.2

4.6   Reusabillity of HMCM-22 catalyst

4.6.1 Characterization of recyclable HMCM-22

The XRD patterns of fresh and 1st reused HMCM-22 catalysts were showed in Figure 4.8. As a result, pattern and peak position of reused were similar as in XRD result of fresh catalyst. The adsorption-desorption isotherms of those catalysts were presented type I isotherm, microporous materials. The used catalyst had the specific surface area of 279 m^3/g that was decreased as compared to the fresh one (Table 4.20). Moreover the external surface area of reused catalyst was enlarged from fresh catalyst due to the fracture of HMCM-22 particles and pore volume was decreased from 0.15 to 0.07 cm^3·g^{-1}. The possible reason may be due to the coke formation and encapsulation of remained reactants and products within pore of catalyst.
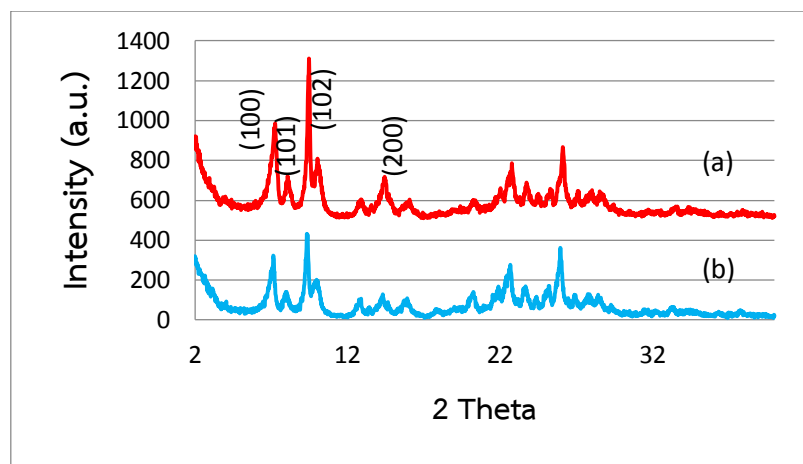
Figure 4. 8 X-ray powder diffraction patterns of (a) fresh HMCM-22 and (b) reused HMCM-22.

**Table 4. 20** Textural properties of fresh and reused HMCM-22

Catalyst	Total specific surface area^a (m^2·g^{-1})	Micropore distribution, d$_p{}^b$ (nm.)	External surface area, S$_{ext}{}^c$ (m^2·g^{-1})	Micropore volume, V$_p{}^c$ (cm^3·g^{-1})	Acid strength^d (mmol/g)
H-MCM-22	384	0.7	61.45	0.15	0.80
Reused MCM-22	279	0.7	76.23	0.07	

^{a}Calculated using the BET plot method,

^{b}Calculated using the MP plot method,

^{c}Calculated using the *t*-plot method

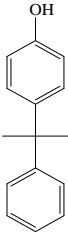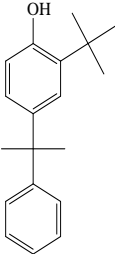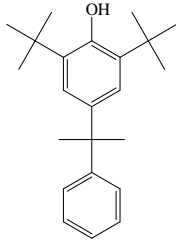^{d}Calculated using the acid titration
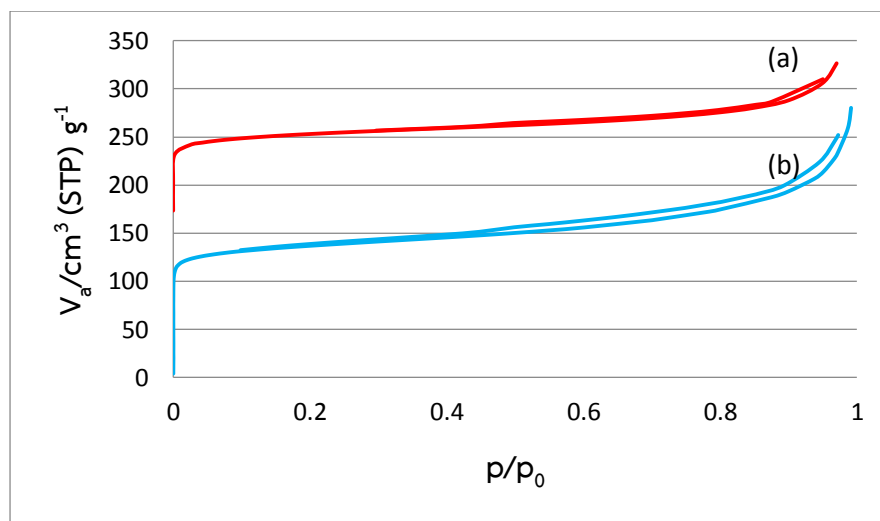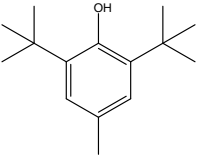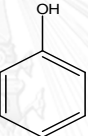
Figure 4. 9 N_2 adsorption-desorption isotherm and MP-pore size distribution of HMCM-22.

4.7   Antioxidant testing
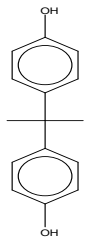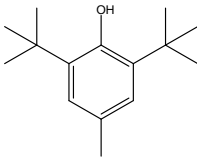
4.7.1   Antioxidant test by UV-visible method

Antioxidant abilities of standard chemical (BHT), reactants (*p*-cumylphenol and BisphenolA), purified products and reaction mixtures were shown in Table 4.20 and Table 4.21. Low of IC_{50} value demonstrated high ability of radical termination. In the case of BisphenolA, radical scavenging capacities were increased as following order; BisphenolA < butylated product. Because the increasing the number of butyl group, as electron-donating group, was enhanced the stabilization of phenoxy radical that occurred after hydrogen atom donating to free radical [50]. Also, this trend was similar to *p*-cumylphenol group result, 2,6-di-*tert*-butyl *p*-cumylphenol showed higher performance of radical scavenger than 2-*tert*-butyl *p*-cumylphenol and *p*-cumylphenol, respectively.

Table 4. 21 Comparison of radical scavenging of p-cumylphenol, butylated p-cumylphenol, BHT and reaction mixtures in continuous flow reactor

p-cumylphenol	2-*tert*-butyl *p*-cumylphenol	2,6-di-*tert*-butyl *p*-cumylphenol
IC_{50} = 1.43 mg/ml	IC_{50} = 0.89 mg/ml	IC_{50} = 0.36 mg/ml
BHT	Phenol	Reaction mixture 1 (optimum cond.) Conversion =98.39%, 2-TBC = 70.20%, 2,6-DTBC = 28.19 % CP:MTBE(1:5),100°C, flow rate:0.03ml/m,hplc pump,100 ml, 100.04g, 26h
IC_{50} = 3.18 mg/ml	IC_{50} = 3.05 mg/ml	IC_{50} = 1.74 mg/ml
Reaction mixture 2 (optimum cond.) Conversion =94.05%, 2-TBC = 75.4%, 2,6-DTBC = 18.7 % CP:*t*-butanol(1:5),100°C, flow rate:0.03ml/m,hplc pump,100 ml, 100.04g, 44h		
IC50 = 4.43 mg/ml		

Table 4. 22   Comparison of radical scavenging of BisphenolA, butylated BisphenolA derivatives and reaction mixtures in batch reactor

 BisphenolA	BisphenolA product (2-TBP and 2,6-DTBP)	 BHT
IC_{50} = 3.18 mg/ml	IC_{50} = 0.49 mg/ml	IC_{50} = 0.17 mg/ml
Reaction mixture 3 (optimum cond.) Conversion =98.0%, 2-TCP = 26.5%, 2,6-DTCP = 6.6% 2,6-DTBPP = 2.5% 4,4-B-2,6-DTBP = 5.4% BPA: MTBE =1:10 by mole, 15 wt% of Amberlyst-15, 120°C, 8 h	Reaction mixture 4 (optimum cond.) Conversion =96.3%, 2-TCP = 15.8%, 2,6-DTCP = 6.4% 2,6-DTBPP = 4.5% 4,4-B-2,6-DTBP = 9.0% BPA: t-BuOH =1:15 by mole, 10 wt% of Amberlyst-15, 120°C, 8 h	Reaction mixture 5 (optimum cond.) Conversion =89.7%, 2-TCP = 11.8%, 2,6-DTCP = 7.3% BPA: MTBE =1:10 by mole, 15 wt% of SBA-15-Pr-SO$_3$H, 120°C, 8 h
IC_{50} = 0.26 mg/ml	IC_{50} = 0.46 mg/ml	IC_{50} = 0.78 mg/ml
Reaction mixture 6 (optimum cond.) Conversion =96.3%, 2-TCP = 16.5%, 2,6-DTCP = 6.4% 2,6-DTBPP = 14.0% BPA: t-BuOH =1:15 by mole, 10 wt% of HMCM-22, 120°C, 8 h		
IC_{50}= 0.96 mg/ml		

Antioxidant ability of reaction mixture was considered to eliminate the separation process. In case of BisphenolA reaction, reaction mixture 3 showed larger efficiency than reaction mixture 4 due to more quantity of alkylation products that exhibited high ability of radical elimination. Moreover, radical scavenging performances of BisphenolA reaction which promoted by SBA-15-Pr-SO$_3$H and HMCM-22 catalysis were increased in following by reaction mixture 5 and reaction mixture 6, respectively. These results of reaction mixture test were presented to relate with amount of alkylation products which could be explained to highly activity.

2,6-DTCP and 2-TCP which promoted by Amberlyst-15 catalysis, respectively, showed higher radical scavenging ability than the other reactions. Both of synthesized reactants could be utilized in antioxidant application in packaging product. Moreover, 2-TCP could be used as intermediate in commercial antioxidant production.
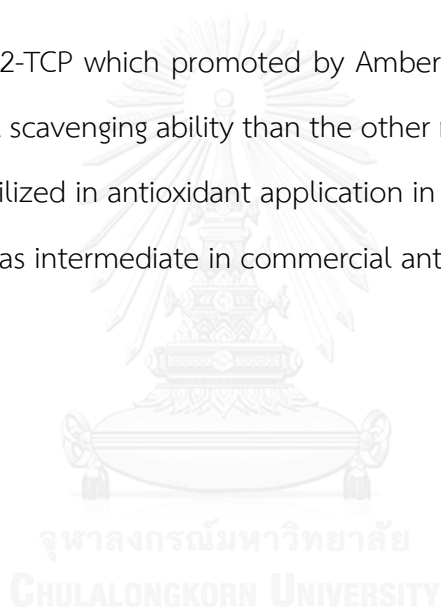
CHAPTER V
CONCLUSION

Continuous flow reactor

In case of the optimum condition of *p*-cumylphenol butylation using Amberlyst-15 as the catalyst in flow reactor with MTBE gave 98.4% *p*-cumylphenol conversion, 70.2% yield of 2-*tert*-butyl *p*-cumylphenol and 28.19% yield of 2,6-di-*tert*-butyl *p*-cumylphenol respectively. That was proceeded with *p*-cumylphenol to MTBE mole ratio as 1:5, flow rate 0.03 ml/min, at 100°C for 26 hrs. Whereas, 94.1% *p*-cumylphenol conversion, 75.37% yield of 2-*tert*-butyl *p*-cumylphenol and 18.67% yield of 2,6-di-*tert*-butyl *p*-cumylphenol, that was received in the optimum condition of *tert*-butanol. That performed with *p*-cumylphenol to *tert*-butanol mole ratio as 1:15, flow rate 0.03 ml/min, at 100°C for 27 hrs. As the results, MTBE exhibited higher performance than *t*-BuOH as a butylating agent.

Batch reactor

The optimum condition over commercial sulfonic resin (Amberlyst-15), total yield of alkylated products was 42.6% and 45.1% when using methyl-*tert*-butyl ether and *tert*-butanol as butylating agents, respectively. In comparison between butylating agents, *tert*-butanol showed higher performance than methyl-*tert*-butyl ether under optimum condition of each butylating agent. Propyl sulfonic functionalized SBA-15 (SBA-15-Pr-SO$_3$H) was successfully synthesized using triblock P123 (poly(ethylene oxide)$_{20}$–poly(propylene oxide)$_{70}$–poly(ethylene oxide)$_{20}$) copolymer as a structure directing agent. SBA-15-Pr-SO$_3$H exhibited well ordered hexagonal mesoporous with rope-like structure that was confirmed by all characterizations (XRD, N$_2$ sorption analysis and SEM). SBA-15-Pr-SO$_3$H activity was examined on butylation of BisphenolA with MTBE. Bisphenol conversion was high as 86.5% and 16.2% total yield of alkylated products in an optimum condition of SBA-15-Pr-SO$_3$H. The appropriate reaction condition was carried out with mole ratio BisphenolA to MTBE as 1: 10, catalytic amount 15wt% based on BisphenolA at 120°C for 8 hrs. SBA-15-Pr-SO$_3$H with large pore size around 8 nm and high acid amount that was suitable for butylated bisphenolA products, that

was the reason for higher reactivity and total yield of product than microporous and other materials. Moreover, HMCM-22 was prepared using hexamethyleneimine as a structure directing agent and showed platelet microporousity material from the characterization. Butylation of BisphenolA was tested with HMCM-22 catalyst. The suitable reaction condition conducted with mole ratio of BisphenolA to *tert*-butanol as 1: 15, catalytic amount 10wt% based on BisphenolA at 120°C for 8 hrs. That gave the highest conversion and total yield of alkylated products as 93.8% and 38.2%, respectively.

From DPPH scavenging assay, IC_{50} value decreased in the following order: BisphenolA > *p*-cumylphenol > 2-*tert*-butyl *p*-cumylphenol > BisphenolA product (2-TBP and 2,6-DTBP) > 2,6-di-*tert*-butyl *p*-cumylphenol. The butylated products of BisphenolA and *p*-cumylphenol are higher antioxidative potential agents than their starting materials which can be used as additive in epoxy resin and polycarbonate production.

The suggestion for future work

To study efficiency of regeneration catalysts in BisphenolA alkylation.

To discover the other group addition to *ortho* position of phenol derivatives in order to increase an antioxidant property.

REFERENCES

[1]   business, I.C. phenol & acetone markets [Online]. 2016. Available from: https://www.icis.com/resources/news/2016/06/09/10006764/market-outlook-phenol-acetone-markets-are-under-ressure-icis-consulting/ [June 9]

[2]   business, I.C. phenol & acetone markets [Online]. 2016. Available from: https://www.icis.com/resources/news/2016/06/10/10006764/market-outlook-phenol-acetone-markets-are-under-ressure-icis-consulting/ [June 10]

[3]   4-cumylphenol [Online]. 4-cumylphenol Available from: http://www.shengshanchem.com/en/p -cumylphenol-13.html [June]

[4]   Phenolic antioxidant compositions for organic polymers. 1982.

[5]   Method for producing 2,6-di-tert.-butyl-4-cumylphenol. 1974.

[6]   Beltrame, P.L., Carniti, P., Gamba, A., Cappellazzo, O., Lorenzoni, L., and Messina, G. Side reactions in the phenol/acetone process. A kinetic study. Industrial & Engineering Chemistry Research 27(1) (1988): 4-7.

[7]   Masagutov, R.M., Spivak, S.I., Akhmadishin, Z.S., Kirichenko, G.N., Grigorieva, N.G., and Tolstikov, G.A. Kinetics of p-cumylphenol alkylation by isobutylene in the presence of p-toluenesulfonic acid. Reaction Kinetics and Catalysis Letters 28(2) (1985): 411-417.

[8]   Kosaka, Y., and Keneth, B. . BisphenolA from phenol and acetone with an ion exchange resin catalyst—union carbide technology [Online]. 1982. Available from: https://www.ihs.com/pdf/RW82-1-1_220283110917062932.pdf [June]

[9]   Zhao, D., et al. Triblock Copolymer Syntheses of Mesoporous Silica with Periodic 50 to 300 Angstrom Pores. Science 279(5350) (1998): 548-552.

[10]   al., M.e. Preparation of sulfonic functionalized mesostructured materials. (2000) (2000).

[11]   Yue, Y., Gedeon, A., Bonardet, J.-L., D'Espinose, J.-B., Fraissard, J., and Melosh, N. Direct synthesis of AlSBA mesoporous molecular sieves: characterization and catalytic activities. Chemical Communications (19) (1999): 1967-1968.

[12]   Ma, J., Qiang, L.-S., Wang, J.-F., Tang, X.-B., and Tang, D.-Y. Effect of different synthesis methods on the structural and catalytic performance of SBA-15 modified by aluminum. Journal of Porous Materials 18(5) (2011): 607-614.

[13]   Shon, J.K., Yuan, X., Ko, C.H., Lee, H.I., Thakur, S.S., Kang, M., Kang, M.S., Li, D., Kim, J.N., and Kim, J.M. Design of mesoporous solid acid catalysts with controlled acid strength. Journal of Industrial and Engineering Chemistry. 13 (2007): 1201.

[14]   Corma, A., Corell, C., and Pérez-Pariente, J. Synthesis and characterization of the MCM-22 zeolite. Zeolites 15(1) (1995): 2-8.

[15]   Asensi, M.A., Corma, A., and Martínez, A. Skeletal Isomerization of 1-Butene on MCM-22 Zeolite Catalyst. Journal of Catalysis 158(2) (1996): 561-569.

[16]   Rigoreau, J., Laforge, S., Gnep, N.S., and Guisnet, M. Alkylation of toluene with propene over H-MCM-22 zeolite. Location of the main and secondary reactions. Journal of Catalysis 236(1) (2005): 45-54.

[17]   Moon, G., Möller, K.P., Böhringer, W., and O'Connor, C.T. Alkylation of phenol with methanol over zeolite H-MCM-22 for the formation of p-cresol. Studies in Surface Science and Catalysis 142 (2002): 635-642.

[18]   Zhang, K., et al. Alkylation of phenol with tert-butyl alcohol catalyzed by large pore zeolites. Applied Catalysis A: General 207(1) (2001): 183-190.

[19]   Kumar, G.S., Saravanamurugan, S., Hartmann, M., Palanichamy, M., and Murugesan, V. Synthesis, characterisation and catalytic performance of HMCM-22 of different silica to alumina ratios. Journal of Molecular Catalysis A: Chemical 272(1) (2007): 38-44.

[20]   Devassy, B.M., Shanbhag, G.V., Lefebvre, F., and Halligudi, S.B. Alkylation of p-cresol with tert-butanol catalyzed by heteropoly acid supported on zirconia catalyst. Journal of Molecular Catalysis A: Chemical 210(1) (2004): 125-130.

[21]   Wu, S., et al. Synthesis, Characterization, and Catalytic Performance of Mesoporous Al-SBA-15 for Tert-butylation of Phenol. Chinese Journal of Catalysis 27(1) (2006): 9-14.

[22]   Catalysis [Online]. 2012. Available from: http://en.wikipedia.org/wiki/Catalysis [June]

[23]   Hagen, J. Industrial Catalysis. . 1999.

[24]   Matias, P., Lopes, J.M., Laforge, S., Magnoux, P., Guisnet, M., and Ribeiro, F.R.
        n-Heptane and methylcyclohexane transformation over a HMCM-22 zeolite.
        Origin of the features typical of large-or of medium-pore zeolites. Reaction
        Kinetics and Catalysis Letters 95(1) (2008): 193-201.

[25]   Breck, D.W. Zeolite molecular sieves: structure, chemistry, and use. . Zeolite
        molecular sieves: structure, chemistry, and use. . 1997.

[26]   Continuation report [Online]. Available from:
        http://mch3w.ch.man.ac.uk/theory
        /staff/student/mbdtscw/transfer_html/node1.html [June]

[27]   Kresge, C.T., Leonowicz, M.E., Roth, W.J., Vartuli, J.C., and Beck, J.S. Ordered
        mesoporous molecular sieves synthesized by a liquid-crystal template
        mechanism. Nature 359(6397) (1992): 710-712.

[28]   Hicks, J.C. Organic/inorganic hybrid amine and sulfonic acid tethered silica
        materials: synthesis, characterization and application. Georgia Institute of
        Technology. 2007.

[29]   Beck, J.S., et al. A new family of mesoporous molecular sieves prepared with
        liquid crystal templates. Journal of the American Chemical Society 114(27)
        (1992): 10834-10843.

[30]   Soler-Illia, G.J.d.A.A., Crepaldi, E.L., Grosso, D., and Sanchez, C. Block
        copolymer-templated mesoporous oxides. Current Opinion in Colloid &
        Interface Science 8(1) (2003): 109-126.

[31]   Athens, G.L., Shayib, R.M., and Chmelka, B.F. Functionalization of
        mesostructured inorganic–organic and porous inorganic materials. Current
        Opinion in Colloid & Interface Science 14(4) (2009): 281-292.

[32]   Melero, J.A., van Grieken, R., and Morales, G. Advances in the Synthesis and
        Catalytic Applications of Organosulfonic-Functionalized Mesostructured
        Materials. Chemical Reviews 106(9) (2006): 3790-3812.

[33]   Wight, A.P., and Dais, M.E. Design and preparation of organic-inorganic hybrid
        catalysts. 2002.

[34]   Kureshy, R.I., Ahmad, I., Pathak, K., Khan, N.H., Abdi, S.H.R., and Jasra, R.V. Sulfonic acid functionalized mesoporous SBA-15 as an efficient and recyclable catalyst for the synthesis of chromenes from chromanols. Catalysis Communications 10(5) (2009): 572-575.

[35]   Amberlyst [Online]. 2010. [June]

[36]   Frija, L.M.T. and Afonso, C.A.M. Amberlyst®-15: a reusable heterogeneous catalyst for the dehydration of tertiary alcohols. Tetrahedron 68(36) (2012): 7414-7421.

[37]   Basic operating principles of the sorptomatic [Online]. 2012. [June]

[38]   Belsorp, B.J., Inc. Analysis software user's manual.

[39]   Gabriel, B.L. SEM: A User's Manual for Material Science. 1985.

[40]   Theory, I.D.a. [Online]. Available from: http://www.sees.manchester.ac.uk/ourresearch/facilities/geochemistry/equipmentandfacilities/icp-ms/instrumentdescriptionandtheory [June]

[41]   DPPH-test [Online]. 2017. Available from: https://en.wikipedia.org/wiki/DPPH

[42]   Mbaraka, I.K., Radu, D.R., Lin, V.S.Y., and Shanks, B.H. Organosulfonic acid-functionalized mesoporous silicas for the esterification of fatty acid. Journal of Catalysis 219(2) (2003): 329-336.

[43]   Chaudhari, S.T.a.B., N.N. Steam gasification of chars and bio-oil. Report to Bioenergy Development Program Renewable Energy Branch, Energy. 2002.

[44]   Stein, Y.S., Antal, M.J., and Jones, M. A study of the gas-phase pyrolysis of glycerol. Journal of Analytical and Applied Pyrolysis 4(4) (1983): 283-296.

[45]   Subramanion, L.J. DPPH free radical scavenging and xanthine oxidase inhibitiory activities of Cassia fistula seeds extract. . Journal of Medicinal Plants Research. (2011).

[46]   Chaudhuri, B., Patwardhan, A.A., and Sharma, M.M. Alkylation of substituted phenols with olefins and separation of close-boiling phenolic substances via alkylation/dealkylation. Industrial & Engineering Chemistry Research 29(6) (1990): 1025-1031.

[47]   Yadav, G.D. and Doshi, N.S. Alkylation of phenol with methyl-tert-butyl ether and tert-butanol over solid acids: efficacies of clay-based catalysts. <u>Applied Catalysis A: General</u> 236(1) (2002): 129-147.

[48]   Yang, J., Yang, J.Y., Zhou, Y., Wei, F., Lin, W.G., and Zhu, J.H. Hierarchical functionalized MCM-22 zeolite for trapping tobacco specific nitrosamines (TSNAs) in solution. <u>Journal of Hazardous Materials</u> 179(1) (2010): 1031-1036.

[49]   Yang, S.-T., Kim, J.-Y., Kim, J., and Ahn, W.-S. CO2 capture over amine-functionalized MCM-22, MCM-36 and ITQ-2. <u>Fuel</u> 97 (2012): 435-442.

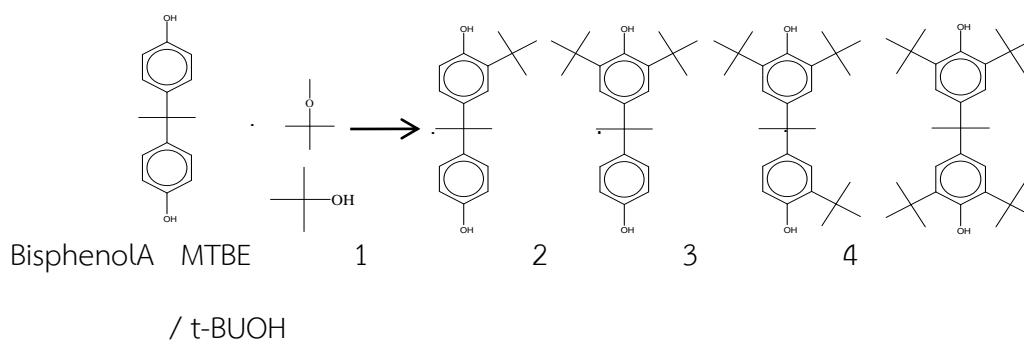[50]   Morales, J.C., and Lucas, R. <u>Olives and Olive Oil in Health and Disease Prevention</u>. 2010.

APPENDIX

CHARACTERIZATION OF AUTHENTIC SAMPLES

BisphenolA   MTBE   1   2   3   4

/ t-BUOH

1.) 2-tert-butyl-4-(2-(4-hydroxyphenyl)propan-2-yl)phenol : 2-TBP

2.) 2,6-di-tert-butyl-4-(2-(4-hydroxyphenyl)propan-2-yl)phenol: 2,6-DTBP

3.) 2,6-di-tert-butyl-4-(2-(3-tert-butyl-4-hydroxyphenyl)propan-2-yl)phenol :
     2,6-DTBPP

4.) 4,4'-(propane-2,2-diyl)bis(2,6-di-tert-butylphenol) : 4,4-B-2,6-DTBP
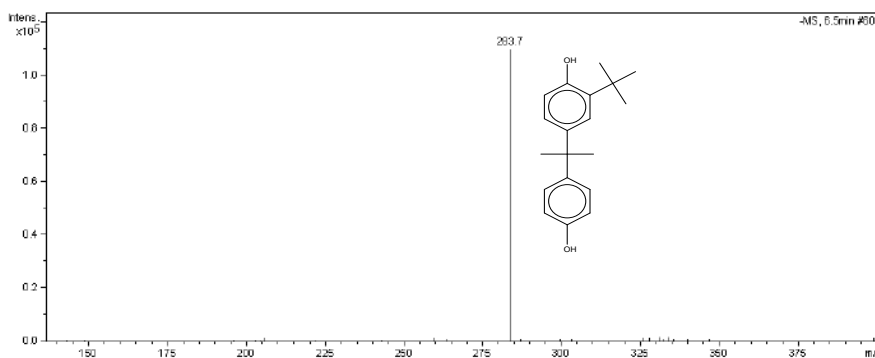

Mass spectrum for t_R 6.5 min

Figure A-1   High-resolution mass spectrumof 2-tert-butyl-4-(2-(4-
                 hydroxyphenyl)propan-2-yl)phenol : 2-TBP.

Mass spectrum for t_R 11.8 min

m/z =339.3   m/z =300

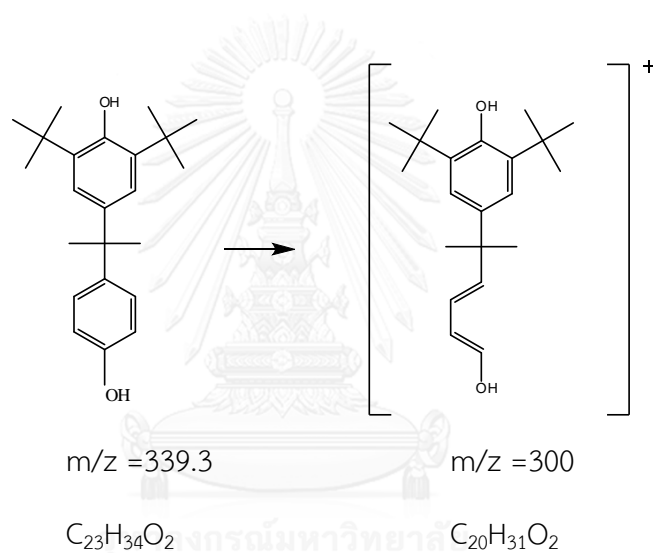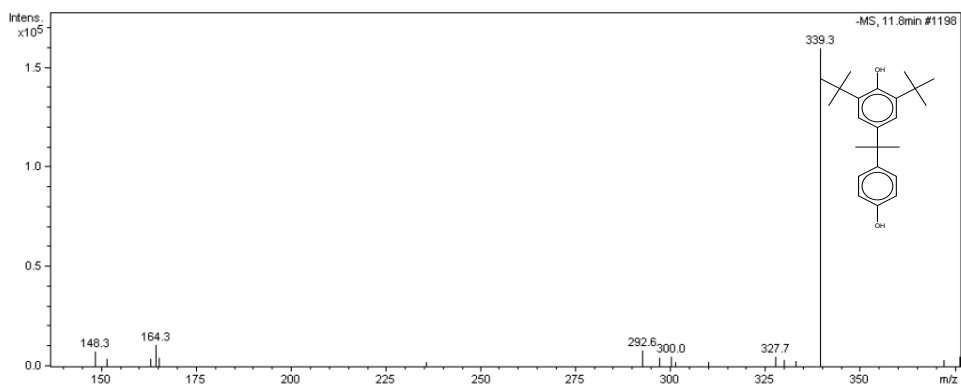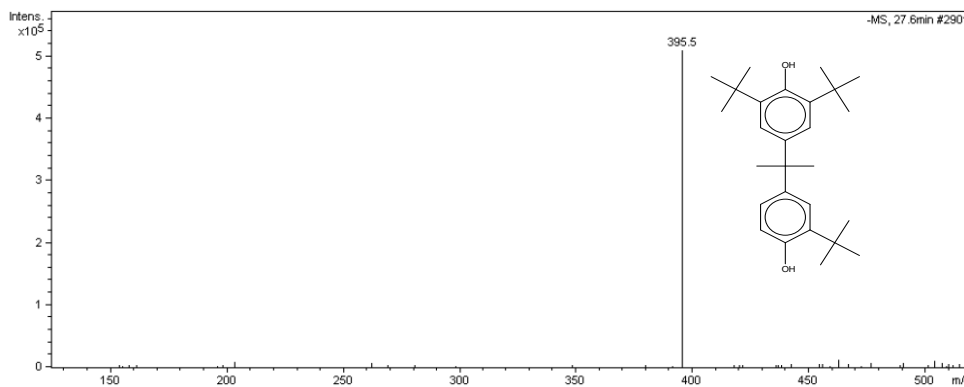$C_{23}H_{34}O_2$ $C_{20}H_{31}O_2$

Figure A-2   High-resolution mass spectrum of 2,6-di-tert-butyl-4-(2-(4-hydroxyphenyl)propan-2-yl)phenol: 2,6-DTBP.

Mass spectrum for t_R 27.6 min

Figure A-3 : 2,6-di-tert-butyl-4-(2-(3-tert-butyl-4-hydroxyphenyl)propan-2-yl)phenol 2,6-DTBPP

HPLC ANALYSIS

1.   Preparation of standard solution and calibration solution

        1.1   *p*-Cumylphenol standard solution

1.1.1   Stock standard solution (2.45×10^{-3} M)

        A 0.0052 g of *p*-cumylphenol was accurately weighed in a 10 ml volumetric flask and made up to the mark with methanol.

1.1.2   Working standard solution (1.85, 1.25, 0.65 and 0.05 [$\times 10^{-3}$] M)

        The working standard solutions were prepared by dilution of the standard solution using a pipette and then made up to the mark with methanol.

        1.2   2-*tert*-Butyl *p*-cumylphenolstandard solution

        1.2.1   Stock standard solution (1.29×10^{-3} M)

        A 0.0034 g of 2-*tert*-butyl *p*-cumylphenolwas accurately weighed in a 10 ml volumetric flask and made up to the mark with methanol.

1.2.2   Working standard solution (0.97, 0.65, 0.33 and 0.005 [$\times 10^{-3}$] M)

The working standard solutions were prepared by dilution of the standardsolution using a pipette and then made up to the mark with methanol.

1.3   2,6-Di-*tert*-butyl *p*-cumylphenolstandard solution

1.3.1   Stock standard solution (1.05×10^{-3} M)

A 0.0034 g of2,6-di-*tert*-butyl *p*-cumylphenolwas accurately weighed in a 10 ml volumetric flask and made up to the mark with methanol.

1.3.2   Working standard solution (0.79, 0.53, 0.27 and 0.004 [$\times 10^{-3}$] M)

The working standard solutions were prepared by dilution of the standard solution using a pipette and then made up to the mark with methanol.

2.   Analysis of the calibration solutions

A 10 μl of each prepared sample was analyzed by HPLC technique. FigureA-9 – A-11 showed calibration curves and linear equations that related between area and concentration of *p*-cumylphenol, mono- and di-butylated products*, all*calibration *curves showed R-square value ca 0.99XX.*
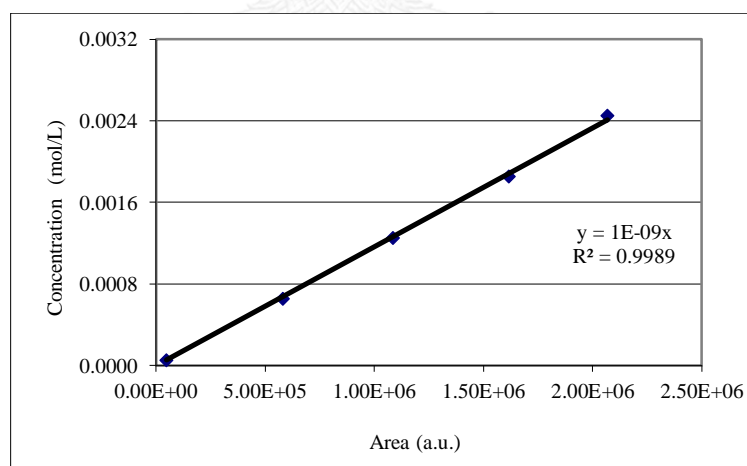

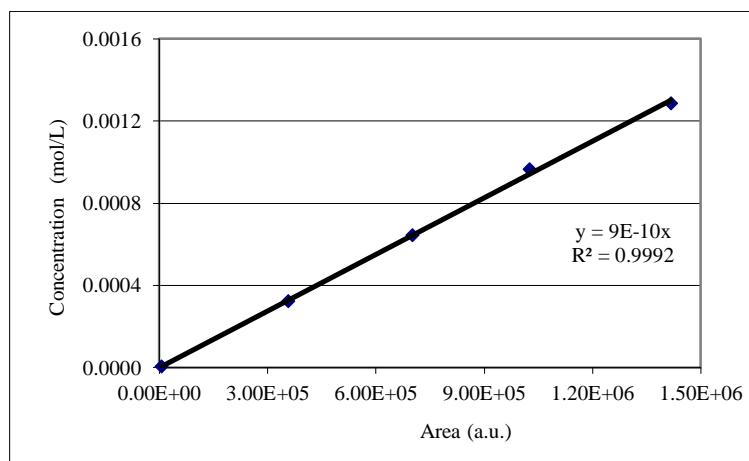Figure A-4   Calibration curve of *p*-cumylphenol

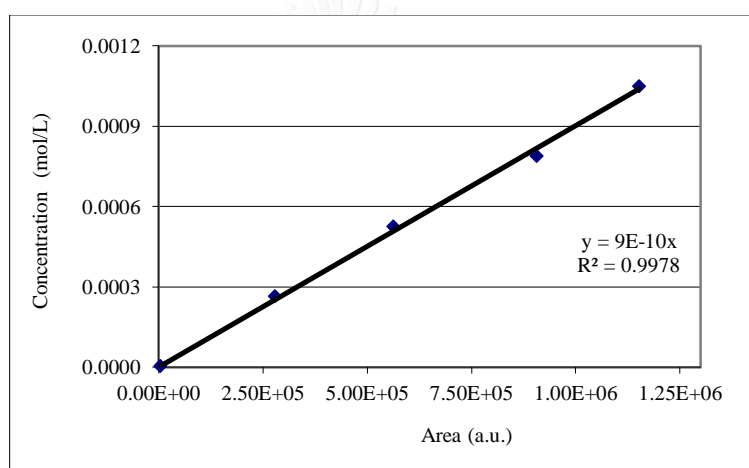Figure A-5   Calibration curve of 2-*tert*-butyl *p*-cumylphenol

Figure A-6   Calibration curve of 2,6-di-*tert*-butyl *p*-cumylphenol

Sample injection: 10 μl

Solvent: MeOH / H_2O = 85%: 15% (v/v)

Flow rate: 0.8 ml/min

Column: Ultra C18 capillary column

(250 mm length $\times$ 4.6 mm inner diameter)

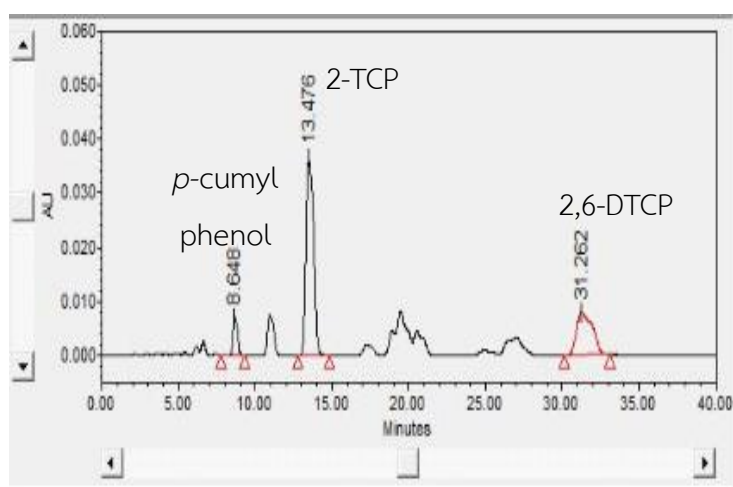Detector: Photodiode array (PDA) at 254 nm.

Figure A-7   HPLC chromatogram of *p*-cumylphenol, 2-TCP and 2,6-DTCP in *p*-cumylphenol butylation reaction (1st monitor) (Reaction condition: *p*-cumylphenol: MTBE = 1:5 by mole, 15 wt% of Amberlyst-15, 100°C, 8 hrs.).

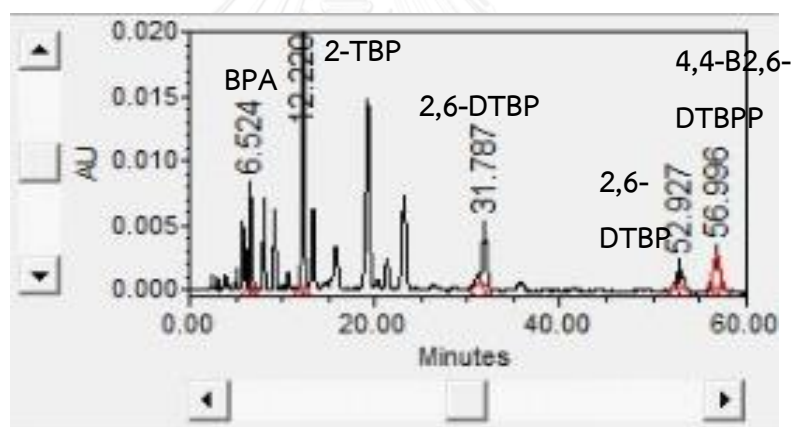

Figure A-8   HPLC chromatogram of BisphenolA (BPA), 2-TBP, 2,6-DTBP, 2,6- DTBPP and 4,4-B-2,6-DTBPin BisphenolA butylation reaction(Reaction condition: BisphenolA: MTBE =1:10 by mole, 15 wt% of Amberlyst-15,
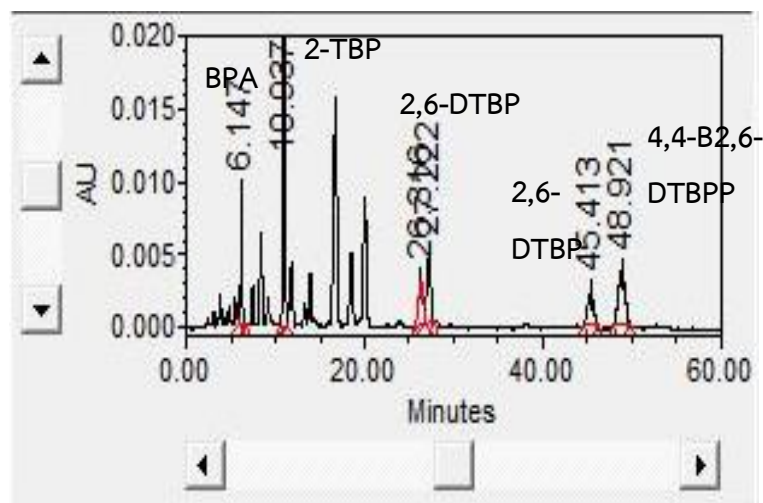
120°C, 8 hrs.).

Figure A-9   HPLC chromatogram of BisphenolA (BPA), 2-TBP, 2,6-DTBP, 2,6- DTBPP and 4,4-B-2,6-DTBP in BisphenolA butylation reaction(Reaction condition: BisphenolA: *tert*-butanol =1:15 by mole, 10 wt% of Amberlyst-15,120°C, 8 hrs.)

3.   Calculation of percent yield and percent selectivity for butylated products

The products of phenol derivative butylation were examine by liquid chromatography analyzer. Butylated products were determined with calibration curve method.

The percent conversion and percent yield were calculated based on the peak area that obtained from liquid chromatography.

For example: a = peak area of the reactant

b = peak area of the product A

c = exact mole of initial reactant (mol)

    d = total weight of the mixture after reaction (gram)

e = mole of product in total reaction mixture (mol)

f = mole of reactant in total reaction mixture (mol)

The concentration of prepared sample was calculate with calibration function can be described as follows:

Y = mX + C

When; Y is concentration (mol/L)

X is peak area

$$\text{Also,} \quad \text{concentration of product A } (Y_A) = mb + c$$

The calculation of mole product A in prepared sample (0.001 gram / 1 ml) can be described as follows:

The amount of mole product in prepared sample

$$= Y_A \times 10^{-3}$$

The calculation of mole product A in total reaction mixture can be described as follows:

The amount of the mole product in total reaction mixture (e)

$$= (Y_A \times 10^{-3}) \times d$$

The calculation of the percent yield can be described as follows:

The percent yield of product A

$$\% \text{ yield of A} = \left(\frac{e}{c}\right) \times 100$$

The calculation of the percent conversion can be described as follows:

$$\% \text{ conversion} = 100 - \left[\left(\frac{f}{c}\right) \times 100\right]$$

The calculation of the percent selectivity of product A can be described as follows:

$$\% \text{ selectivity of A} = \left(\frac{\% \text{ yield of A}}{\% \text{ conversion}}\right) \times 100$$

CALCULATION OF ANTIOXIDANT TEST BY UV-VISIBLE METHOD

Sampling 50 µl of sample solutions (1 ppm, 0.5 ppm, 0.25 ppm, 0.125 ppm and 0.0625 ppm in methanol) to the microplate

Add 250 µl DPPH (11.8 mg/100 ml of methanol) to all of them

Detect by UV-visible spectroscopy at 517 nm

Calculate the radical scavenging percentage

$$\% \text{ radical scavenging} = \left(\frac{A_{blank} - A_{sample}}{A_{blank}} \right) \times 100$$

Where A_{blank} = absorbance of DPPH radical without the sample

A_{sample} = absorbbance of DPPH radical and added of sample

Plot graph of % radical scavenging (Y) relative with concentration (X)

Calculate IC_{50} value or concentration at 50% radical scavenging

Example: BisphenolA (MW = 228.29 g/mol)

Table C-1   Absorbance of BisphenolA sample with various concentrations

Concentration	absorbance					
(ppm)	1	0.5	0.25	0.125	0.0625	control
Run 1	1.212	1.698	1.927	2.071	2.127	2.150
Run 2	1.217	1.752	1.808	1.998	2.123	2.146
Run3	1.365	1.768	1.903	2.097	2.110	2.112
Avg.	1.265	1.739	1.879	2.055	2.120	2.136
% radical scavenging	40.79	18.57	12.01	3.77	0.74	

$$\% \text{ radical scavenging}$$
$$= \left[1 - \left(\frac{\text{avg. absorbance of 1 ppm conc.}}{\text{avg. absorbance of control}} \right) \right] \times 100$$
$$= \left[1 - \left(\frac{1.265}{2.136} \right) \right] \times 100$$
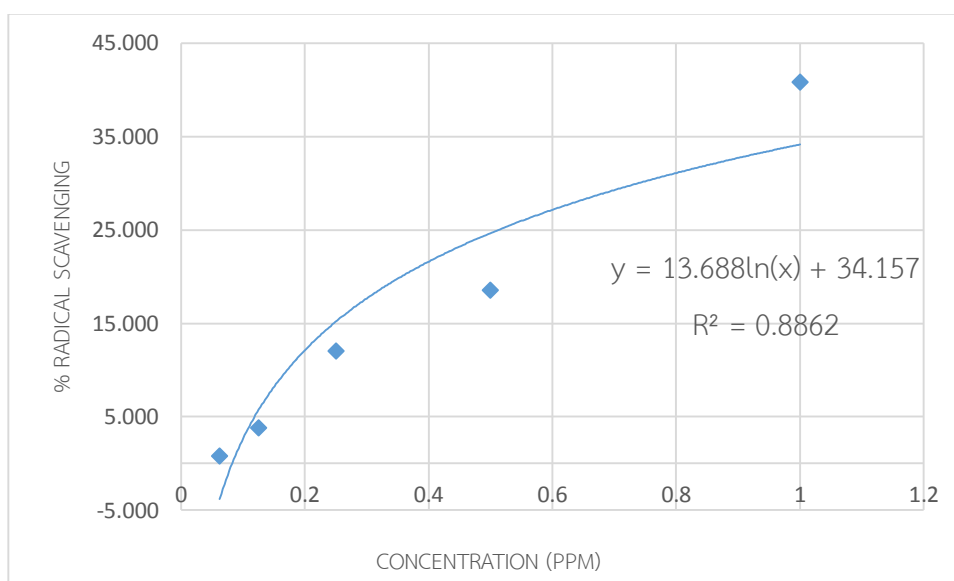
= 40.79 %

Figure C-1   Curve of concentration versus % radical scavenging of *p*-cumylphenol.

From linear equation;

$$Y = mX + c$$

$$X = \frac{Y - c}{m}$$

In this case, the resulting curve was performed the logarithm function

Also,

$$\ln X = \frac{Y - c}{m}$$

If   Y = 50, when c = 34.157, m = 13.688

 X = 3.180 mg/ml

   = (3.180mg/ml)/MW

   = (3.180mg/ml)/ (228.29 g/mol)

   = 13.92 mM

      IC_{50} = 3.180 mg/ml = 13.92 mM

VITA

Miss Warumporn Singhapan was born on March 14, 1990 in Bangkok, Thailand. She received a Bachelor Degree of Applied Science, major in Industrial Chemistry from King Mongkut's University of Technology North Bangkok in 2012. Since 2013 she has been a graduate student in the program of Petrochemistry and Polymer Science, Faculty of Science, Chulalongkorn University and completed her Master of Science Degree in 2017.

In 9-11January 2016,she participated the Pure and Applied Chemistry International Conference (PACCON 2016) at Bangkok International Trade & Exhibition Centre (BITEC) approval of proceeding and poster presentation in the title of "Preparation of Butylated Cumyl Phenol in Flow Reactor".